COLORED TITANIUM PASSIVE FILMS. PREPARATION, CHARACTERIZATION, APPLICATIONS, AND SURFACE MODIFICATION

by

Sabahudin Hrapovic

Thesis submitted to the Département de chimie
in fulfillment of the requirements for the degree of master ès sciences (M. Sc.)

FACULTÉ DES SCIENCES
UNIVERSITÉ DE SHERBROOKE

Sherbrooke, Québec, Canada, July 2000

Le 1er juillet 2010, le jury suivant a accepté ce mémoire dans sa version finale.
date

Président-rapporteur:	M. Jean Lessard Département de chimie	_____
Membre:	M. Jean-Marc Chapuzet Département de chimie	_____
Membre:	M. Gregory Jerkiewicz Département chimie	_____
Membre:	M. Dennis Dong Huron Tech.	_____
Membre:	M. Zbigniew Twandowski Kvaerner Chemetics Ltd	_____

SOMMAIRE

L'application de la polarisation par courant alternatif (CA) sur le titane dans le NH_4BF_4 aq. a permis d'obtenir des couches passives colorées brillantes et uniformes. Ces types de films révèlent une gamme de couleurs plus étendue comparativement à ceux obtenus par la technique de la passivation en phase gazeuse aux températures élevées. De plus, ces couches peuvent être formées en quelques secondes contrairement aux heures ou même aux journées nécessaires avec un traitement thermique en phase gazeuse sous atmosphère d'oxygène. Ces films démontrent de nouvelles propriétés comme protectrices et décoratives.

L'influence des différents paramètres expérimentaux (ex.: le pH et la concentration de l'électrolyte, le temps de polarisation et le type de voltage appliqué) sur la coloration, l'uniformité et la brillance du film ainsi que sa morphologie a été étudiée. La comparaison avec la polarisation par courant constant (CC) était également effectuée.

Les résultats expérimentaux démontrent que les couches passives colorées adhèrent bien au substrat de Ti et ne peuvent en être arrachées. Les analyses au moyen du microscope optique et du microscope à balayage électronique (MEB), confirment que la polarisation par un courant alternatif a formé des couches passives compactes ne révélant pas de fracture ou de fissure contrairement aux couches formées thermiquement en phase gazeuse. L'adhérence du film passif dépend du pré-traitement mécanique du Ti métallique avant sa formation. En général, l'adhérence est meilleure quand les films sont formés sur une surface rugueuse obtenue par décapage. Dans le cas d'un film formé sur une surface de Ti polie mécaniquement, l'adhérence est plus faible et le polissage ou le frottement provoque le détachement du film.

La caractérisation par spectrométrie des photoélectrons (XPS) des couches passives colorées, révèle que la composition chimique de la surface dépend du voltage lors de la polarisation CA.

Les principaux constituants de la couche passive sont Ti^{z+}, O^{2-} et F^- (z varie de 4 à 2 selon la profondeur du film). Le fluorure dans le film provient de la décomposition du NH_4BF_4 s'accumulant à l'interface entre le métal et le film. L'étude de la variation de la composition chimique en fonction de la profondeur nous montre que plus le voltage appliqué est élevé, plus la couche passive est épaisse.

La combinaison de la coloration électrochimique du Ti avec la technique de masquage utilisée dans l'industrie des semi-conducteurs a mené au développement de la lithographie électrochimique du titane. Cette technique pourrait être utile dans l'industrie de la décoration et aussi pour l'industrie des semi-conducteurs et des circuits imprimés.

Les propriétés électrochimiques des couches passives colorées du Ti sont déterminées en enregistrant des courbes de polarisation dans la région de – 0,8 à 3,2 V selon par rapport d'électrode réversible à hydrogène (ERH) et aussi en réalisant des courbes de Tafel dans la région de la réaction de dégagement d'hydrogène (RDH) dans une solution aqueuse d'H_2SO_4 1.0 M. Les courbes de polarisation démontrent que le potentiel de corrosion des couches passives colorées se déplace vers des potentiels moins négatifs, montrant que ces couches sont plus stables que le titane dans les mêmes conditions. Les courbes de Tafel pour la RDH démontrent que les couches passives ont une activité beaucoup plus élevée que le Ti pour cette réaction. La relation de Tafel révèle de nouvelles propriétés qui peuvent être associées à l'altération / décomposition de la couche passive, à l'absorption d'hydrogène ou à la formation d'hydrure de titane. Les couches passives peuvent aussi être utilisées comme barrière interfaciale contre la diffusion d'hydrogène.

Des études morphologiques et des caractérisations électrochimiques de l'Ebonex® ont aussi été menées. Ebonex® est un matériau céramique produit à partir des suboxydes de titane de type Magneli. Ce matériau possédant des caractéristiques physico-chimiques spécifiques est très difficile à mouler en pièces précises, ce qui n'est pas le cas des couches passives colorées de

Ti. Ebonex® a été utilisé pour comparer ses propriétés électrochimiques à celles des couches passives de Ti et aussi à celles des couches passives modifiées de Ti.

L'un des objectifs spécifiques de ces travaux était de modifier la surface de ces films de Ti par déposition d'oxyde de ruthénium et/ou d'oxyde d'iridium. Dans l'industrie chloro-alcaline, le rôle et l'importance des électrodes de RuO_2 et/ou de IrO_2 sont bien connus. La méthodologie de modification de la surface des couches passives colorées implique une technique de décomposition thermique des chlorures de ruthénium et/ou d'iridium. L'efficacité de cette technique de décomposition thermique, ainsi que la composition chimique de la surface et la morphologie de ces couches passives modifiées ont été vérifiées et confirmées par analyse élémentaire à rayons-X en sélection d'énergie (EDX) et par MEB. La couche passive de RuO_2 au-dessus de la couche passive de Ti ne révèle pas de fracture ou de fissure. Par contre, la couche passive de IrO_2 et celle de IrO_2+RuO_2 possèdent des fissures très prononcées. La morphologie des couches passives de Ti après leur modification par RuO_2 et/ou par IrO_2, donne des nouvelles caractéristiques électrochimiques, et aussi un comportement tout à fait différent comparativement aux couches passives colorées de Ti. L'évaluation de leur activité électrocatalytique et de leur stabilité sur de longues périodes de polarisation cathodique a été effectuée en utilisant les mêmes techniques électrochimiques que pour la caractérisation du Ti, des couches passives colorées de Ti et enfin pour Ebonex®.

ABSTRACT

Brightly and uniformly colored passive layers on Ti are prepared by application of AC polarization in aqueous NH_4BF_4. Such formed films reveal a wider spectrum of colors that those prepared by gas-phase techniques at elevated temperatures and can be formed within seconds (vs. hours or days in the case of thermal treatment in an oxygen-containing atmosphere). These films demonstrate novel properties as protective and decorative layers.

The influence of different experimental parameters (electrolyte pH and concentration, duration of polarization, type of applied voltage) on the coloration, uniformity, brightness, and morphology of the colored films is examined. The comparison with DC polarization was also studied.

Experimental results demonstrate that the colored, passive films well adhere to the Ti substrate and do not peel off from it. Optical microscopy and Scanning Electron Microscopy (SEM) analysis confirm that AC polarization formed passive films are compact and do not reveal fractures or cracks unlike thermally formed layers. The adherence of the passive films depends on the mechanical pretreatment of the metallic Ti prior to the film formation. In general, the adherence is greater when the films are formed on a rough, chemically etched Ti substrate. In the case of the films formed on a mechanically polished Ti, the adherence is lower and polishing or rubbing can result in the film's removal.

X-ray Photoelectron Spectroscopy (XPS) characterization of the colored passive layers reveals that their surface-chemical composition depends on the AC polarization voltage. The main constituents of the passive layers are Ti^{z+}, O^{2-}, and F^- (z varies from 4 to 2 depending on the film's depth). Fluoride in the film originates from decomposition of NH_4BF_4 and it

accumulates at the inner metal/passive-film interface. XPS depth profiling shows that the higher the AC voltage applied, the thicker the passive film formed.
A combination of the electrochemical coloring of Ti with masking techniques used in the semiconductor industry leads to the development of electrochemical lithography and pattern design on titanium. This technique could be useful in the decorative, semiconductor and printed circuit boards industries.

Electrochemical properties of the colored Ti passive layers are determined by recording polarization curves in the – 0.8 - 3.2 V vs. RHE range and Tafel plots in the hydrogen evolution reaction (HER) region in 1.0 M aqueous H_2SO_4 solution. The polarization curves show that the corrosion potential of the colored passive layers shifts towards less-negative potential, indicating that they are more stable than Ti under the same conditions. The Tafel plots for the HER demonstrate that the passive layers have much higher activity than Ti towards the HER. The Tafel relations reveal new features that can be associated with the partial breakdown/decomposition of the passive layers, H absorption, and Ti hydride formation. The passive layers can be used as an interfacial barrier against hydrogen embrittlment.

Studies of morphology and electrochemical characterization of Ebonex® are also carried out. Ebonex® is a ceramic material made from Magneli suboxides on titanium. This material having specific physicochemical characteristics is very difficult to machine, in contrast to the case of colored Ti passive layers. This material is used in order to compare its electrochemical characteristics with those of the multicolored Ti passive layers and chemically modified passive layers.

One of the objectives of this work was the preparation of Ti-based electrode materials for Hydrogen Evolution Reaction (HER) by surface modification of colored Ti passive layers through RuO_2 and/or IrO_2 depositing/doping. The surface modification of the passive layers was accomplished using thermal decomposition technique of $RuCl_3$ and/or $IrCl_3$. The

achievement of this doping technique, and the surface chemical composition and morphology of such modified layers are verified and confirmed by Energy Dispersive X-Ray microanalysis (EDX) and Scanning Electron Microscopy analysis (SEM). The RuO_2 oxide layer on top of the Ti passive film reveals no cracks and fractures. On the other hand, the IrO_2 and IrO_2/RuO_2 layers are cracked with very pronounced fractures. The surface morphology of Ti passive layers obtained by depositing/doping with RuO_2 and/or IrO_2 gives new electrochemical characteristic and different behavior to the colored titanium passive films. The evaluation of their electrocatalytic activity and stability upon prolonged cathodic polarization was carried out using the same electrochemical techniques used for the characterization of Ti, colored Ti passive layers and Ebonex®.

ACKNOWLEDGEMENTS

I would like to present my gratitude and great appreciation to Professor Gregory Jerkiewicz for his direction, guidance and support during the course of this research. Professor Jerkiewicz has been always ready to help, to discuss the results and to provide useful ideas. He was not only my professor, but also like my friend, joyful and helpful in establishing my new life in my new homeland.

I would like to express my gratitude to my friends and colleagues in our laboratory: Sonia Blais M.Sc., Dr. Alireza Zolfaghari, Dr. Gholam Vatankhah, Mathieu D'Amours and Jean-Pierre Tessier, friends always ready to help and resolve numerous electrochemical problems. I wish to thank the Chemistry Department professionals, Mr. Pierre Magny for excellent SEM analysis, Mr. Denis Poulin of the Mechanical Workshop who was able to fabricate and machine numerous electrodes. Thanks to Mr. Réal Dubuc, master glassblower and artist in his job.

I would like to express my special respects and gratitude to my parents, Zekir and Aisha, and to my sister Selma, for their support and encouragement during the course of my studies which I started in my native land, Bosnia, and which I could not finish there because of the war. Even while being so far away, they have always been with me.

I would like to acknowledge the financial support from the Natural Sciences and Engineering Research Council of Canada (NSRCC) through a Strategic Research Grant, and two industrial supporters, namely Huron Tech Canada Inc., of Kingston, Ontario, and Kvaerner-Chemetics Inc., of Vancouver, British Columbia.

Above all, I would like to thank my dear wife, Zorana, for her love and help. She was and is always supporting and giving me the energy and courage to continue my work. Thank you!

TABLE OF CONTENTS

LIST OF FIGURES

LIST OF TABLES

INTRODUCTION

The importance of titanium and its rapidly increasing utilization and applications lie in its exceptional physico-chemical characteristics. Titanium is the fourth most abundant metal and ninth most common element in the Earth's crust. With a density of 4.5 g cm^{-3}, it lies halfway between aluminum (2.7 g cm^{-3}) and iron (7.9 g cm^{-3}). Titanium is diamagnetic and has good heat-transfer properties. Its coefficient of thermal expansion is somewhat lower than that of steels and less than half of aluminum. Titanium is non-toxic and generally biologically compatible with the human tissues and bones. The combination of high strength, low density, and excellent corrosion resistance makes titanium and its alloys useful in many industrial domains. The aircraft industry is the single largest market for titanium products primarily due to the exceptional strength-to-weight ratio, high melting point and corrosion resistance. Titanium applications are most significant in jet engine and airframe components that are subject to temperatures up to 600°C and for other critical structural parts. Its use is widespread in most commercial and military aircraft. Titanium is also used in spacecraft where the most of the physical and mechanical properties of titanium are effectively utilized.

Development of highly efficient gas turbine engines is possible only through the use of titanium-based alloys in components such as fan blades, compressor blades, discs, hubs and numerous non-rotor parts. The key advantages of titanium-based alloys in this application include high strength at moderate temperatures and good resistance to creep and fatigue. The development of titanium aluminides will allow the use of titanium in hotter sections of a new generation of engines. Titanium condensers, shell and tube heat exchangers, plate and frame heat exchangers are used extensively in power plants, refineries, air conditioning systems, chemical plants, offshore platforms, surface ships and submarines. Extended life time, increased energy efficiency, and greater product purity are factors promoting the use of titanium electrodes in electro-winning and electro-refining of copper, gold, manganese and manganese dioxide. Titanium is widely used for implants, surgical devices, pacemaker cases

and centrifuges. Titanium is the most biocompatible of all metals because of its total resistance to attack by body fluids, high strength and low strength modulus. In hydrocarbon processing, the need for long lifetime equipment, coupled with requirements for low downtime and maintenance, favors the use of titanium in heat exchangers, vessels, columns and piping systems in refineries and offshore platforms. Titanium is immune to general attack and stress corrosion cracking brought about by hydrocarbons, H_2S, brines and CO_2.

Because of exceptional erosion/corrosion resistance, titanium is currently being used for submarine ball valves, fire pumps, heat exchangers, castings, hull material for deep-sea submersibles, water jet propulsion systems, shipboard cooling and piping systems. Titanium vessels, heat-exchangers, tanks, agitators, coolers, and piping systems are utilized in the processing of aggressive compounds such as nitric acid, organic acids, chlorine dioxide, inhibited reducing acids and hydrogen sulfide (1,2).

The enigma of such a large utilization of titanium is its ability to passivate by forming surface oxides which provide a high degree of immunity to attack by most mineral acids and chlorides (3). However, in reducing environments in which the oxide film is not self-healing, it often becomes the anodic member of the couple. The corrosion potential of titanium in sea water is –0.10V vs. RHE which places it below that of 18-8 stainless steel and above that of silver in the sea water galvanic series (4). Titanium is cathodic to aluminum, carbon steel, zinc and magnesium in sea water, and the rate of corrosion of these less-noble metals will be affected by the ratio of the surface areas. Because of the electrical resistivity of the oxide films that are formed on titanium, the metal loss or corrosion due to the galvanic couple is less than it would be in an electrochemical couple between metals of similar position in the galvanic series that do not have a dielectric coating (2,5).

Protection of titanium against corrosion is achieved by means of passive, self-healing films which form on the metal surface. Film formation depends on the environment to which metal is exposed. Under oxidizing, neutral, or naturally occurring conditions, titanium shows

immunity to corrosion as an oxide film is formed and maintained. In strongly reducing solutions in which protective films cannot be formed (aqueous HF), rapid attack can occur. In slightly reducing or complexing environments, titanium behavior depends on the presence of metal ion inhibitors, alloying elements, the temperature, and other variables (6).

The protective crystalline oxide film that normally passivates titanium is believed to forme instantaneously on exposure to the air. The initial film is 12-16 Å in thickness. After about 70 days it reaches 50 Å, and after 4 years it grows to about 250 Å (3). The thickness of the films varies with temperature and oxidation conditions. The film composition changes across its thickness. Near the metal surface it contains TiO, and at the outer surface it is TiO_2, but in the interior it contains Ti_2O_3 (7,8). The surface passive film affects heat transfer because the thermal conductivity of titanium is greater than the thermal conductivity of Ti oxides. The increased hardness of the surface film provides resistance to abrasion and cavitation erosion.

The passivation of titanium in aqueous reducing acidic media shifts the corrosion potential in the noble (positive) direction where oxide film stability is promoted. There are different ways and methodologies of improving titanium stability in corrosive environments (1):

(a) Anodic polarization of titanium or its alloy by applied anodic current, or galvanic coupling to a less noble metal.

(b) Presence of dissolved oxidizing species in the environment acting as cathodic depolarizers.

(c) Presence of certain alloying elements in titanium which decrease the cathodic (hydrogen) overvoltage, thereby depolarizing the cathodic process.

(d) Increase of surface oxide thickness by thermal oxidation.

(e) Increase of surface oxide thickness by anodization.

The anodization of titanium by direct current (DC) application is a known and established method. In the past, a variety of solutions have been employed for formation of anodic films

on titanium: alcoholic-organic acid baths containing small amounts of phosphoric acid for developing of the anodic film on titanium metal (9); acetic-perchloric acid baths (10). They produced pure oxide films, but extremely poor in adherence. New methods were developed in order to improve the poor adherence of Ti oxides formed in sulfuric acid solutions (11). Much better results were obtained when using hydrochloric-nitric-sulfuric acid baths for polishing the surface followed by anodization in a borate buffer solution (12). Some authors recommend a two-step anodizing procedure employing first a phosphoric acid-glycol bath, and then a boric acid bath for final film formation (13). The aqueous solution of phosphate salts including sodium and potassium orthophosphates and sodium, potassium and ammonium acid phosphates, and also ammonium tartaric acid baths) are the most commonly used aqueous salt solutions . A large spectrum of colors can be obtained in aq. 3-5 wt. % trisodium phosphate (13,14).

One of the objectives of this work was the examination of the corrosion resistance of the colored passive layers on titanium and their applications as electrode materials. A methodology of preparation of colored passive layers on Ti already invented in our laboratory was improved. The formation of multicolored passive films on titanium was created by potentiostatic alternating current (AC) polarization of titanium in aq. NH_4BF_4 solution which produces passive films with a wide spectrum of uniform and well-defined colors (15). The coloration originates from the constructive light interference between the beam reflected at the outer oxide-air interface and the inner metal-oxide one, a phenomenon referred to as *iridescence* (16). This is characteristic for thin transparent films, where part of the light is reflected by the outer surface layer, and part at the inner one. Whether the beams reinforce or cancel out depends on the nature and thickness of the film, the angle of reflection, and the light wavelength. If the film has a uniform thickness, different wavelengths emerge at different angles. If the layer varies in thickness, then at any given viewing angle, a different color appears (17). The same effect is also observed for metals such as Zr, Nb, and Ta. This phenomenon can be used in electrochromic process technology (18) and in the domain of decorative art (19).

A separate part of this work is the chemical modification of the titanium multicolored passive layers by doping with IrO_2 or/and RuO_2. Pure and mixed metal oxide coatings on titanium are materials widely used as anodes in a variety of industrial electrochemical processes such as the chloro-alkali industry. These types of materials are usually prepared by thermal decomposition of the corresponding metal chloride solutions ($IrCl_3$ or $RuCl_3$) applied to the titanium substrate by immersion or by painting (20-29). Some authors proposed the sol-gel method as an alternative to obtain mixed oxide films on metallic substrates and to avoid the presence of residual chloride (30-32). These kinds of electrodes containing conductive metal oxides reveal some desirable properties such as: (a) high surface area (33), (b) excellent mechanical, electrical and electrocatalytic properties, (c) catalytic properties that can be modified by introducing a modulating oxide (34). The surface doping of TiO_2 with IrO_2 or RuO_2 modifies the electronic properties of TiO_2 from semi-conducting to electronically conducting. Such prepared chemically modified mixed oxide layers reveal good catalytic properties towards the electrolytic O_2 and Cl_2 generation, and are used as anode materials (35-37). Our interest in surface modified Ti electrodes arises not only from their application as anodes but also from the necessity to develop a suitable Ti-based cathodic material for the chloro-alkali industry where the carbon-steel electrode is unable to withstand the highly corrosive environment and has to be periodically replaced (38). Nanocrystalline Ti-Ru alloys prepared by ball milling (39), as well as mixed Ti-Ru-Fe oxides (40) reveal favorable electrocatalytic properties as a cathode material for water electrolysis owing to a low overpotential of the hydrogen evolution reaction (HER), long-term mechanical stability, and high real-surface area. On the other hand, titanium oxides electronically modified through Pd implantation can be used as a suitable substrate in electrolytic bulk Cu deposition (41,42).

Another important objective of this work, which is described in a separate chapter, was to study and characterize Ebonex® on titanium in order to compare its electrochemical properties with those of multicolored titanium passive layers and also with modified passive layers.

Ebonex® is a ceramic material based on Magneli suboxides on titanium (43). The non-stoichiometric oxides having the general formula Ti_nO_{2n-1}, where n = 4-6, are dark blue-black in color and electrically conducting, whilst retaining corrosion resistance and low toxicity of the parent material (44). Ebonex® materials are currently being explored for a diverse range of technological applications such as chlorine generation, sodium chlorate production, electroflotation devices, battery materials, and fuel cells (45). In electroplating, for the regeneration of hard chrome plating solutions, lead dioxide electrode coated with Ebonex® are used (46). New systems using Ebonex® are being developed for cathodic protection of metals in concrete and for marine applications (47).

CHAPTER 1

THEORETICAL ASPECTS OF CORROSION OF TITANIUM AND TITANIUM PASSIVE LAYERS

Corrosion is an electrochemical process in which the surface of a metal in contact with an electrolyte is oxidized with the simultaneous reduction of some species in the electrolyte on the metal surface, and which, over time, results in the deterioration of the majority of metals. Generally, a corrosion process can proceed via one of the three modes, depending on the compactness and stability of the corrosion products: (a) direct dissolution without hindrance from corrosion products, (b) direct dissolution with hindrance from corrosion products, and (c) indirect dissolution through the formation of passive films (48,49).

The rate in which the corrosion reaction proceeds is related to the electrolyte composition and physico-chemical characteristics of the metal. One of the very best ways for obtaining information about corrosion kinetics is through an analysis of anodic polarization curves recorded in the electrolyte of interest (50). The polarization curve for a metal that passivates will have the general shape shown in Fig. 1 (1). The current-potential, or polarization, curve can be divided into number of regions. In region AB, the active region, metal dissolution occurs. At the potential B, the current decreases to a very low value. The electrode is said to have undergone under an active-passive transition, and at the point C, the electrode becomes passive. The potential at which the current falls to the passive value is called the passivation potential. For $E > E_{pass}$, the metal is said to be in the passive region. In this region, the current is independent of potential, and metal dissolution occurs at a low constant rate. For potentials greater than the point E, oxygen evolution can occur on the outside of the oxide film. This is possible because the passive films are commonly thin (nanometers) and possess semiconducting properties. The dashed line in Fig. 1, (potential region D to E), represent the

transpassive region. In this region, the oxide film starts to dissolve, generally as a hydrolyzed cation in a higher oxidation state.

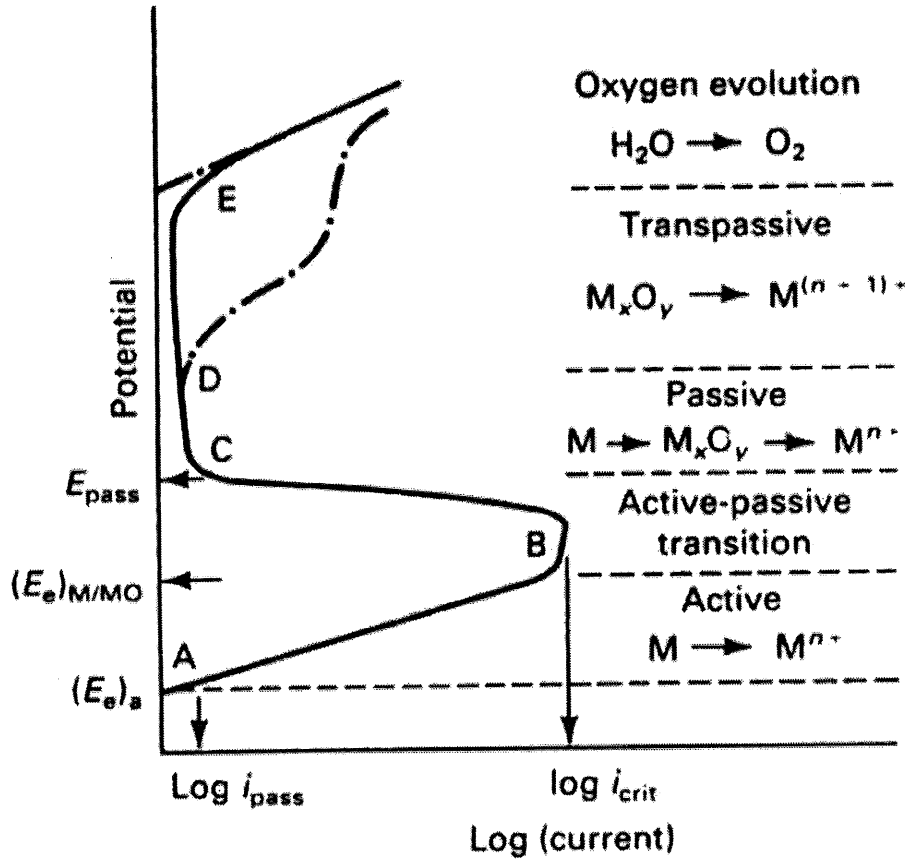

Figure 1. A typical polarization curve for a metal/metal ion system that undergoes an active to passive transition followed by transpassive transition (49).

Another excellent way of graphical presentation of the domain of stability of metal ions, oxides, and other species in solution is a potential vs. pH (Pourbaix) diagram that is shown in Fig. 2. The lines that show the limits between two domains express the value of equilibrium potential between two species as a function of pH. They are computed from thermodynamic data using the Nernst equation. These diagrams show also the equilibrium of acid-base reactions independent of the potentials. These equilibria are represented by vertical lines at specific pH's. Potential-pH diagrams provide important information that is useful in corrosion

science and technology. Fig. 2 (52) shows a Pourbaix diagram for titanium indicating the domain of stability as well as the regions of corrosion of titanium for given values of potential and pH. Oxide stability over the full pH scale is indicated over a wide range of highly oxidizing to mildly reducing potentials, whereas oxide film breakdown and the resultant corrosion of titanium occur under reducing acidic conditions. Under strongly reducing (cathodic) conditions, titanium hydride formation is predicted.

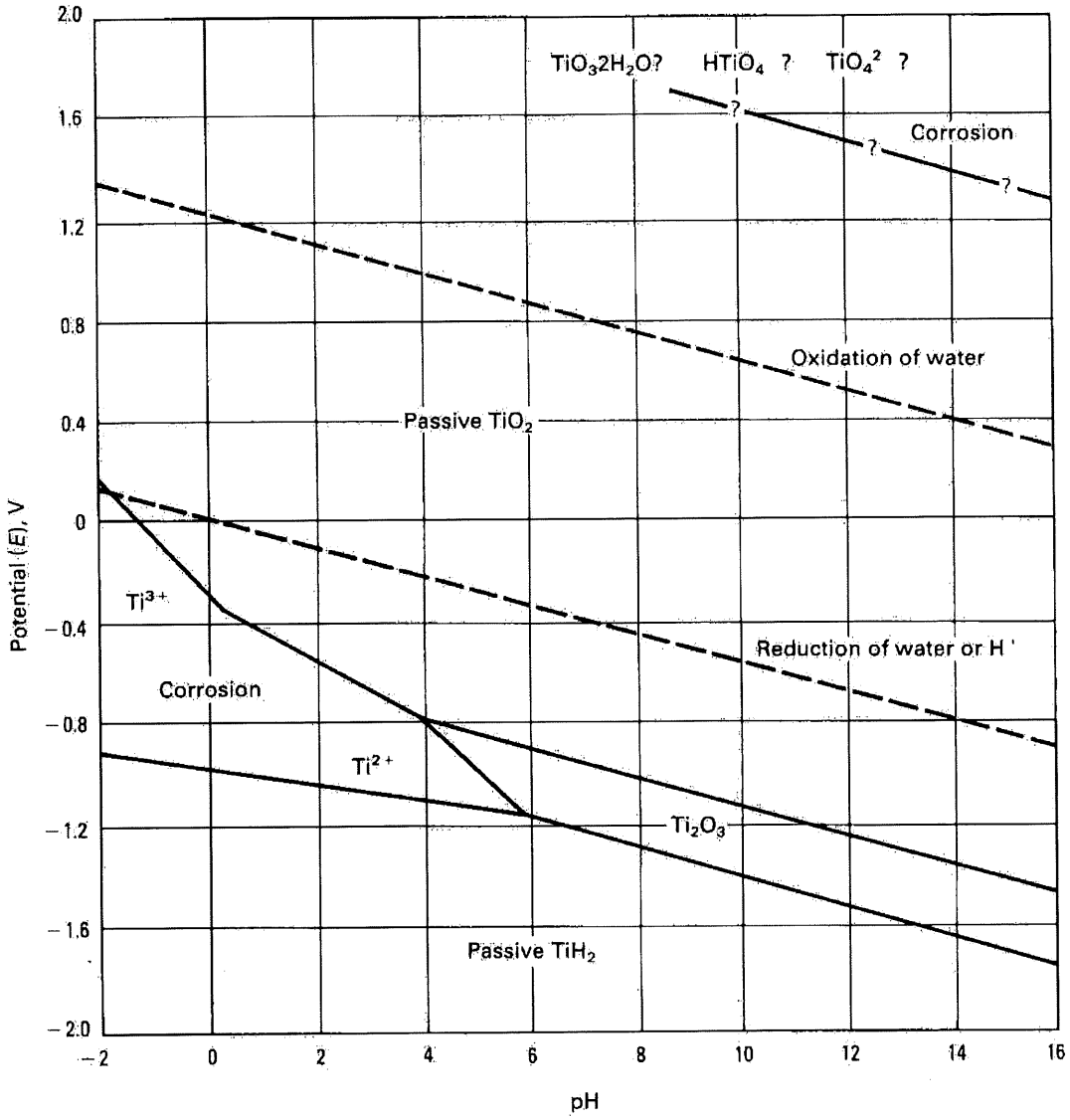

Figure 2. Pourbaix (potential versus pH) diagram for the titanium-water system at 25°C (52).

1.1 Forms of titanium corrosion

The form of corrosion can be defined according to the nature of corrosion such as galvanic corrosion and crevice corrosion or according to the effect of the corrosion on the surface morphology i.e. general corrosion and pitting corrosion, and also according to its effect on bulk properties, such as intergranular corrosion and stress corrosion cracking (4).

1.1.1 Galvanic corrosion

Galvanic corrosion, also called bimetallic corrosion, occurs when two different metals are in electrical contact. The coupling of titanium with dissimilar metals usually does not accelerate the corrosion of titanium, with the exception of strongly reducing media in which titanium severely corrodes and does not passivate (4). In this uncommon situation, accelerated corrosion may occur when titanium is coupled with more noble metals. In its normal passive state, titanium is beneficially influenced by materials that exhibit more noble (positive) corrosion potentials (graphite, Pt, Pd, Au, Ru, Ir). When coupled with these materials, titanium anodic protection increase by further stabilizing the oxide film on titanium at more noble potentials. The corrosion potential of titanium in seawater is – 0.10 V vs. RHE which places it below 18-8 stainless steel and above silver in the sea water galvanic series (4). The anodic/cathodic nature of titanium depends on the other metal and its place and potential in the galvanic series. Titanium is cathodic to aluminium, carbon, steel, zinc, and magnesium in seawater, and the rate of corrosion of those metals is affected by the ratio of the surface areas of the two metals. Because of the electrical resistivity of the oxide films that are formed on titanium, the metal loss or corrosion due to the galvanic couple is less than it would be with a couple between metals of similar position in the galvanic series that do not have a dielectric coating (3).

1.1.2 Crevice corrosion

Crevice corrosion is a localized form of corrosion proceeding at a fast rate within a crevice. Titanium and titanium alloys generally exhibit superior resistance to crevice corrosion as compared to stainless steel and nickel-based alloys. The susceptibility of titanium to crevice corrosion should be considered when tight crevices exist in hot aqueous chloride, bromide, iodide, or sulfate solutions. Factors that affect crevice attack includes alloy composition, pH of electrolyte, temperature, halide concentration, presence of oxidizing species, sample surface condition and crevice geometry. The model for crevice corrosion in aqueous chloride media is represented in Fig. 3 (51). Dissolved oxygen or other oxidizing species in the bulk solution are not present in the restricted volume of solution in the crevice. As a result, metal potential in the crevices become active (negative) relative to metal surface exposed to the bulk solution. This creates an electrochemical cell in which the crevice becomes anodic and corrodes, and the surrounding metal surface is cathodic. Titanium chlorides formed within the crevice are unstable and tend to hydrolyze, forming hydrochloric acid and titanium oxide as corrosion products. Because of the small volume of the solution in the crevice, a decrease of pH value as low as 1 and below, can be observed. This involves an additional growth of the crevice and a progress of corrosion.

One way of preventing crevice corrosion is to avoid the imperfections of the materials and the machining failures during the design stage. Rivets, which favor crevice corrosion, could be replaced by welding or they could be covered by coatings (49). Under certain conditions, usually associated with halide solutions, crevice corrosion of titanium can occur in gasket joints, and under heavy scale deposits. Teflon and fluorocarbon adhesives, when coupled in a crevice, accelerate the corrosion of titanium. The severity of attack increases with an augmentation of temperature, halide ion concentration, and a decrease of pH.

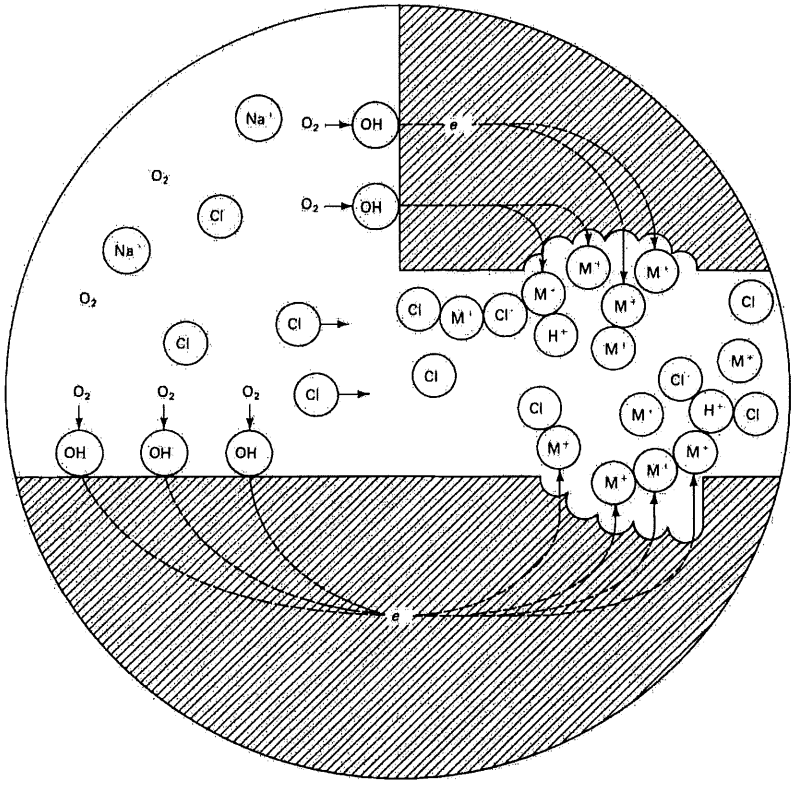

Figure 3. Schematic representation of the mechanism of crevice corrosion for titanium in aqueous chloride media (51).

1.1.3 Stress corrosion and hydrogen embrittlement

This form of corrosion is a mechanical failure of a metal by cracking caused by the combined effect of a corrosive environment and a tensile stress. The numerous factors that influence stress corrosion are: metal purity and alloy composition, thermal/metallurgical treatment, metallurgical factors, tensile stress, and the environment.

Titanium is subject to stress corrosion cracking in a limited number of strong oxidizing and halogen-containing agents. Since the metal has found wide use in these environments, failures appear to be limited to extreme operating conditions. Stress corrosion of titanium has been observed in red fuming nitric acid, nitrogen tetroxide, liquid cadmium, chloride salts at elevated temperatures, bromine at elevated temperatures, and in certain chlorinated and

brominated organic compounds at elevated temperatures. In each case susceptibility manifests itself in many small branching cracks. Initiation can occur in an untouched material at relatively low stress levels. Alloying with certain metals can increase the sensitivity to stress corrosion, and mill processing also influences susceptibility.

A special type of stress corrosion is hydrogen-assisted cracking, so-called hydrogen embrittlement. The phenomenon is based on hydrogen absorption near the crack tip. Hydrogen absorption leads to embrittlement of the metal and promotes formation of cracks which may cause a severe loss of ductility and other physical properties of the metal. A photomicrograph of severely hydrided titanium is shown in Fig. 4 (52). Hydrogen-assisted cracking can affect zirconium, titanium, and other metals forming hydrides. The metal becomes brittle and subject to mechanical failure. Moreover, hydrogen frequently concentrates near dislocations, pits, cracks, or inclusions, thus leading to preferential cracking in these areas (49). Brittle type failures in normally ductile material were shown to have abnormal hydride contents. Under cathodic conditions, titanium is known to embrittle rapidly and cracks, due to the formation of titanium hydride crystals. In aqueous halide-containing solutions certain titanium alloys show reduced fracture toughness. This phenomenon is considered by many to be a modified form of stress corrosion (52).

This disintegration mechanism depends on the nature of the metal, the electrolyte, temperature, current density, etc. As regards Ti, the formation of TiH_x is of particular importance. Atomic hydrogen, formed on the cathodic surface, penetrates into the grain boundaries to form TiH_x (53). This ability of hydrogen to penetrate into titanium is responsible for its hydrogen embrittlement.

Typically, the oxide film on titanium acts as an effective barrier for hydrogen penetration. However, under conditions that allow hydrogen to enter titanium and exceed the concentration needed to form a hydride phase (about 100 to 150 ppm), embrittlement can occur. Hydrogen absorption has been observed in alkaline solutions at temperatures above the boiling point. Acidic conditions that cause the oxide film to be unstable, may also result in embrittlement

under conditions in which hydrogen is generated on the surface. The hydrogen penetration may reduce ability to resist erosion, resulting in a higher rate of different forms of corrosion. The presence of as little as 2% of moisture effectively prevents the absorption of hydrogen up to temperatures as high as 315°C. Anhydrous environments and those lacking a source of oxygen to maintain the oxide film intact on titanium should be avoided, because absorption of hydrogen will occur at temperatures above 75°C. A photomicrograph of hydrided unalloyed titanium surface is shown in Fig. 4 (54).

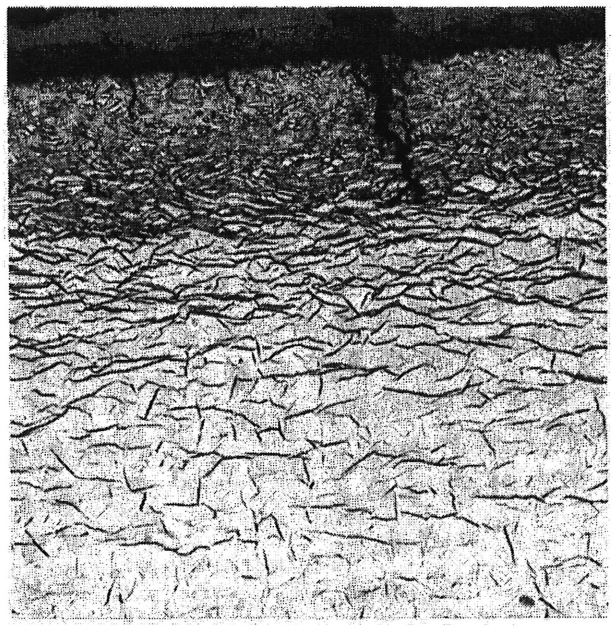

Figure 4. Photomicrograph of severely hydrided unalloyed titanium at the magnification of 200 × (54).

1.1.4 Erosion corrosion and cavitation

When abrasion or erosion occurs at a metal in a corrosive environment, there is a very effective combination of mechanical and chemical conditions than can result in a rapid deterioration and failure of the material. All metal alloys are susceptible to erosion-corrosion, especially alloys that form a protective surface passive film; the abrasive action may erode

away the film, leaving a naked metal surface exposed to electrolyte. If the coating is not capable of reforming a protective barrier, corrosion may be severe (55). In normal passive environments, titanium is highly resistant to erosion corrosion, because of the presence of protective surface oxide films as a barrier. The ability of an oxide film to repair itself when damaged, also contributes to excellent resistance to erosion corrosion of titanium. The contour of the metal surface, the amount of suspended solids, and the temperature affects the rate of the attack (3). Recent studies have shown that initiation and propagation of fatigue micro-cracks at the cavitated surface can play a major or even dominant role in cavitation erosion (49).

1.1.5 Localized corrosion (pitting)

Pitting corrosion is a localized corrosion that proceeds rapidly at small spots where the attack penetrates deep into the metal. Once the pitting has started, it penetrates to the point of perforation. Pitting is usually difficult to detect, especially in the early stage. One characteristic feature is that pitting generally occurs on metals and alloys whose surface is in a passive state, with severe dissolution of the metal at localized points and relatively little dissolution of the rest of the exposed surface. Another feature is that it usually occurs in a medium that contains aggressive anions, such as traces of fluoride or chloride ions, which cause local breakdown of the passive surface, thus exposing the underlying metal to the corrosive medium (48).

In the case of titanium, the protective oxide film must be destroyed before localized attack can take place. Once the film becomes powdery and porous, the localized attack proceeds. Titanium has good resistance to a localized attack. Although many metals pit in hypochlorites, seawater, calcium chloride, hydrogen sulfide, and at places where surface deposits accumulate, titanium is resistant in these circumstances (3). A general representation of the development of pitting corrosion is shown in Fig. 5 (1).

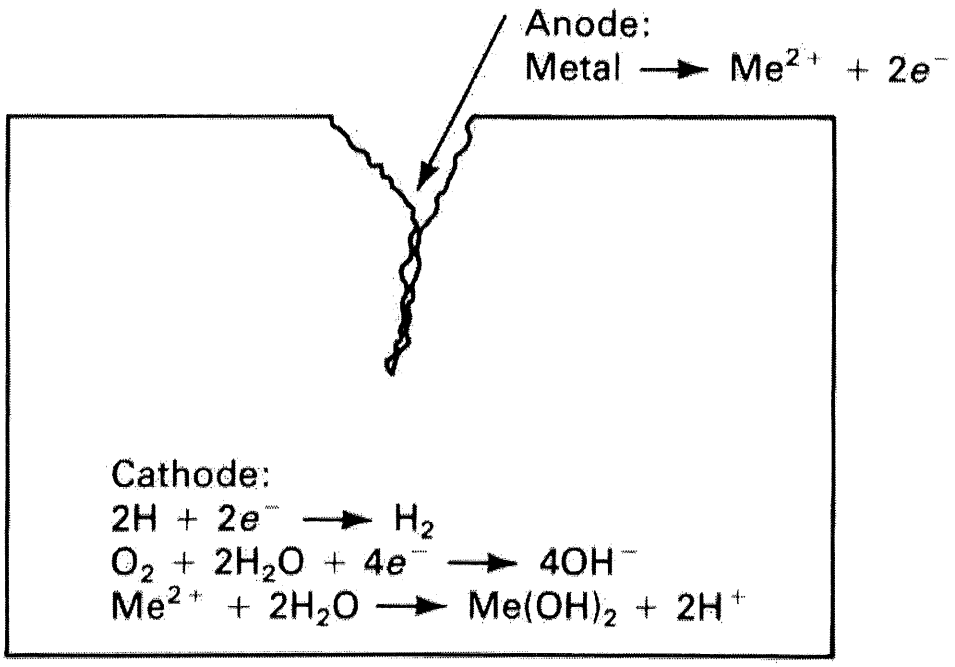

Figure 5. Schematic representation of the mechanism of pitting corrosion (49).

1.2 Corrosion resistance of titanium in specific media

Titanium, through the presence of the native surface oxide, is completely resistant to distilled water at all oxygen levels. No attack occurs in high-purity water in nuclear-reactor coolant systems at the pressure and the temperature conditions normally used (P = 4500 kPa, and T = 530 K) (56). The exposure of titanium to the seawater shows no attack on the metal (57). Similar tests in Atlantic Ocean at various depths show no variation of corrosion rates of titanium. Only biological organisms present in the sea adhere to the titanium surface, but they do not promote any attack. The effect of temperature of the seawater is negligible up to 320°C. Above this point, the corrosion process most likely originates from a difference of the thermal expansion coefficients of titanium and titanium oxide. However, the physical properties of titanium do not appear to suffer from exposure to seawater.

Titanium has excellent resistance to wet chlorine gas, although it is corroded by dry chlorine. The moisture content necessary for passivation depend on environmental conditions such as

temperature, pressure, degree of gas movement, geometry of the part, and extent of mechanical damage to the surface oxide film. Titanium has a high degree of immunity to such media as chlorinated brine, chlorine dioxide, chlorates, hypochlorites, and boiling solutions of sodium chlorate. In chloride environments, titanium may suffer crevice corrosion.

Titanium has been employed to a considerable extent for the handling of nitric acid. At numerous temperatures, concentrations, and other conditions, it has a low corrosion rate. Only fuming nitric acid with less than 1.34% of water, or more than 6% of NO_2, is capable of making sensible titanium and its alloys to the point where violent pyrophoric reaction may develop. The corrosion rate of titanium at high temperatures in nitric acid is shown in Fig. 6 (56).

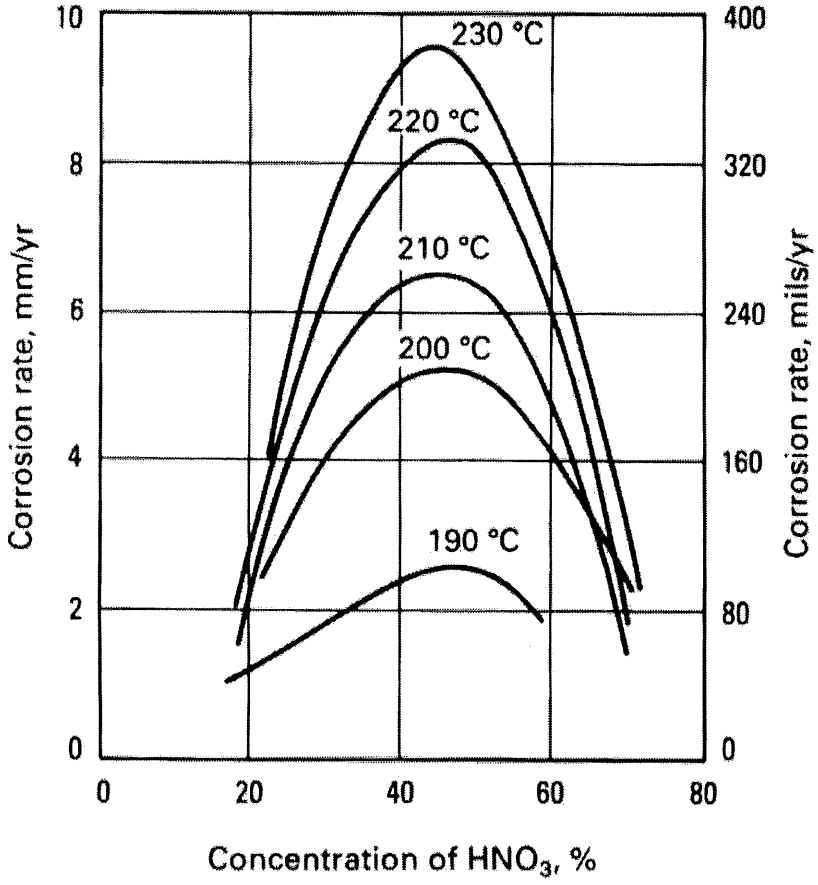

Figure 6. Corrosion rate of unalloyed titanium in high temperature HNO_3 solutions (56).

Titanium is resistant to dilute solutions of sulfuric acid at low temperatures. Although laboratory test data show that the attack is severe at higher concentrations and temperatures, titanium is used successfully where test data indicated poor performance. This phenomenon is generally explained by the fact that minor amounts of many metal ions such as Fe^{3+} and Cu^{2+}, often present when the acid is used in production cycles, dramatically lower the corrosive attack on titanium. Accordingly, titanium is frequently found to be resistant in a sulfuric acid environment. Titanium is corroded in hydrochloric acid, where the presence of ferric or cupric ions, chromic acid or nitric acid in hydrochloric acid, can have a beneficial effect in passivating titanium (58).

1.3 Enhancement of the corrosion resistance of titanium

Despite, in generaly, excellent corrosion properties of titanium, its use in more and more severe and aggressive solutions requires an improvement and expansion of the corrosion behavior of titanium. There are numerous ways of enhancing the corrosion stability of titanium such as alloying of titanium, inhibitor addition, precious metal surface treatment, thermal oxidation, and electrochemical oxidation.

1.3.1 Alloying of titanium

The most effective and preferred means for extending resistance to general corrosion into reducing environments has been alloying titanium with certain elements. These additions facilitate cathodic depolarization by providing sites of low hydrogen overvoltage, which shift the alloy corrosion potential towards more positive values where the formation of oxide passive films is possible. Relatively small amounts of certain precious metals, of the order of 0.1 wt.%, are sufficient to expand significantly the corrosion resistance of titanium in reducing media. These beneficial alloying additions have been incorporated in several commercially available alloys including titanium-palladium alloys (grades 7 and 11), Ti-0.3Mo-0.8Ni (grade 12), Ti-3Al-8V-6Cr-4Zr-4Mo, Ti-15Mo-5Zr, and Ti-6Al-2Sn-4Zr-6Mo (51). The high-

molybdenum alloys offer a unique combination of high strength, low density and superior corrosion resistance.

1.3.2 Inhibitor addition

Various oxidizing species can effectively inhibit the corrosion of titanium in reducing acidic environments when present in very small concentrations. Typical potent inhibitors for titanium and titanium alloys in aggressive reducing acids are picric acid, m-nitroacetanilide, trinitrobenzoic acid, oxidizing metal cations (Ti^{4+}, Fe^{3+}, Cu^{2+}, Ce^{4+}, Sn^{4+}...), oxidizing anions (ClO_4^-, $Cr_2O_7^{2-}$, MoO_4^{2-}, WO^{4-}, IO^{3-}...), precious metal cations (Pt^{2+}, Pt^{4-}, Pd^{2+}, Ru^{3+}, Ir^{3+}...). Many of these inhibitors are effective at levels as low as 20-100 ppm, depending on the acid concentration and temperature.

1.3.3 Precious metal surface treatment

Precious metals such as platinum and palladium can be ion plated, ion implanted, or thermally diffused into the titanium alloy surface to achieve improved resistance to reducing acids. This approach has not been used commercially for industrial components, because of high cost, coating application limitations (mechanical and corrosion damage), normally associated with very thin surface films. However, ion plated platinum or gold surface films impart significant improvements in titanium alloy oxidation resistance at temperatures up to 650°C (59). In the case of palladium surface treatment of titanium (Fig. 7), the addition of palladium provides cathodic sites on the surface of titanium which tend to increase the thickness of the oxide film and the resistance of titanium to aggressive environments (3).

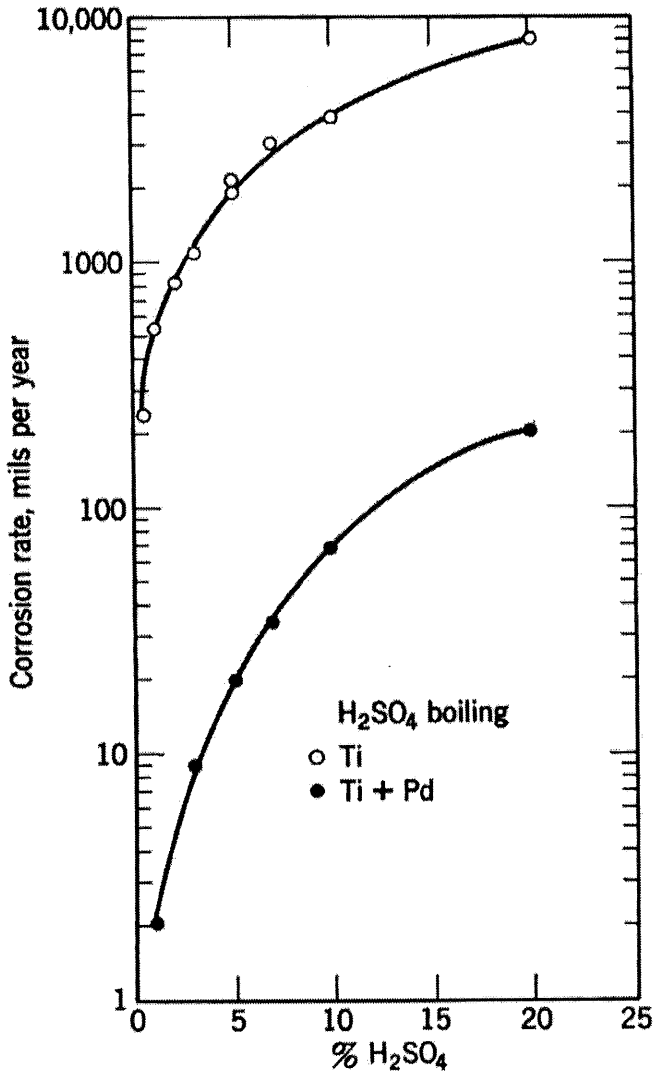

Figure 7. Comparison of titanium and Pd-ion treated titanium surface in boiling sulfuric acid (3).

1.3.4 Thermal oxidation

Protective thermal oxide films can be formed when titanium is heated in air at temperatures of 600 to 800°C for 2-10 min. The growth rate of the thermal oxide films on titanium in air is shown in Fig. 8 (51). The rutile TiO_2 film measurably improves resistance to dilute reducing acids as well as absorption of hydrogen under cathodic charging or gaseous hydrogen absorption. Corrosion studies in hot dilute HCl have confirm its superior resistance. Like anodization, thermal oxidation offers no improvements in titanium resistance in highly alkaline media.Although the thermal oxide has proved to be protective in relatively short-term

tests in dilute reducing acids, the long-term performance has not been fully demonstrated. Moreover, in the case of thermal oxidation, the same crack-free morphology is difficult to accomplish at elevated temperatures because the metal and the oxide have different thermal expansion coefficients and different partial molar volumes, which are the origin of cracking upon cooling down to room temperature. Mechanical damage and plastic strain of thermally oxidized components must be avoided for effective protection. The oxide has been successfully applied on tubing and small components, but may be impractical for large components or where component distortion may occur during thermal oxidation (heating). The growth of the thermal oxide films on unalloyed titanium in air is shown in Fig. 8 (4).

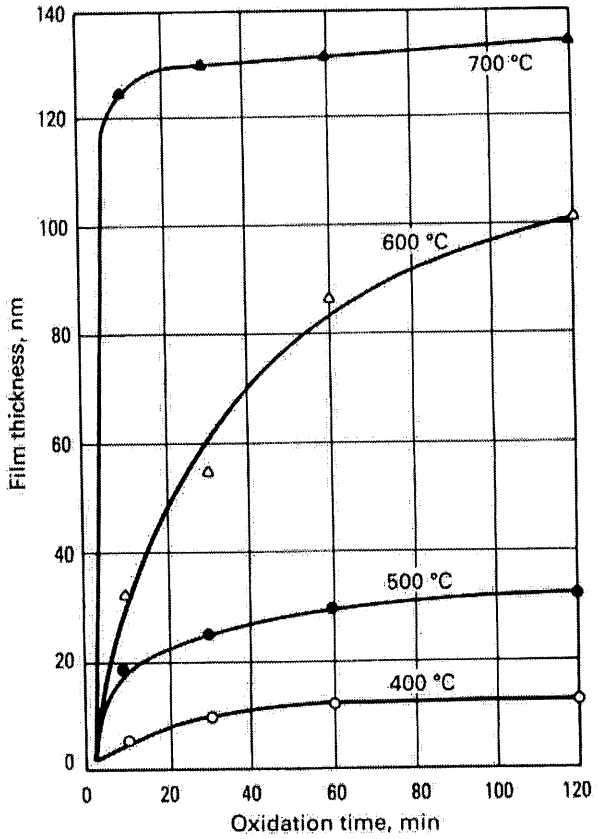

Figure 8. Growth of the thermal oxide films on unalloyed titanium in air (4).

1.3.5 Electrochemical oxidation

This procedure resembles closely standard electroplating techniques. A well-established method is DC anodization of titanium in different electrolytes (8-11, 19). During the anodization, a current passes through the bath and oxygen evolution occurs on the anode surface. Oxygen combines with the reactive titanium to form an oxide. This transparent oxide increases in thickness in relation to the amount of applied voltage. While oxygen is formed on the anode, hydrogen is generated on the cathode. The cathode may be any inert metal, but titanium and stainless steel are also convenient.

One method of electrooxidation of titanium is an application of an alternating current (AC) in NH_4BF_4 electrolyte (See Chapter 2). While the formation of oxide films on noble and non-noble metals by anodization (potentiostatic and galvanostatic), or by potential cycling is quite well documented in the electrochemical literature, the oxide growth behavior and its morphology and electrochemical characteristics upon application of AC polarization are not well known or established (60). In order to properly understand the mechanism of formation of Ti passive films and their physico-chemical properties, a careful attention must be given to all the reactions taking place at the electrode surface upon polarization. The possible anodic reactions are:

(a) Surface metal oxidation: $Ti + {}^{x}/_{2} H_2O \rightarrow TiO_x + xe^- + xH^+ \quad (x = 2,,3,4\ldots)$ [1.1]

(b) Metal dissolution: $Ti \rightarrow Ti^{+z} + ze^-$ [1.2]

(c) Surface fluoride formation: $Ti + xF^- \rightarrow TiF_x + xe^-$ [1.3]

(d) Oxygen evolution reaction: $2H_2O \rightarrow O_2 + 4H^+ + 4e^-$ [1.4]

The oxidation state of titanium in oxides and fluorides may be +2, +3, or +4. It should be emphasized that the products of the processes (a) to (c) may undergo subsequent reactions such as: oxide dissolution, oxide conversion to a different oxide state, or oxide hydration (61).

Also the fluorides may undergo similar reactions or dissolution forming complex compounds. Both the surface oxide and fluoride may be influenced by the strong electric field, which accelerates the ion (O^{2-}, OH^-, or F^-) migration and incorporation within it.

CHAPTER 2

EXPERIMENTAL PART

2.1 Electrode preparation

According to the specific objectives of this work, titanium electrodes of different shape and geometric surface area were prepared and pretreated as described below.

2.1.1 Titanium electrodes

Two different types of Ti electrodes were prepared: (a) circular electrodes, and (b) wire electrodes. Circular titanium electrodes of 10 mm in diameter and 0.89 mm in thickness, were prepared from Ti foil (Johnson-Matthey, 99.6 wt. % containing 0.12% Fe, 0.08% Si, 0.05% C, 0.10% O and 0.04% N). The geometric surface area of this type of electrode was 2.198 cm^2. They were spot-welded to a Ti wire of 0.81 mm diameter (Aldrich, 99.7 wt.%) for electrical contact (Fig. 9a). This type of titanium electrodes was used in order to examine the impact of variation of experimental conditions (pH, V_{AC}, i_{AC}, T, t) and to establish optimal conditions for obtaining a wide and well defined set of colored titanium passive layers. Circular Ti electrodes were also very practical for surface morphology examination (Optical Microscopy, SEM, and AFM) and chemical composition analysis (XPS Depth Profiling). To study the influence of the surface area ratio between the working and counter electrodes, Ti electrodes of 5, 15, 20, and 25 mm in diameter were prepared.

The second type of Ti electrode (wire-shaped) was used in electrochemical characterization of the colored Ti passive layers. These electrodes were made from a titanium wire of 0.81 mm diameter (Aldrich, 99.7 wt.%). One side of the wire was mounted to one end of a special electrical connector. The other side of this connector was connected to copper wire (Fig. 9b).

Upon the verification of electrical contact, the area between the Ti wire and the connector was sealed with Struers epoxy resin. After hardening of the epoxy resin, the wire was cut to 10 mm of length. Finally, the electrode tip was polished mechanically using Struers mechanical polisher (model LaboPol-5) with 2400 grade silicon polishing paper. The electrode's diameter was determined with a Vernier Microscope with the precision of 0.001mm (Precision Tool & Instrument Co. Ltd, Thorthon Heath Surrey, England).

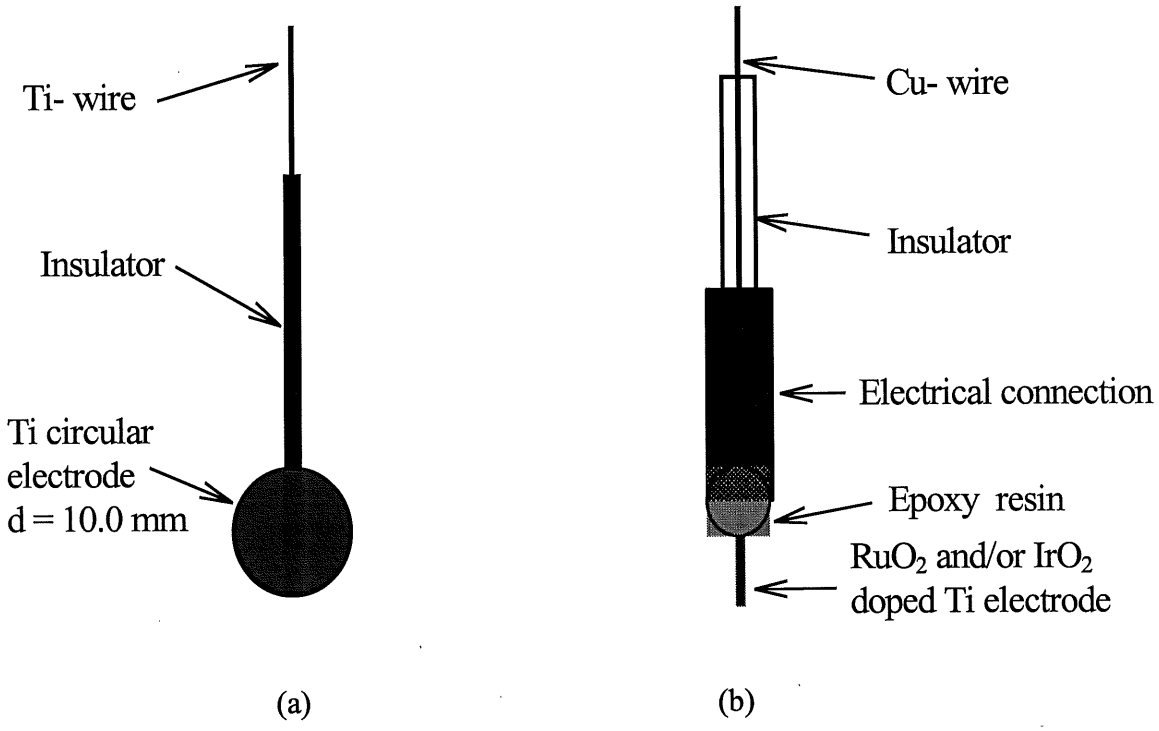

Figure 9. Circular titanium electrode used to establish optimal conditions for surface coloration (a), and wire-shaped titanium electrode utilized for electrochemical characterization of the colored Ti passive layers (b).

Both types of electrode were pretreated similarly. The electrodes were degreased in acetone under reflux in order to remove any organic impurities. Subsequently, they were etched for 1-2 min. in solution made from 30 cm^3 of concentrated HF and 50 cm^3 of concentrated HNO_3 diluted to 1000 cm^3 with H_2O; afterward, they were rinsed with Nanopure water, 18 MΩ (62). To avoid any traces of the aggressive etching solution, which, with time, can damage and dissolve the colored passive layer, the Ti electrodes were sonicated in an ultrasonic bath (Branson) for 1 min, and than rinsed again carefully with Nanopure water.

2.1.2 RuO_2 or/and IrO_2 doped titanium passive-layer electrodes

Titanium wire (Aldrich Chemical Co. 99.7%) of 0.81mm diameter and 25 mm length was mechanically polished, chemically degreased and etched as described in Section 2.1.1. Such a pretreated electrode was ready for AC polarization. It was polarized by application of a given AC voltage in aq. $NH_4 BF_4$ 7.5 wt. %. In this case, the time of AC polarization was 10 sec., and the applied AC voltage was 20, 40, and 60 V, respectively (60).

After the preparation of the colored Ti passive layers, thermal decomposition technique was applied to deposit RuO_2, IrO_2, and RuO_2+IrO_2 layers. The AC-colored electrode was immersed in 20% HCl aqueous solution of 0.1M $RuCl_3$ x H_2O (Aldrich), 20% HCl aqueous solution of 0.1M $IrCl_3$ x $3H_2O$ (Aldrich), or 1:1 (by volume) mixture of these solutions. After immersion, the electrode was dried at 80°C for 15 min. After each drying procedure, the layer was treated in a furnace (air environment) at 450°C for 15 min (Fig. 10a). Three subsequent immersions and heating procedures were applied to increase the thickness of the deposit and the Ru, Ir, or Ru+Ir loading. After the deposition of the third layer, the material was annealed at 450°C for 1 hour (Fig. 10b).

After the thermal treatment, the electrodes (25mm in length) were connected to a copper wire using an electrical connector to get a good electrical contact, degreased and sealed with Struers Epofix resin (See Fig. 9b).

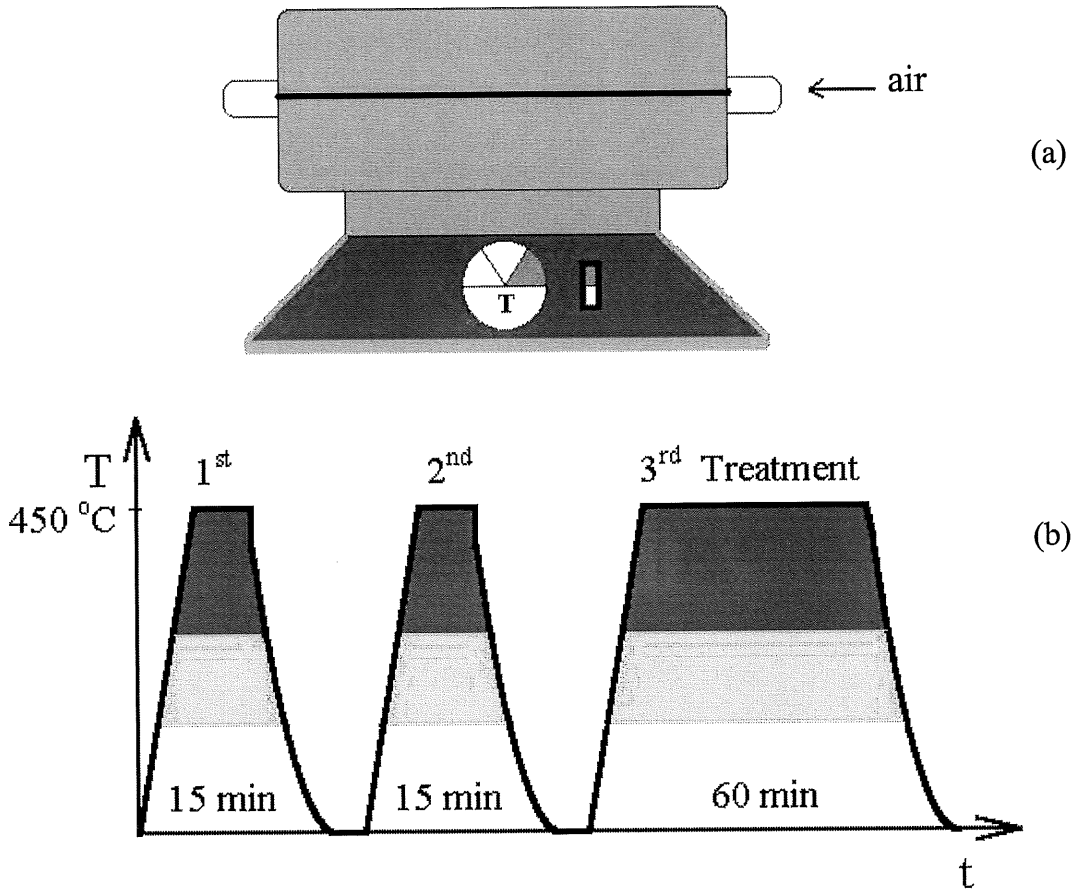

Figure 10. Schematic representation of the thermal treatment procedure applied to prepare RuO_2, IrO_2, and $RuO_2 + IrO_2$ doped colored Ti passive-layer electrodes : (a) furnace used for thermal decomposition, (b) three-step program applied during the thermal treatment procedure.

2.2 Electrolyte and cell for AC polarization

The solution was prepared by dilution of analytical grade NH_4BF_4 (97 wt. % Aldrich) or by neutralizing HBF_4 (48 wt. % Aldrich) with NH_4OH (29 wt. % Aldrich) in stoichiometric proportions. In this solution, the electrolyte anion is principally BF_4^-. A one-compartment

all-glass cell with two electrodes was used. The counter electrode was made of Pt foil. The geometric surface area ratio between the Pt counter electrode and the Ti working electrode was at least 2. The standard electrode distance was 5cm (this separation was sufficient for effective circulation of the electrolyte between the electrodes to expel the gases generated during the AC polarization), the time of polarization was 10 sec., and the usual electrolyte concentration was 7.5 wt. %. A stream of nitrogen gas (99.9 wt. % in purity) was passed through the electrolyte in order to expel the gases generated while passivating Ti; the N_2 gas also increased the cooling rate of electrolyte (Fig. 11). The electrolyte was stirred mechanically in order to sustain uniform temperature distribution.

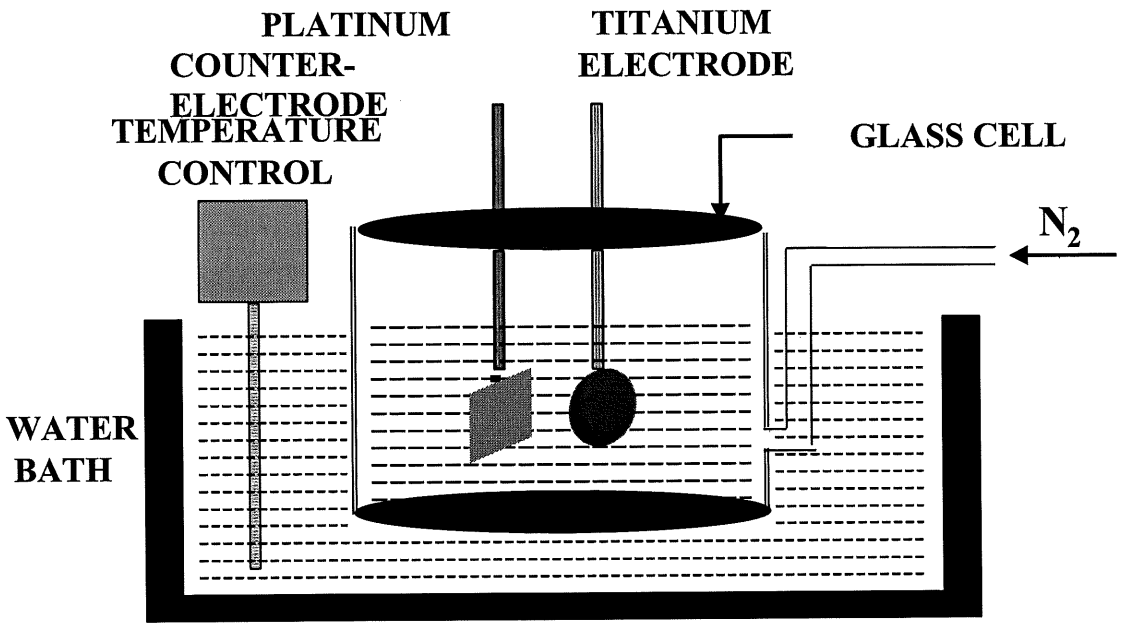

Figure 11. Schematic representation of the cell used for preparation of colored passive layers on titanium.

In order to analyze the influence of the separation between two electrodes (see Results) and to examine the influence of the surface area ratio on the film coloration, the cell shown in the

Fig. 12 was used. This cell allowed one to vary the electrode distance from 1 to 25 cm and it allowed one to place two counter electrodes. Because of the large active volume of this cell (1.8 dm^3), it was possible to use a very different electrode surface area and to examine the uniformity of the coloration in specific conditions.

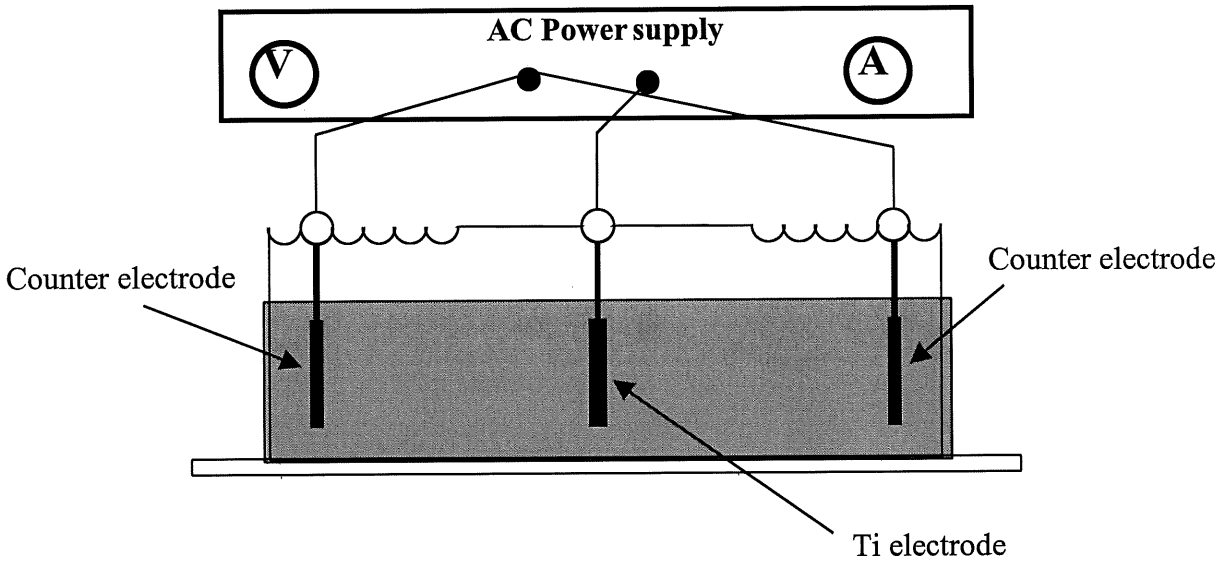

Figure 12. Schematic representation of the cell used to study the influence of the distance between the Ti electrode and the Pt counter electrode on the surface coloration.

2.3 Electrolyte and cell for electrochemical characterization

The polarization curves and Tafel plots for Ti, colored Ti passive layers, RuO_2 and/or IrO_2 doped titanium passive layers, and Ebonex® on Ti, were recorded in a 1.0 M aqueous H_2SO_4 solution (Aldrich, 98.0 wt. %, heavy metals as Pb < 1 p.p.m., Fe < 0.2 p.p.m., Hg < 0.005 p.p.m.) in a standard three-compartment electrochemical cell (63) shown in Fig. 13 (64). A stream of N_2 gas (99.99 wt. %) was passed through electrolyte to expel any gases generated

during the electrochemical characterization. A Pt/Pt black reversible hydrogen electrode (RHE) was used as the reference electrode in the electrochemical characterization (polarization curves and Tafel plots). We selected the 1.0 M aqueous H_2SO_4 as electrolyte for electrochemical characterization of the colored Ti passive layers in order to relate their electrochemical characteristics to the polarization curves of Ebonex® as well as IrO_2- surface modified Ebonex®, whose electrochemical characteristics were acquired in this particular electrolyte (65).

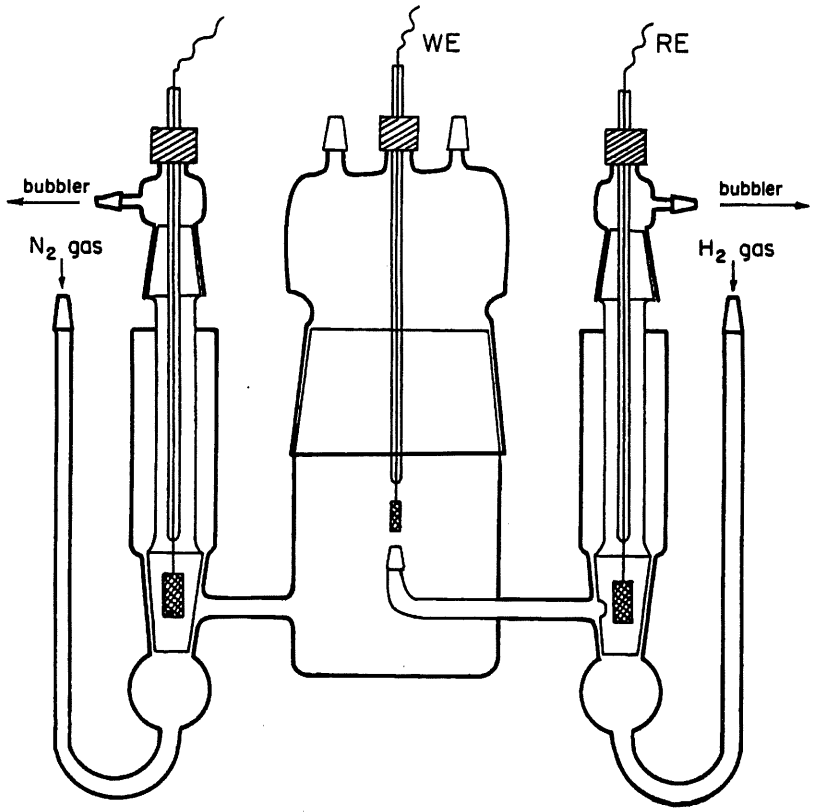

Figure 13. Schematic representation of the three-compartment cell used for electrochemical characterization of the colored titanium passive layers, RuO_2 or/and IrO_2 doped Ti passive layers, and Ebonex®.

2.4 Instrumentation for colored Ti layer preparation

The Ti coloration was accomplished using a variable AC power supply, 60 Hz (Vector-Vid, Instrument Division, model WP32) and the AC voltage was monitored by means of a multimeter (Fluke 45). The current passing during the polarization was controlled with a digital ammeter (Phillips). The voltage applied was in the 5 – 90 V range and the current density measured with respect to the geometric surface area, was from 230 mA cm^{-2} to 2800 mA cm^{-2}. The coloration of titanium by DC polarization was accomplished using a DC power supply (6034A system power supply, Hewlett Packard) in electrical circuit with the same multimeters used in the case of the AC polarization of Ti.

It should be emphasized that it was essential to sustain a constant temperature in order to achieve passive films of uniform thickness and coloration. Because the Ti passivation was carried out at high current densities, heat was generated during the process and it was necessary to cool the cell by its immersion in a thermostated water bath (Haake B3).

2.5 Instrumentation for electrochemical characterization

Electrochemical characterization was carried out using EG&G model 273 potentiostat. EG&G M270 and M353 electrochemical and corrosion software packages were used to control the experimental parameters and to acquire the data. Polarization curves of the wire-shaped Ti electrodes in 1.0 M aqueous H_2SO_4 solution were obtained in the – 0.8 - 3.2 V, RHE, potential range. Tafel polarization measurements were conducted in the 0.0 - (– 0.8) V, RHE, potential range in order to assess the activity of the colored Ti towards the HER. In these measurements, the counter electrode was made of a platinum gauze and its surface area was over 10 times that of the Ti electrodes. All current densities are reported with respect to the geometric surface area of the passivated Ti electrodes.

2.6 Instrumentation and techniques for morphology and surface composition analysis

The examination of the morphology of Ti and colored Ti passive layers, RuO_2 and/or IrO_2 doped layers, and also Ebonex® on Ti, was carried out by means of Optical Microscopy, Scanning Electron Microscopy, and Atomic Force Microscopy. Surface-chemical composition of the electrodes was examined by X-Ray Photoelectron Spectroscopy coupled with Ar^+-ion depth profiling.

2.6.1 Optical Microscopy

An optical microscopy analysis was carried out using a SEIWA Optical, Correct Metallurgical Microscope, model SDM-TR in order to analyze the uniformity of the surface coloration and the morphology of the colored Ti passive layers. The electrodes were analyzed at different magnifications from 50 × to 600 ×.

Three-dimensional optical microscopy analysis was performed using an optical microscope, model New View 5000 Zygo (Zygo Corporation, USA). This analysis was carried out to generate quantitative three-dimensional images. The principle of the technique is based on scanning white-light interferometry, a traditional technique in which a pattern of dark and bright lines (fringes) result from an optical path difference between a reference and a sample beam. The incoming light is split inside an interferometer, one beam going to an internal reference surface, and the other one to our sample. After reflection, the beams recombine inside the interferometer, undergoing constructive and destructive interference and producing light and dark patterns. This type of analysis gives information not only about the topography of the samples, but also about their roughness showing high quality 3D images. The results of the analysis are presented as a filled contour plot (two-dimensional plot, which shows the surface heights as viewed along the instrument's z-axis top view). Different height is represented by different colors. The red shows high points and the violet, low points. The horizontal lines found in the filled contour plot represent the cross-section found in the profile

plot. Solid plot displays surface area data as a function of the slope as viewed along the instrument's z-axis. Areas with different slopes are represented by different shades. The profile plot shows two-dimensional slices through the filled plot. The x-axis shows lateral dimensions. The y-axis provides the height information. Ti and Ti colored passive films samples were analyzed at different magnifications (100 × and 1000 ×), working distance 3.4 mm, lateral resolution 0.64 μm and field of view 0.14 x 0.11mm.

2.6.2 Scanning Electron Microscopy (SEM)

As a tool for examining surfaces, the scanning electron microscope (SEM) offers two major advantages over the optical microscope: (a) an improvement in resolution, and (b) a depth of field. This technique provides images at magnifications up to 100 000 × and a resolution of features down to 3 nm, depending on the sample. SEM is a very useful technique in observation of grain boundaries on etched and unetched samples, in an analysis of the morphology of ferromagnetic materials, and in evaluation of the crystallographic orientation of grains with diameter down to 2 to 10 μm. A scanning electron microscope JEOL, model JSM 840-A in topography mode, was used in surface analysis of the colored Ti passive layers, RuO_2 and/or IrO_2 doped layers, and also for the examination of the morphology of Ebonex® on Ti. The magnification in the SEM analysis was 1000, 3000, and 10 000 ×. The JEOL scanning electron microscope allowed one to perform a bulk chemical analysis via the Electron Diffraction Analysis (EDX). This analysis was used in order to verify the extent of doping the colored Ti passive layer with RuO_2 or/and IrO_2.

2.6.3 Atomic Force Microscopy (AFM)

AFM allows us to perform surface morphology analysis at magnifications not attainable by SEM. This method is particularly useful for analyzing thin and thick film coatings, ceramics, composites, glasses, synthetic and biological membranes, metals, polymers, and

semiconductors. The AFM can be applied to study phenomena such as abrasion, adhesion, cleaning, corrosion, etching, friction, lubrication, plating, and polishing.

Titanium passive layers formed by AC polarization were analyzed by using Digital Instruments, NanoScope III Atomic Force Microscope. The most common mode, so called, the contact mode, where the tip scans the sample in close contact with the surface, was applied for the analysis of colored titanium passive layers. In AFM, an atomically sharp tip is scanned over a surface with feedback mechanisms that enable the piezo-electric scanners to maintain the tip at a constant force (to obtain height information), or height (to obtain force information) above the sample surface. Tips are typically made from Si_3N_4 or Si. As the tip scans the surface of the sample, moving up and down with the contour of the surface, the laser beam is deflected into a dual element photodiode. The photodetector measures the difference in light intensities between the upper and lower photodetectors, and then converts to voltage. Feedback from the photodiode difference signal, through software control from the computer, enables the tip to maintain either a constant force or a constant height above the sample. In the constant force mode, the piezo-electric transducer monitors real time height deviation. In the constant height mode, the deflection force on the sample is recorded. The latter mode of operation requires calibration parameters of the scanning tip to be inserted in the sensitivity of the AFM head during force calibration of the microscope (66).

2.6.4 X-ray Photoelectron Spectroscopy (XPS/ESCA)

The chemical composition of titanium oxide layers formed under electrochemical or gas-phase conditions can be evaluated by means of Auger electron spectroscopy (AES) and X-ray photoelectron spectroscopy (XPS). XPS or ESCA (Electron Spectroscopy for Chemical Analysis) is a technique which gives the elemental analysis of a surface, identification of chemical state of surface species, in-depth composition profiles in thin films, or determination of oxidation states of metal atoms in metal oxide surface films (15).

Fig. 14 shows a block diagram of the basis of XPS/ESCA technique (67). Thus, an XPS spectrometer consists of an x-ray source, an electron energy analyzer, an electron detector, and instrumentation for data acquisition. One of the most important capabilities of XPS is its ability to mesure shifts in the binding energy of core electrons resulting from a change in the chemical environment. Such changes in binding energy, termed the chemical shift, can result from a change in the nearest neighbor, the oxidation state, the compound formation, or the crystal structure.

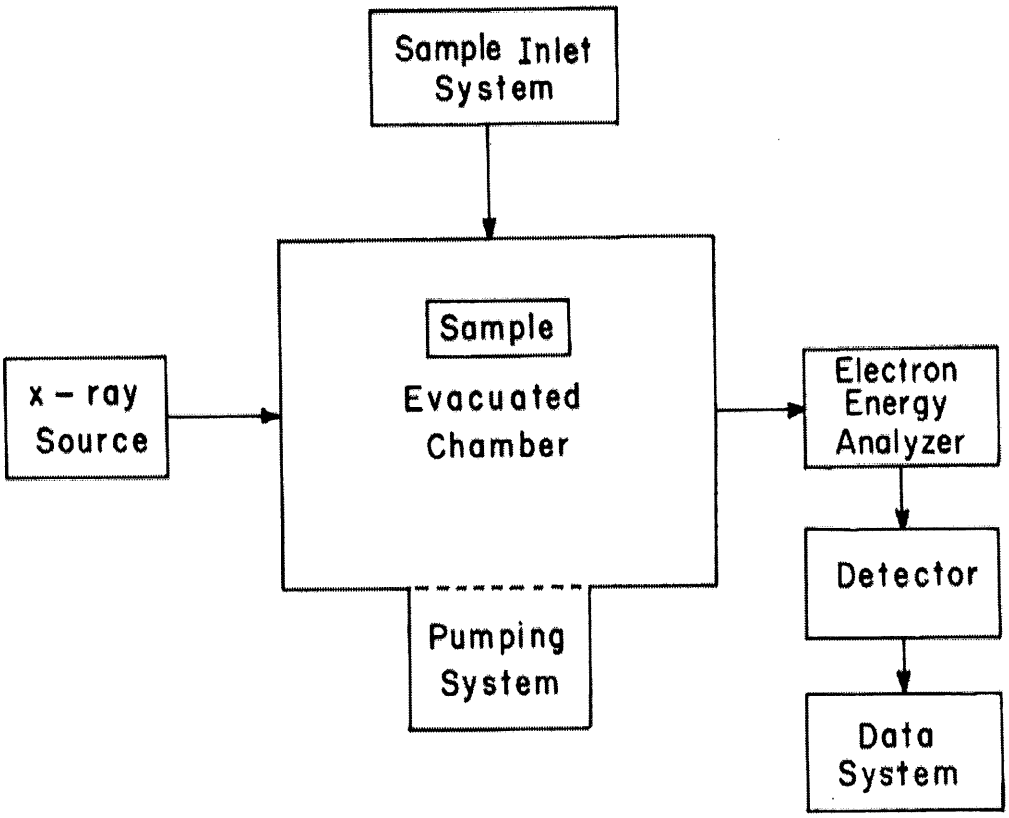

Figure 14. Block diagram of XPS/ESCA system for surface analysis (67).

The XPS depth profile analysis was of particular importance for this project, because this aspect of ESCA gives the information about the thickness (d/nm) of the colored passive layers in relation to the applied AC voltage. A way of obtaining a depth-composition profile is to bombard the sample with a beam of inert gas ions, usually argon or xenon. Sputtering rates can be varied from a few angstroms per minute to several hundred angstroms per minute by changing the ion current and the accelerating potential. The surface-chemical composition and depth profile analysis (68) were conducted on colored Ti samples transferred via air using a fully automated PHI Quantum 2000 Scanning ECSA Microprobe. The X-ray beam was of 200 μm in diameter. Photoelectrons were generated by Al ($K_{\alpha 1,2}$) X-ray radiation (energy of 1486.6 eV) at 50 W of power and the calibration was based on the C (1s) spectrum at the 284.8 eV binding energy (69-71). First, a survey spectrum of each Ti sample was acquired followed by a high-resolution spectra acquisition. Each sample was sputter depth profiled using 3 keV Ar ion beam and Zalar Rotation™. The unique Zalar Rotation™ system allowed us to minimize sputter-induced surface roughening and to enhance interface resolution. Survey and high-resolution spectra were acquired at each stage of depth profiling. XPS spectra were treated using the PHI MultiPak™ linear least squares (LLS) fitting routines. The Ti XPS spectrum did not represent a single spectrum and was deconvoluted into two components, one characteristic of Ti^{z+} and one of Ti^0 (metallic Ti). The positions of the following XPS lines were considered in the depth profile evaluation: Ti ($2p_{3/2}$), Ti ($2p_{1/2}$), O (1s), F (1s), and C (1s). The binding energy and the chemical shift of each XPS line were compared to the standards and the data were sensitivity-factor corrected. Based on the sensitivity-factor corrected XPS data, we evaluated the O to Ti atomic ratio, N_O/N_{Ti}, in relation to the AC voltage applied to form the colored passive layers (the amount of Ti bound to O was corrected for a small amount of Ti bound to F). Finally, the thickness of each passive layer was determined by measuring the depth at which the intensity of the O (1s) signal dropped to 50% of its maximal value.

CHAPTER 3

PREPARATION OF COLORED PASSIVE SURFACE LAYERS ON TITANIUM

The main objective of this project was to examine the impact of the variation of experimental conditions (pH, V_{AC}, time of polarization, current density, concentration of electrolyte, distance between the electrodes, electrode surface ratio) on the coloration of titanium passive layers and to establish optimal conditions for obtaining uniform and bright colors. Another important objective was to compare the results obtained by application of AC polarization and DC anodization of titanium.

3.1 Relation between current density and polarization time during film formation

A relation between the AC polarization time and the current density is shown in Fig. 15. The current was measured and recorded every 10 seconds (peak-to-peak) at two selected voltages, 10 and 20 V_{AC}. In both cases, the current density decays over the initial 50 seconds and, then, levels off. The coloration of the electrode remained unchanged. At 20 V_{AC}, small modifications of the coloration were observed after 200 seconds. The initial decay of current density is due to the resistivity of the passive film (53).

3.2 Relation between current density and distance between the working and the counter electrodes for different applied AC potentials

This experiment was done in order to examine how the distance between two electrodes (titanium and platinum) influences the current passing through the cell. The current was measured after 10 sec of polarization at the different potentials in the 20 - 60 V_{AC} range. The distance was changed from 1 to 20 cm for each measurement.

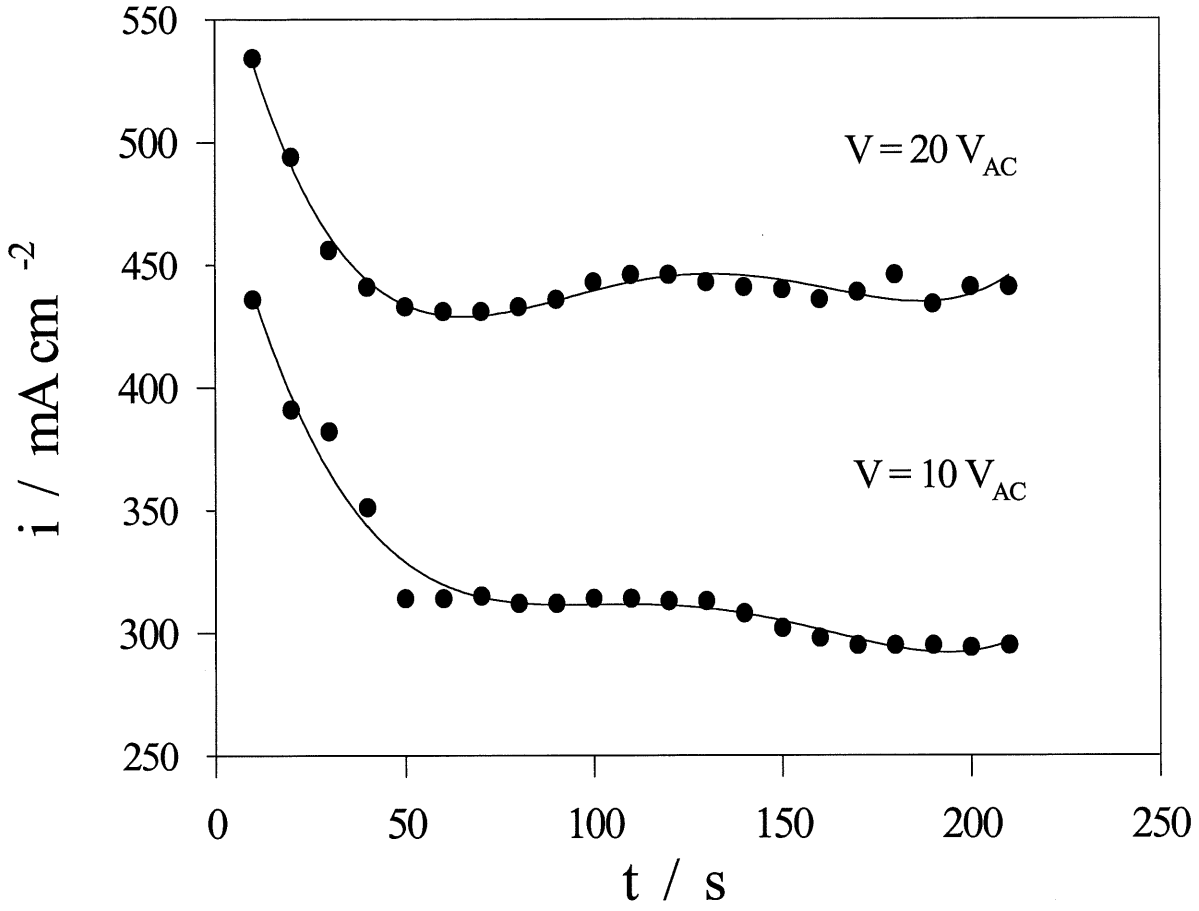

Figure 15. Current density vs. polarization time for applied 10 and 20 V_{AC} in aq. 7.5 wt. %NH_4BF_4, t = 10 s, T = 298 K (Error bars are omitted to facilitate the graph analysis).

After each polarization, the colored films were etched again, rinsed with distilled water, and the electrode was polarized again, this time at a new distance from the Pt electrode. As can be seen in Fig. 16, the highest current drop associated with the separation change is observed for the applied AC potential of $60V_{AC}$, and the lowest for $20V_{AC}$. Only minor changes in coloration of the electrodes were observed as the distance was changed from 1 to 20 cm.

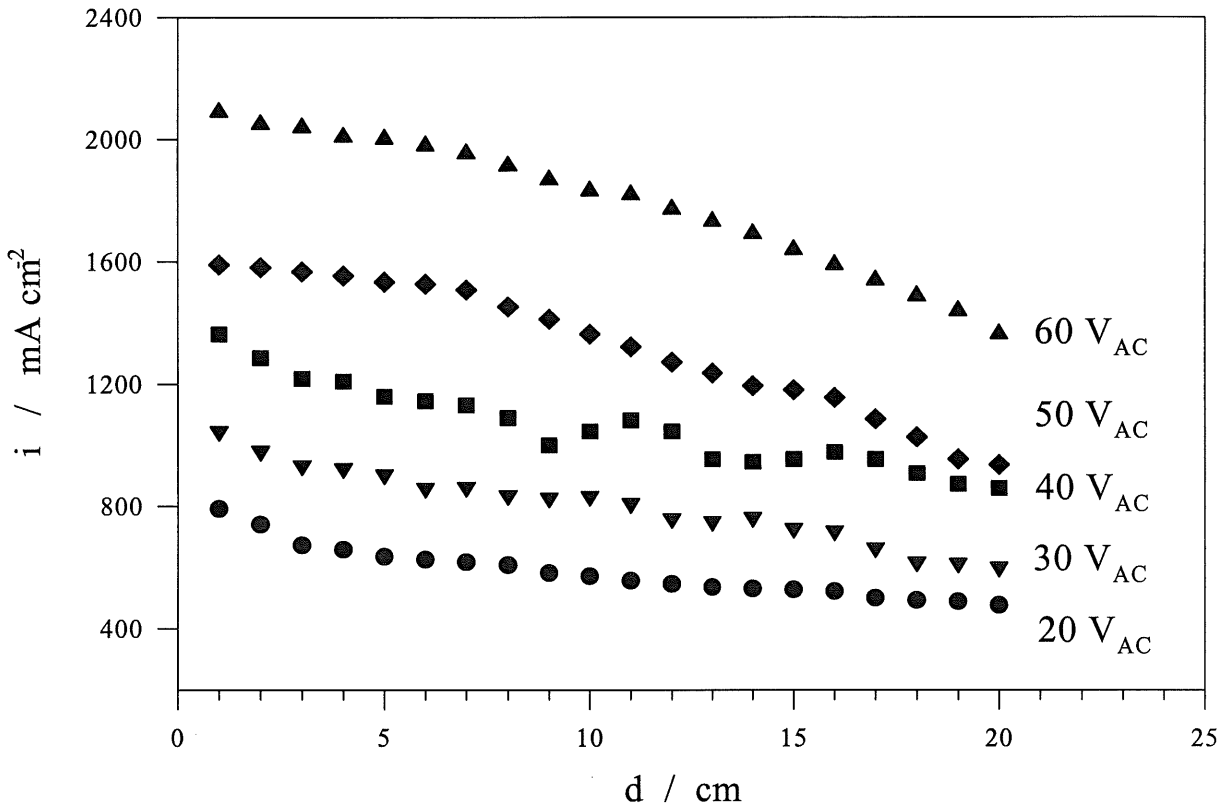

Figure 16. Current density vs. distance between the working and the counter electrodes for different applied AC potentials from 20 to 60 V_{AC} in aq. 7.5 wt. %NH_4BF_4 for t = 10 s, T = 298 K.
(Error bars are omitted to facilitate the graph analysis).

3.3 Comparison of Ti surface coloration accomplished by AC and DC polarization

These experiments were carried out in order to compare the impact of two different types of polarization (AC vs. DC) while maintaining other parameters constant. Because of the different properties of the AC and DC polarization (19), we have noticed that to achieve the same coloration (the coloration was determined by eye), it was necessary to apply a 20% higher DC voltage than the AC voltage (Fig. 17). This could be explained by the different nature of AC and DC current. In the case of DC current, the current passes only in one

direction, whereas in the case of AC current the current direction changes with certain frequency (60 Hz).

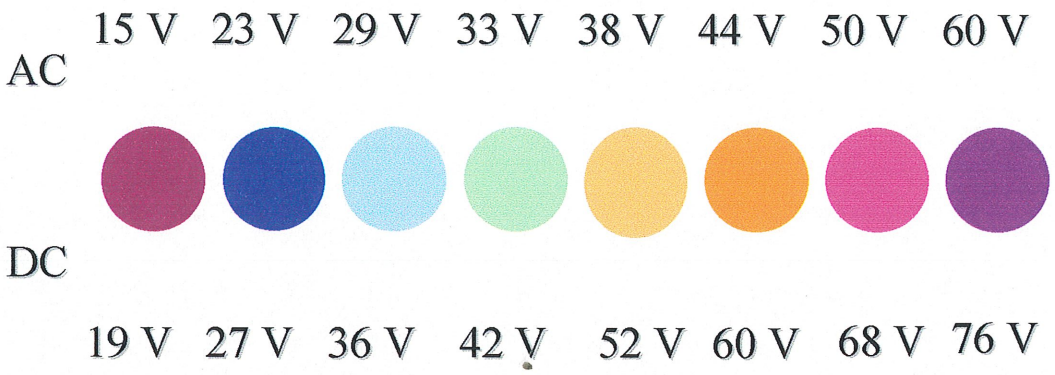

Figure 17. AC and DC voltages required to reach the same surface coloration of Ti in aq. 7.5 wt. %NH_4BF_4, t = 10 s, T = 298 K.

In the case of DC polarization, the current drops to zero after a certain period of time which is not the case for the AC polarization. Fig. 18 shows the time necessary for the DC current to drop to zero for different applied DC voltages. At the beginning of the anodization, the reaction rate is expressed as $i = i_{pass} + i_{gas\ evol.}$ and the reaction is very vigorous with gas evolution at both electrodes. Few seconds later, the reaction becomes tranquil and the coloration variation of passive layers ends. The duration of the DC polarization depends on the applied DC voltage, and generally, the higher the applied voltage, the longer the anodization time. The higher is applied voltage, the losses of current are bigger and the most of current is consumed on gas evolution. The DC current at one point can not traverse the big resistance barrier due to the growth of titanium passive film (53). As shown in Fig. 18, after a short period of time (3-7.5 sec) the current drops, and the anodization is finished. As the DC current ceases, the anodization finishes and the reactive BF_4^- anion attacks and easily dissolves the colored passive layer, even in a pH neutral environment if the electrode is kept in the

electrolyte (53). In order to maintain the DC formed color layer, one needs to quickly withdraw the electrode from electrolyte and to rinse it very well with water.

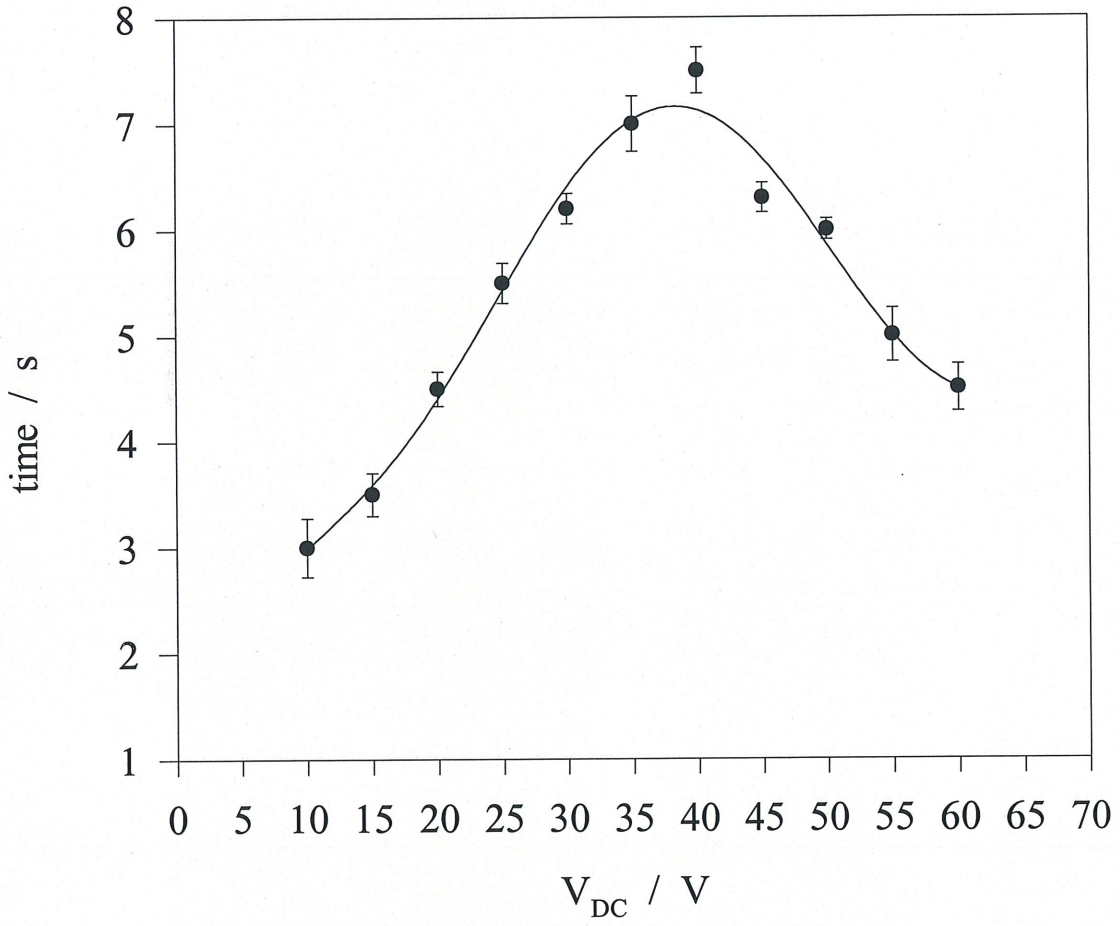

Figure 18. Time required for DC current density to decay to a zero value during DC polarization of titanium from 10 – 60 V_{DC} in aq. 7.5 wt. %NH_4BF_4, t = 10 s, T = 298 K.

3.4 Impact of AC voltage, polarization time, concentration, and pH on the coloration of titanium

The application of an AC voltage initiates the formation of colored Ti passive layers with a wide spectrum of very bright and well-defined colors. In general, the coloration depends on

numerous parameters such as: (i) the applied AC voltage; (ii) the polarization time; (iii) the electrolyte concentration; and (iv) the pH of the electrolyte (if the electrolyte is a non-stoichiometric mixture of NH_4OH and HBF_4). The results presented in Fig. 19 show the spectrum of colors that can be obtained. In the case of the AC voltage (V_{AC}) increase, whilst maintaining other parameters constant, the coloration varies from brownish purple to green.

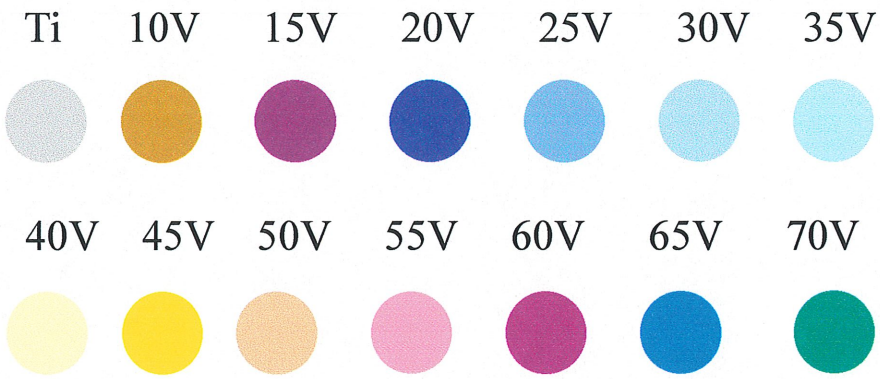

Figure 19. Colored passive layers of Ti obtained by applying different AC voltages (10-70 V_{AC}) in aq. 7.5 wt. %NH_4BF_4, t = 10 s, T = 298K.

When increasing the polarization time, t_{polar}, again whilst maintaining other parameters constant, the coloration of the passive layer gradually changes due to its ever-increasing thickness (Fig. 20). However, it is worthwhile noticing that while the coloration change is very pronounced within the initial 1 s of t_{polar}, a further extension of t_{polar} contributes only to a slight modification the shade of the colored layer rather than to the coloration itself.

In a separate series of experiments, the impact of the electrolyte concentration on the Ti coloration of titanium was examined. The results may be summarized as follows (Fig. 21):

(a) the data indicate that one can increase the AC voltage towards high values (V_{AC} > 60 V) by decreasing the NH_4BF_4 concentration; and (b) this experimental approach permits preparation

of green and turquoise colored layers, thus two colors that are impossible to achieve at high concentrations of NH_4BF_4 (Fig. 21).

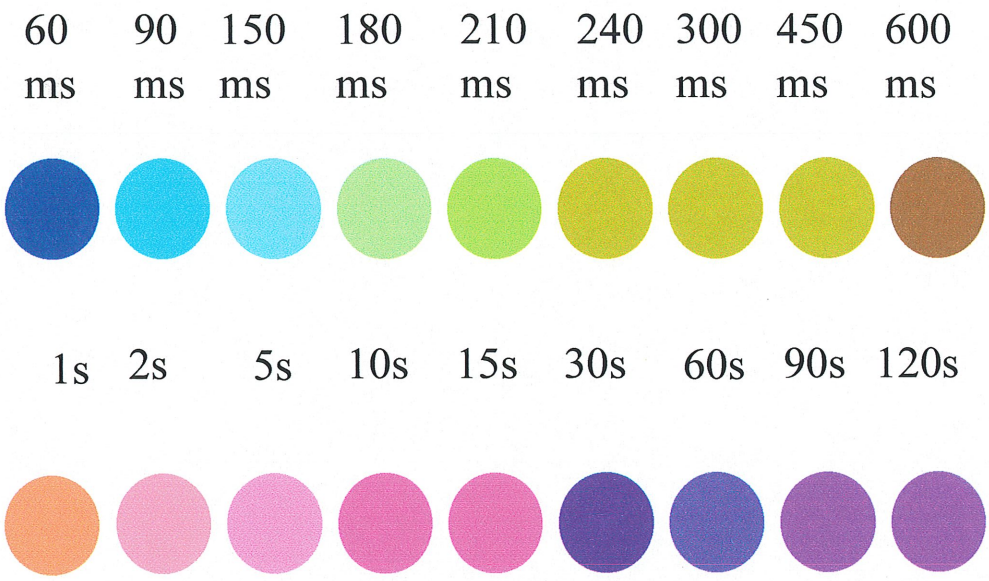

Figure 20. Coloration changes with the time of AC polarization in aq. 7.5 wt. % NH_4BF_4, t = 60 ms – 120 s, T = 298 K.

However, when increasing the AC voltage beyond 60 V_{AC}, the amount of heat generated at the interface is so great that it is difficult, yet feasible, to accomplish uniform green or turquoise coloration. The passive film has some grains that have already undergone electric breakdown, especially in the case of layers formed at very high voltages. Consequently, the coloration of Ti is not always uniform and strongly depends on the applied potential and the concentration of the electrolyte. Small dots or large spots in Fig. 21 are presented in the case of the $V_{AC} \geq 60$

V and the concentrations 2.5 -7.5%. For higher concentrations of the electrolyte ($\geq$ 10%) and $V_{AC} \geq 60$ V, the coloration disappears after 2-3 seconds. In the case of further increase of the AC voltage, say $V_{AC} \geq 85$ V, there exists almost instantaneous electric breakdown of the passive film with sparking at the Ti surface in electrolyte.

Finally, we examined the influence of the pH of the electrolyte prepared by mixing NH_4OH and HBF_4 in different proportions so that pH could vary from 2 to 11. The results (Fig. 22) reveal that modification of pH is one of the suitable means for adjusting the coloration of the Ti passive layers. In particular, the green and turquoise layers that require high AC voltages (V_{AC} > 60 V) in a low concentration of NH_4BF_4 can be easily prepared already at 60 V if the pH of the solution is in the 8 - 10 range. Thus, by modifying the electrolyte composition and pH, we avoid the difficulties of working at the limiting experimental conditions (in NH_4BF_4 only) and we were still able to prepare uniformly colored deep green and turquoise layers.

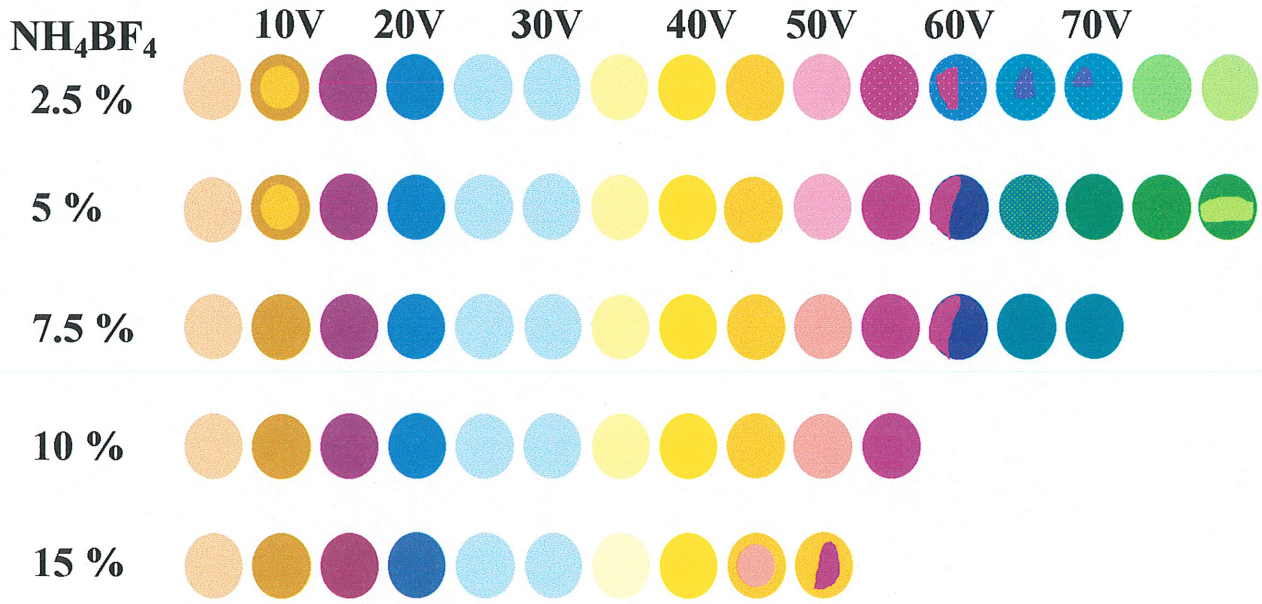

Figure 21. Impact of electrolyte concentration and applied voltage on titanium coloration in aq. 7.5 wt. %NH_4BF_4, t = 10 s, T = 298 K.

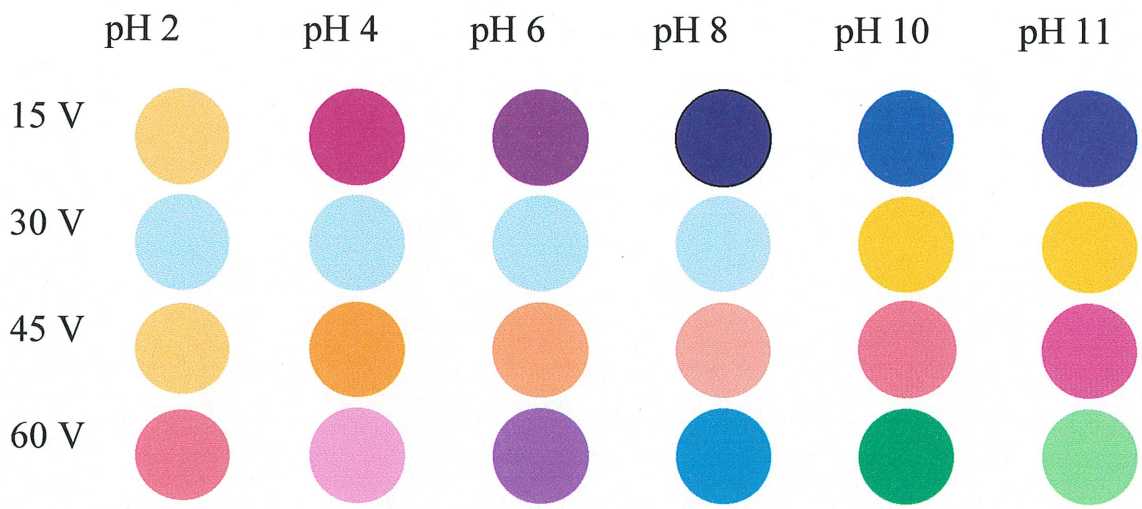

Figure 22. Influence of the pH of the electrolyte on the coloration of titanium in aq. 7.5 wt. % NH_4BF_4, t = 10 s, T = 298 K.

3.5 Color switching during AC polarization of titanium

An interesting phenomenon was observed during the AC polarization. The results are shown in Fig. 23. The experiment was carried out by applying a given AC potential for 5 sec and the coloration was examined. Then, after each 5 sec, the AC potential was increased step-wise for 5 V, and the color was examined. As the applied voltage increases, a whole spectrum of colors was observed. Interestingly, once the highest potential and the last color were reached, it was possible, by decreasing the AC voltage, to observe the previous colors in the spectra. The realization of this experiment required the maintenance of a sufficient distance between the electrodes (20.0 cm). The color switching effect can be explained as follows. At a given AC voltage, the color film formation proceeds, while at the same time the color layer undergoes dissolution: a steady-state condition is achieved. As one decrease V_{AC}, the dissolution rate increases until a new steady-state (thickness) is accomplished.

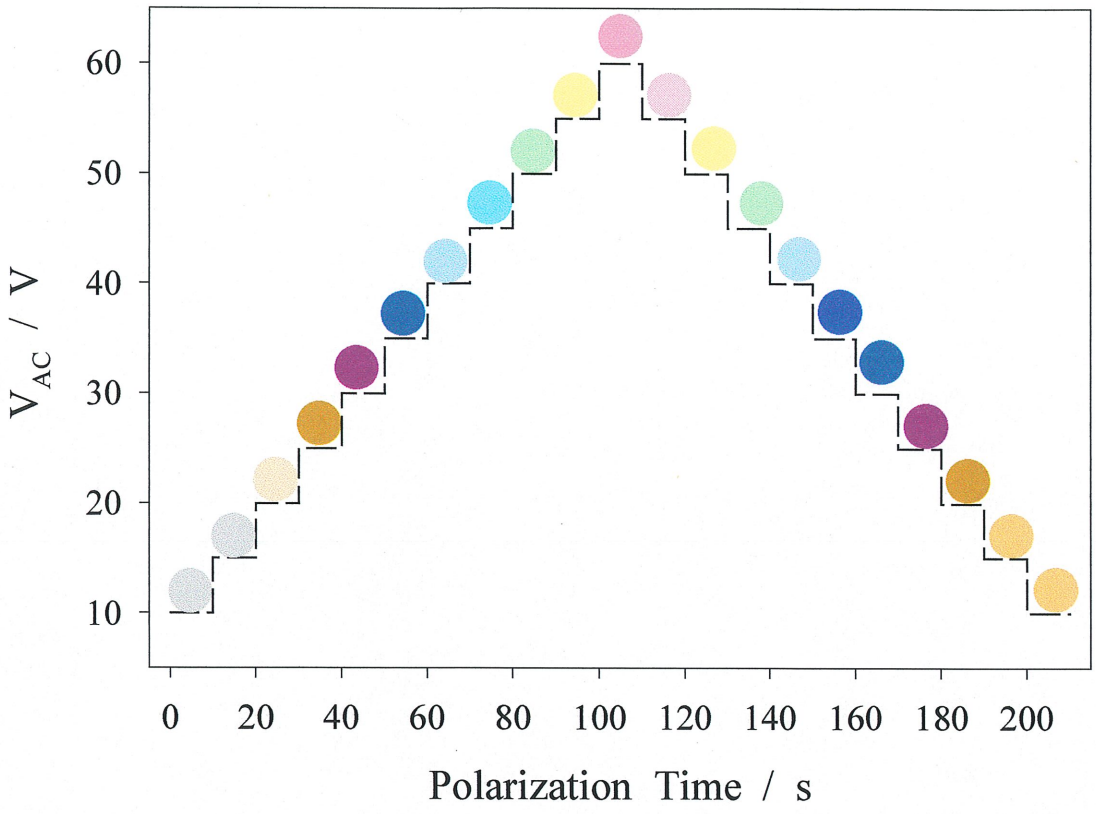

Figure 23. Color switching effect characteristic of only AC polarization. Possibility of changing the coloration in opposite directions by decreasing or increasing the applied V_{AC} in aq. 7.5 wt. % NH_4BF_4, T = 298 K, t = 5 s.

3.6 Colored passive layers on titanium alloys

The majority of titanium applications are attributed to Ti alloys, and that was the reason to verify if the same methodology could be used to color Ti alloys. A set of Ti-6Al-4V alloy electrodes was colored using AC polarization. The results of the chemical analysis of this alloy are as follows: C (0.01 wt.%), N (0.006 wt.%), O (0.13 wt.%), Fe (0.20 wt. %), Al (6.24 wt. %), V (4.02 wt. %), H (42 ppm), Y (50 ppm), and Ti (balance). The preparation procedure applied to prepare the Ti-alloy electrodes, was the same as the procedure for electrooxidation of pure titanium. Two sets of samples were prepared. In the first set, the samples were polished with a Struers polishing machine (paper grade 2400 and 4000) to a mirror-like finish.

After that, the samples were degreased in acetone under reflux, and finally polarized by applying different AC voltages in 7.5 wt. % aq.NH_4BF_4. This way of coloring the alloys provides very shiny samples with wide spectrum of colors. In the second set, the samples were etched prior to the AC polarization. Due to the presence of Al in the alloy, the etching solution used for Ti (30 cm^3 of concentrated HF and 50 cm^3 of concentrated HNO_3 diluted to 1000 cm^3 with H_2O) was found too agressive. After dilution of this solution with distilled water (1:1 ratio, per volume), the alloy surface was uniformly etched and ready for the coloration. Both methods (polishing and etching) give the same spectrum of well-defined and uniform colors, yet the surface coloration accomplished at a given V_{AC} differs from that accomplished for Ti under the same experimental conditions. The difference of surface coloration is due to the different surface morphologies (pure Ti and Ti alloy).

3.7 Development of electrochemical lithography on titanium

After mastering the experimental conditions for titanium coloration, it was possible to proceed further and to develop a special technique of pattern design on titanium (72,73) - electrochemical lithography on titanium. This technique could be useful in surface finishing and the decorative industry, and also in semiconductor and printed circuit boards industries. Electrochemical lithography is a combination of the AC polarization of Ti with the masking technique for microlithographic applications in the semiconductor and microelectronics industries.

The consecutive steps of the electrochemical lithography technique are described below and presented in Fig. 24.

1) Application of positive photoresist (Olin Microelectronics Materials, Norwalk, USA) either on pure titanium, or on pre-colored Ti surface. This photoresist layer is formed by immersion of the Ti sample followed by drying.

2) Placement of the previously prepared mask in order to expose the surface areas that will polymerize and, afterward, colored by application of AC polarization.

3) Application of UV light for 10 – 15 min to polymerize the photoresist (the areas which are not exposed do not polymerize).

4) Removal of the unpolymerized surface using remover solution (Olin Microelectronics Materials, Norwalk, USA). After this step, two different zones are visible: one is the Ti surface, which will be polarized during the AC polarization, and the other is masked and protected.

5) Chemical etching for 10 sec (the same solution as described previously for color film preparation), in order to prepare the surface of Ti for electrochemical passivation.

6) Electrochemical passivation of the unprotected titanium surface. Upon this process, after 5 sec, the exposed areas become colored. In order to achieve a desired color, the experimental conditions must be selected very carefully as described in the Section 3.4 by selecting the AC voltage, polarization time, electrolyte concentration, and pH. Upon application of $V_{AC} \geq 45$, there is a possibility of peeling off the photoresist, hence one needs to modify the pH of the electrolyte in order to decrease the AC voltage to obtain a given coloration.

7) Removal of the photoresist by immersion in acetone.

This methodology allowed us to prepare patterns which comprised three or more different colors. Moreover, many logos and numerous graphics and drawings were successfully created in our laboratory. The color uniformity and high linear resolution (a few μm) was confirmed by an optical microscopy analysis.

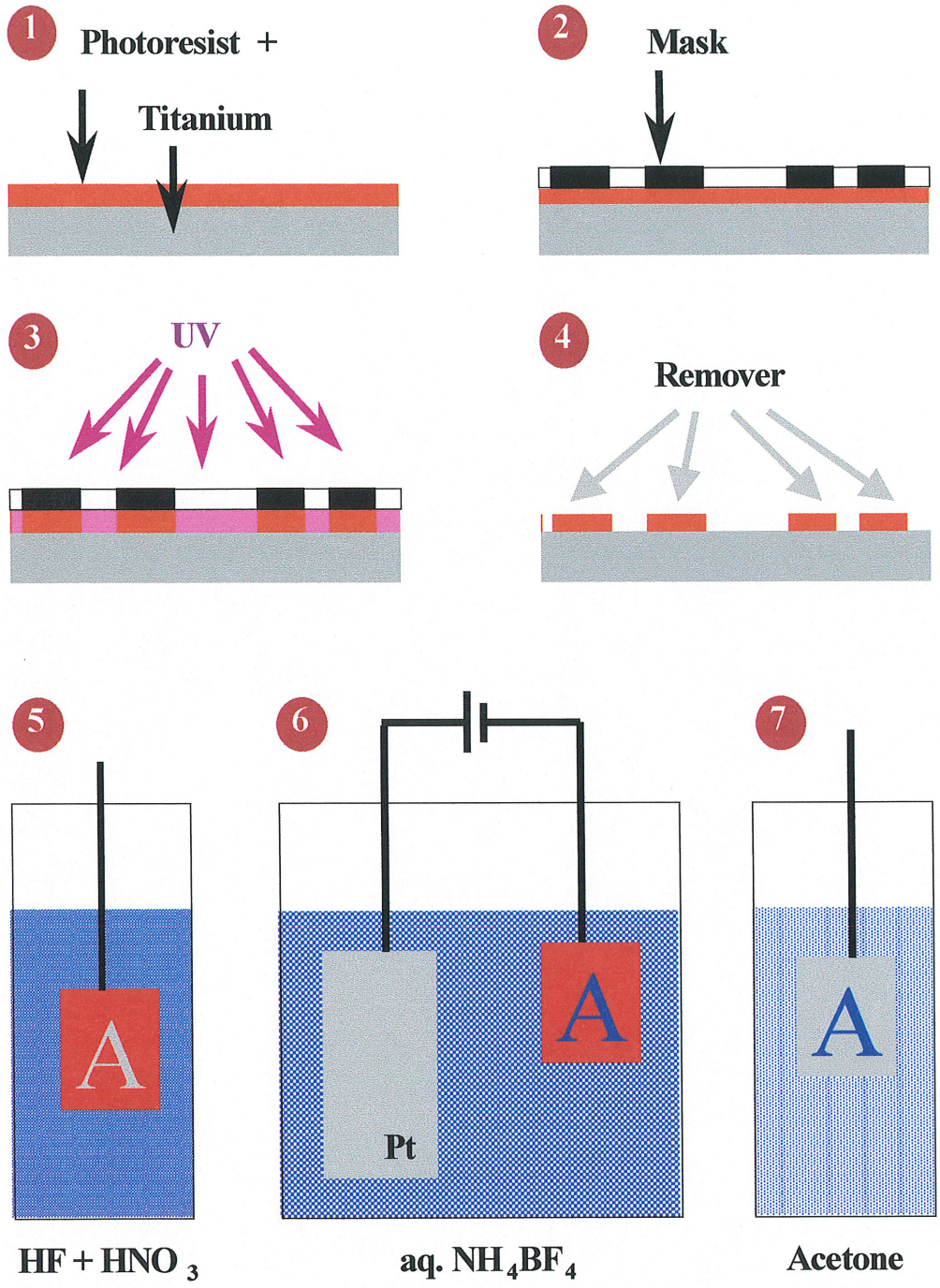

Figure 24. Schema of electrochemical lithography technique: (1) application of photoresist on Ti, (2) placement of mask to mark the surface for coloring, (3) application of UV light – polymerization, (4) removal of the polymerized surface, (5) chemical etching, (6) electrochemical oxidation of unprotected titanium surface, and (7) removal of photoresist by immersion in acetone.

CHAPTER 4

SURFACE CHEMICAL CHARACTERIZATION AND CHEMICAL COMPOSITION OF MULTICOLORED TITANIUM PASSIVE LAYERS

4.1 Optical microscopy analysis of Ti passive films

The Ti samples used in the course of research were of polycrystalline nature and after cleaning and etching, they revealed a well-defined grain structure (Fig. 25), with each grain behaving like a single crystal. Thus, it became necessary to evaluate whether: (a) the passive films revealed the same coloration on different grains; (b) the surface roughness underwent any changes upon the color film formation, and if so how it depended on the applied AC voltage; and (c) the colored passive films revealed cracks or fractures.

The relation between the grain structure and the coloration of particular grains, thus the uniformity of AC-polarization induced coloration, was evaluated by optical microscopy at various magnifications but the visualization at 200 × provided the best results. Fig. 25 represents the surface morphology pictures of Ti and colored passive films formed at five different voltages (10, 15, 30, 50 and 60 V_{AC}) that are representative of the overall tendency. The results may be summarized as follows:

(i) The surface coloration is predominantly uniform in the sense that each grain had the same color;

(ii) Certain grains show slightly different coloration than that expected for a particular AC voltage (see 30 and 60 V_{AC} in Fig. 25), yet they are the neighbor colors of the principal one according to the coloration versus voltage dependence shown in Fig. 19. For instance, the blue passive layer (Fig. 25, 30 V_{AC}) reveals some purple and pale-blue

grains, thus the "neighbor colors" of the principal one since a purple layer is formed at 20-25 V_{AC} and the pale-blue one at 35 V_{AC}. Similarly, the brownish pink sample (Fig. 25, 60 V_{AC}) reveals gold and purple grains with some characteristics of non-uniformity due to the lines and scratches on the electrode.

(iii) Since the XPS depth profile analysis (see Section 4.5) displays that the coloration depends on the thickness of the passive layer, it may be concluded that the thickness of the passive layer is not exactly the same on all grains owing to the polycrystalline nature of the sample. Yet, since most of the grains reveal the coloration representative of the applied voltage (the principal coloration), it is rational to say that the thickness of the colored passive layer is similar across the entire sample.

(iv) The optical microscopy shows that the passive layers were free of micrometer-sized cracks or fractures.

4.2 3D Optical microscopy of multicolored titanium passive layers

Fig. 26 shows the results of 3D optical microscopy analysis of an as-received Ti samples which were only cleaned in acetone under reflux. All heights vs. distance plots clearly display the imperfections on the surface such as grains, grain boundaries, scratches and lines due to the manufacturing of the titanium plate, which gives a rough, irregular polycrystalline surface. Fig. 27 presents Ti being etched for 1min. The etching resulted in a fast dissolution of titanium. This procedure results in higher surface roughness as revealed in the contour and surface profile plots (Fig. 27). However, the etching of Ti results in a regular titanium surface showing the grain structure and the polycrystalline nature of Ti. The results allowed us to access to the real morphology characteristics of the pure metal and to relate them to the features of the colored layers. Fig. 28 represents the 3D optical microscopy analysis of the 20V_{AC} passive layer. On the macroscopic or micrometers level, there are no major differences between the etched titanium sample and the colored films on titanium.

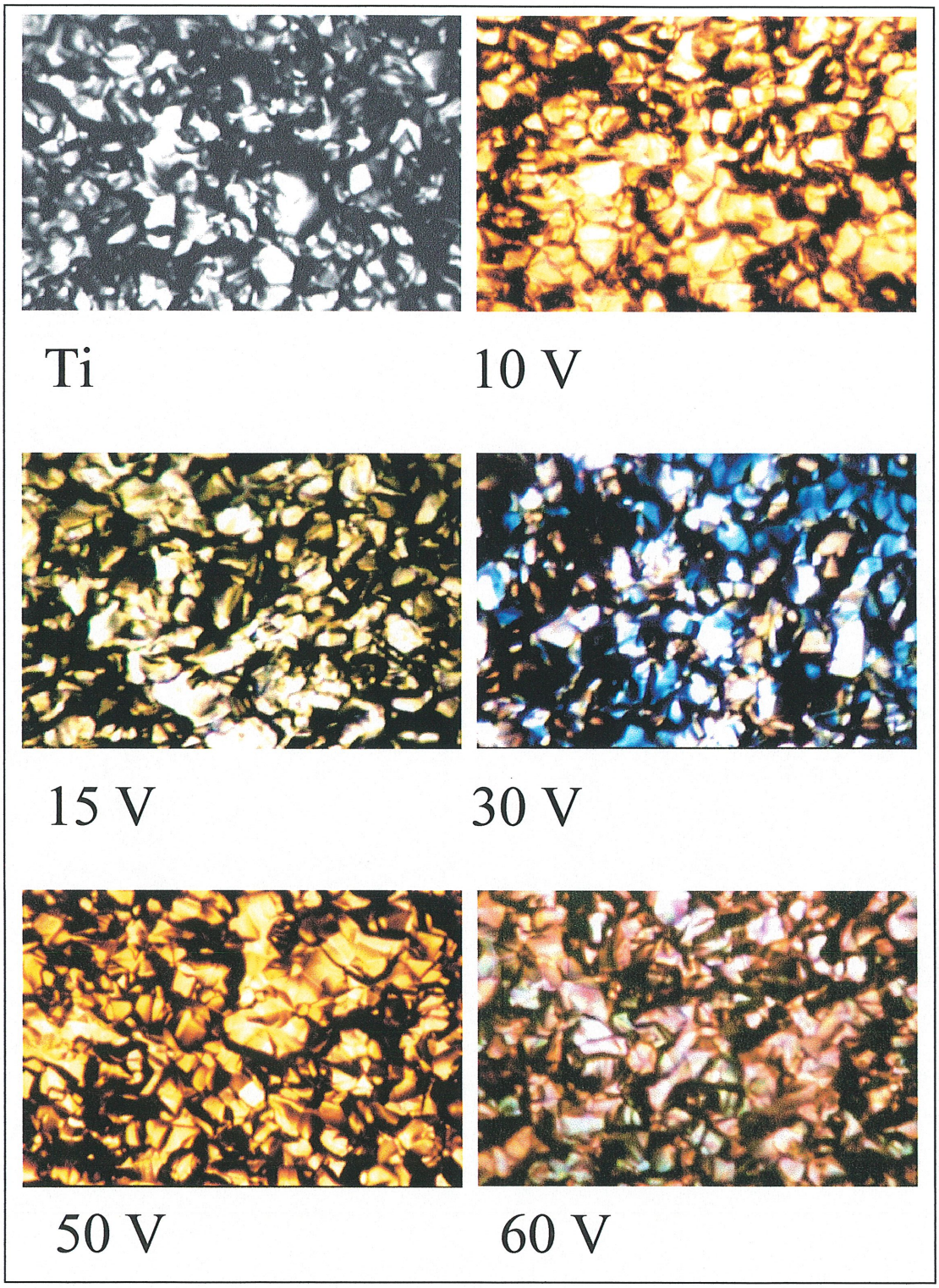

Figure 25. Optical microscopy analysis (200 ×) of Ti and Ti passive films formed at 10, 15, 30, 50 and 60 V_{AC} in aq. 7.5 wt. % NH_4BF_4, T = 298 K, t = 10 s.

However, the surface profile plot (on the bottom of Figs. 26-30) shows a decrease of the surface roughness upon the color film formation. Fig. 29 shows the 3D optical microscopy analysis of the 40 V_{AC} passive layer. New features associated with surface smoothing can be observed. This becomes easily visible in the surface profile curve, which becomes smoother in the case of 40 V_{AC} film than in the case of the etched Ti or the film formed at 20 V_{AC}. Fig. 30 shows the 3D optical microscopy analysis of the 60 V_{AC} passive film, the passive layer having the greatest thickness and the smoothest surface (see surface profile plot). The solid plot gives some new features: the grains and grain boundaries are more pronounced in the case of the 60 V_{AC} film than in the case of 20 and 40 V_{AC}. In general, the New View 5000 3D Optical Microscopy results are in agreement with the classical optical microscopy results, and goes further giving additional information about the surface roughness of Ti and the colored passive layers. The effect of smoothing of the surface of titanium by applying the higher AC voltage was also verified.

4.3 Scanning electron microscopy characterization of Ti and Ti passive layers

The results of the surface morphology analysis of Ti and of the colored passive layers by SEM are as follows:

a) The colored layers sustain a grain structure which is in conformance with the morphology of titanium metallic substrate;
b) The passive layer development is more pronounced at the grain boundaries which is visible on both Figs. 31 and 32;
c) The grain structure of the passive layer formed at 10 V_{AC} (Figs. 31B and 32B) resembles that of Ti (Figs. 31A and 32A); in this case, the passive layer is the thinnest;
d) The morphology of the passive layers formed at 20 V_{AC} (Figs. 31C and 32C) and 30 V_{AC} (Figs. 31D and 32D) is similar to that of other passive films; here, the grain boundaries become less visible due to the increased thickness of the passive layer;

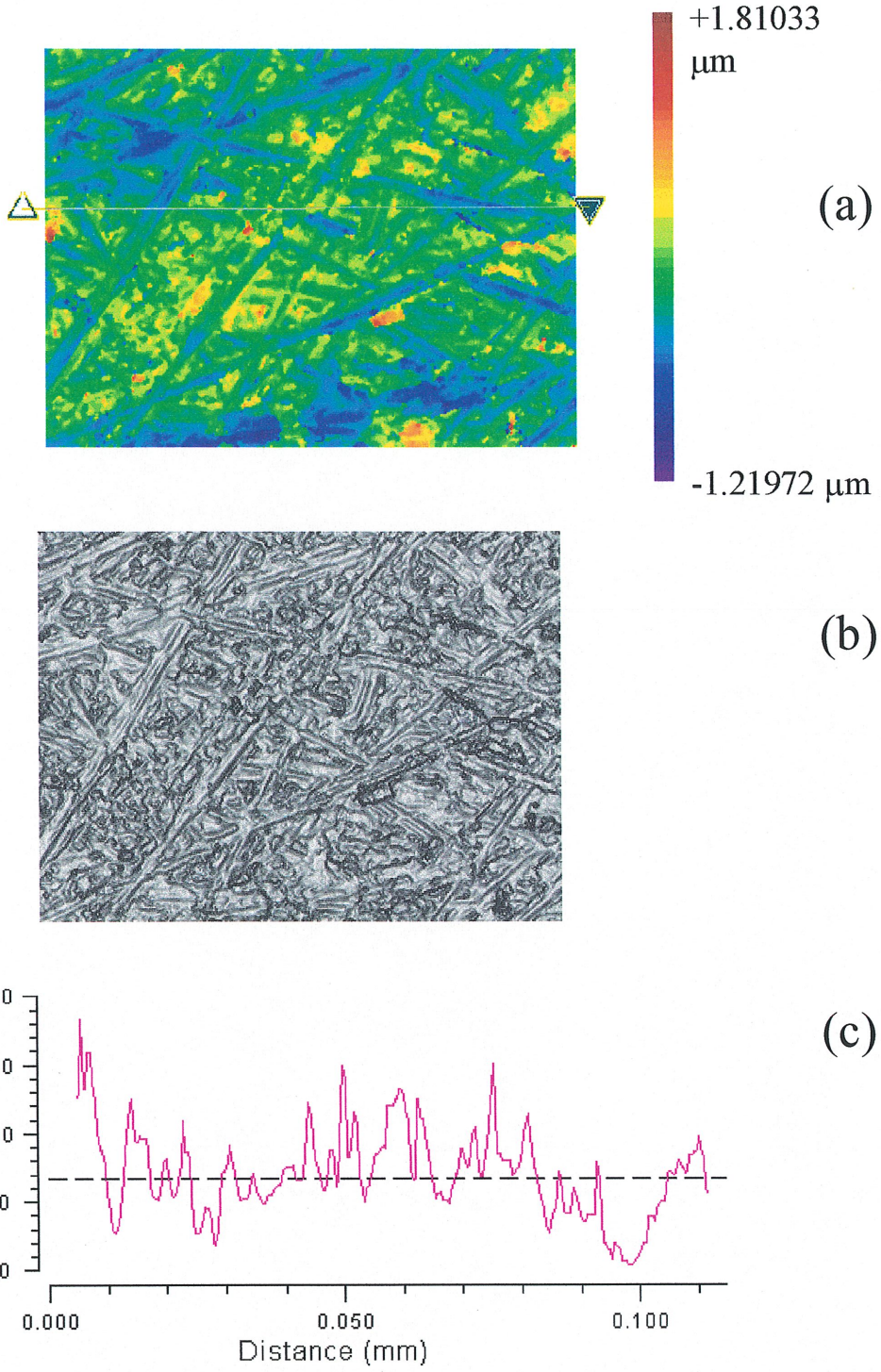

Figure 26. New View 5000 3D Optical Microscopy analysis of an as-received Ti sample. (a) Filled plot, (b) Solid plot, (c) Profile plot at the magnification of 1000 ×; working distance 3.4 mm, lateral resolution 0.64, field of view 0.14 x 0.11 mm.

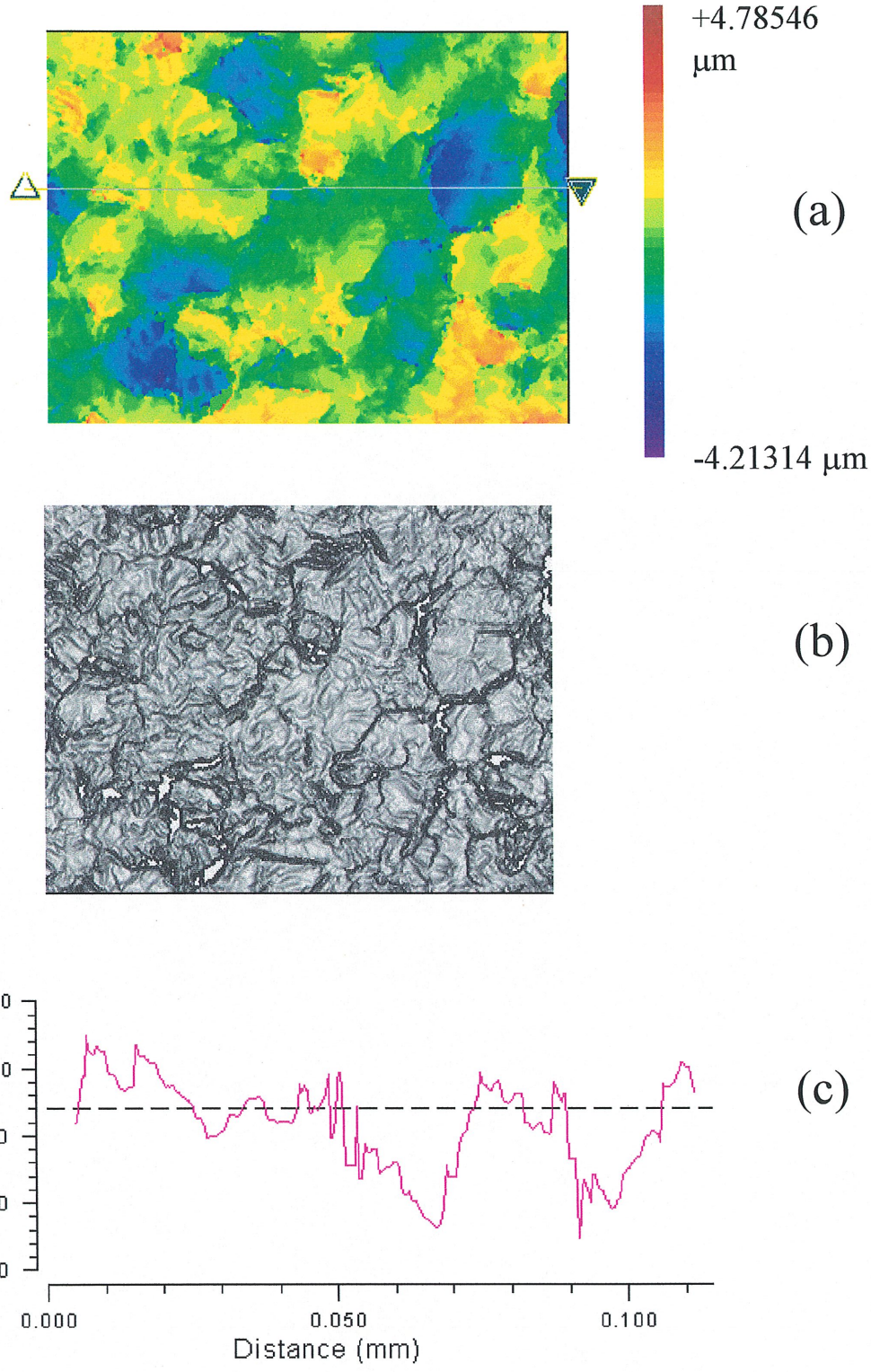

Figure 27. New View 5000 3D Optical Microscopy analysis of the etched Ti sample. (a) Filled plot, (b) Solid plot, (c) Profile plot, at the magnification of 1000 ×; working distance 3.4 mm, lateral resolution 0.64 µm, field of view 0.14 x 0.11 mm.

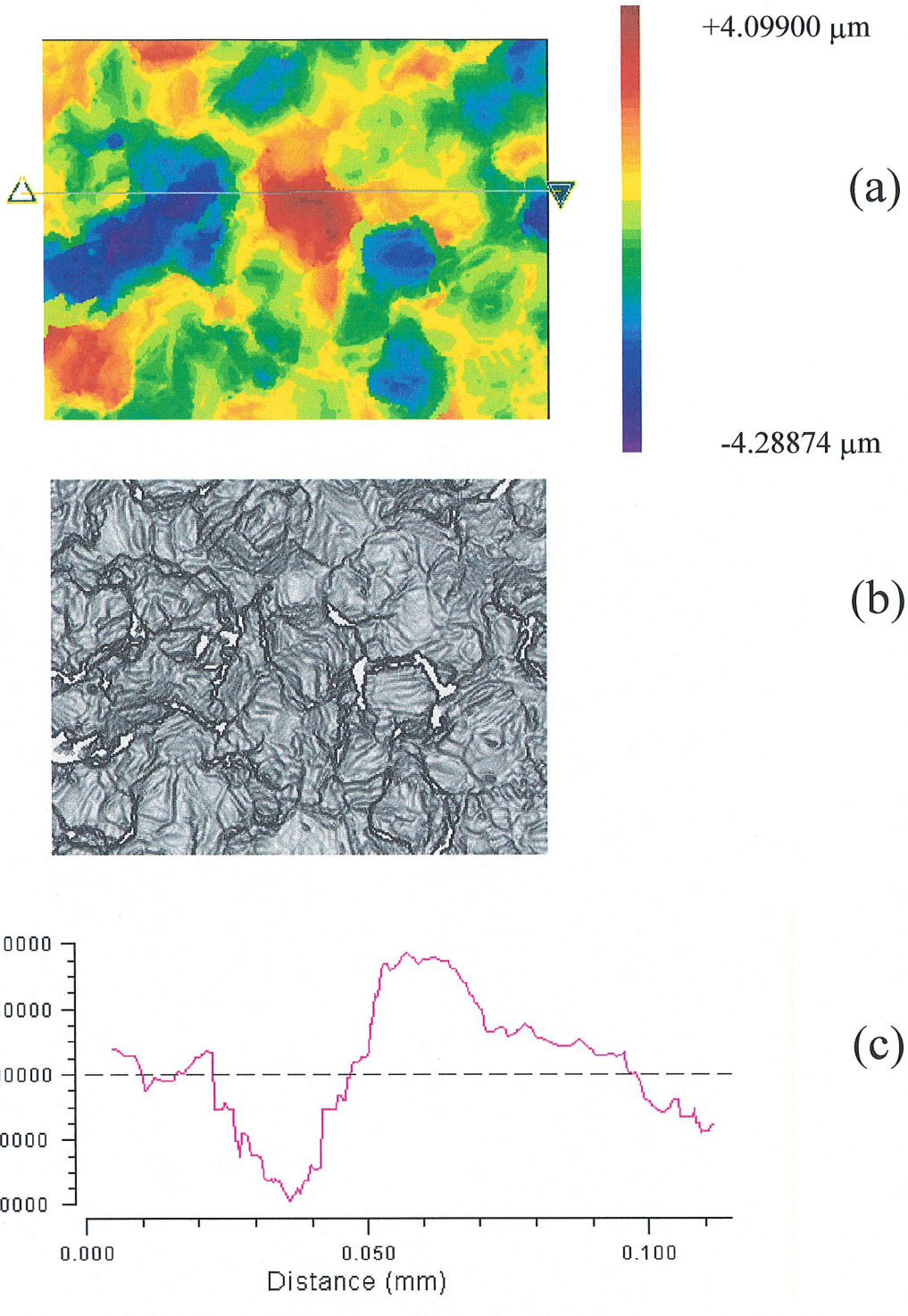

Figure 28. New View 5000 3D Optical Microscopy analysis of the 20 V_{AC} colored passive layer on Ti formed in aq. 7.5 wt. % NH_4BF_4, T = 298 K, t = 10 s. (a) Filled plot, (b) Solid plot, (c) Profile plot, at the magnification 1000 ×; working distance 3.4 mm, lateral resolution 0.64 µm, field of view 0.14 x 0.11 mm.

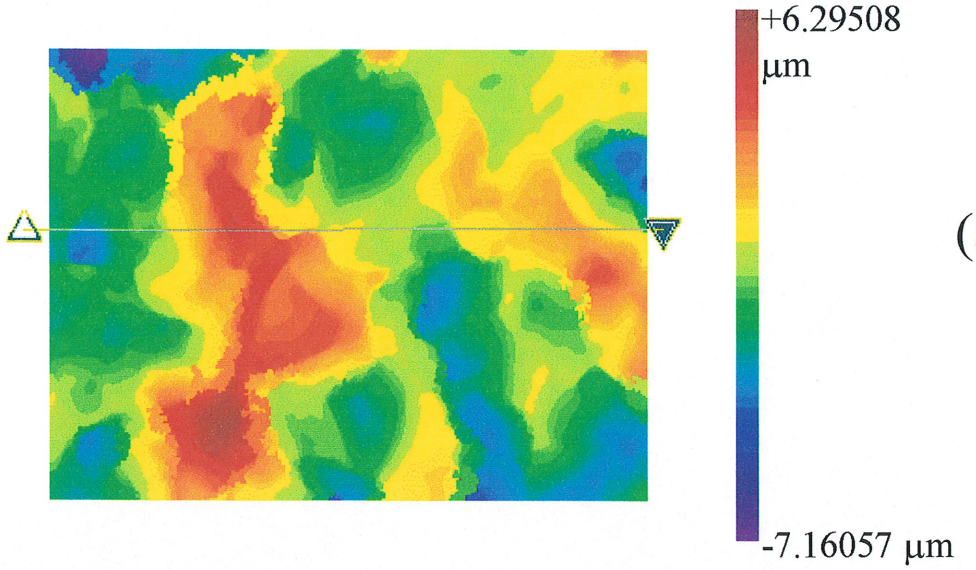

(a)

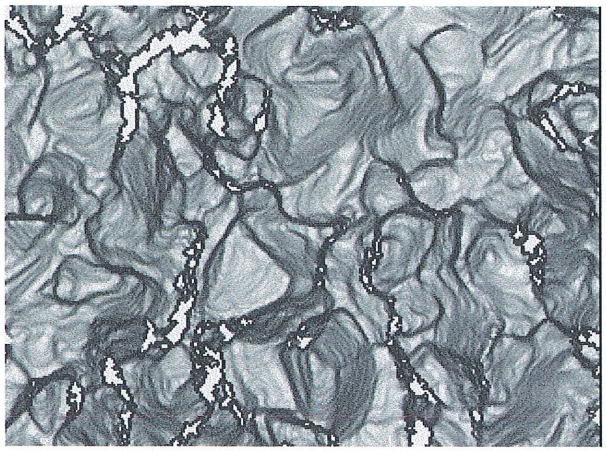

(b)

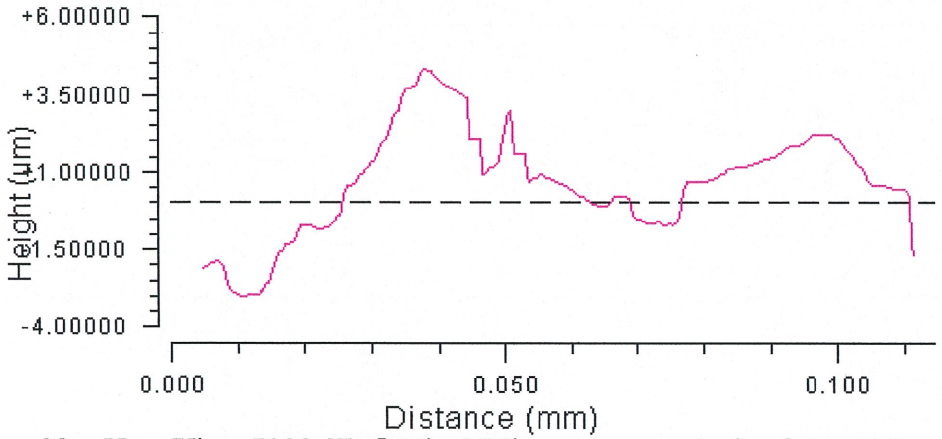

(c)

Figure 29. New View 5000 3D Optical Microscopy analysis of the 40 V_{AC} colored passive layer on Ti formed in aq. 7.5 wt. % NH_4BF_4, T = 298 K, t = 10 s. (a) Filled plot, (b) Solid plot, (c) Profile plot, at the magnification 1000 ×; working distance 3.4 mm, lateral resolution 0.64 µm, field of view 0.14 x 0.11 mm.

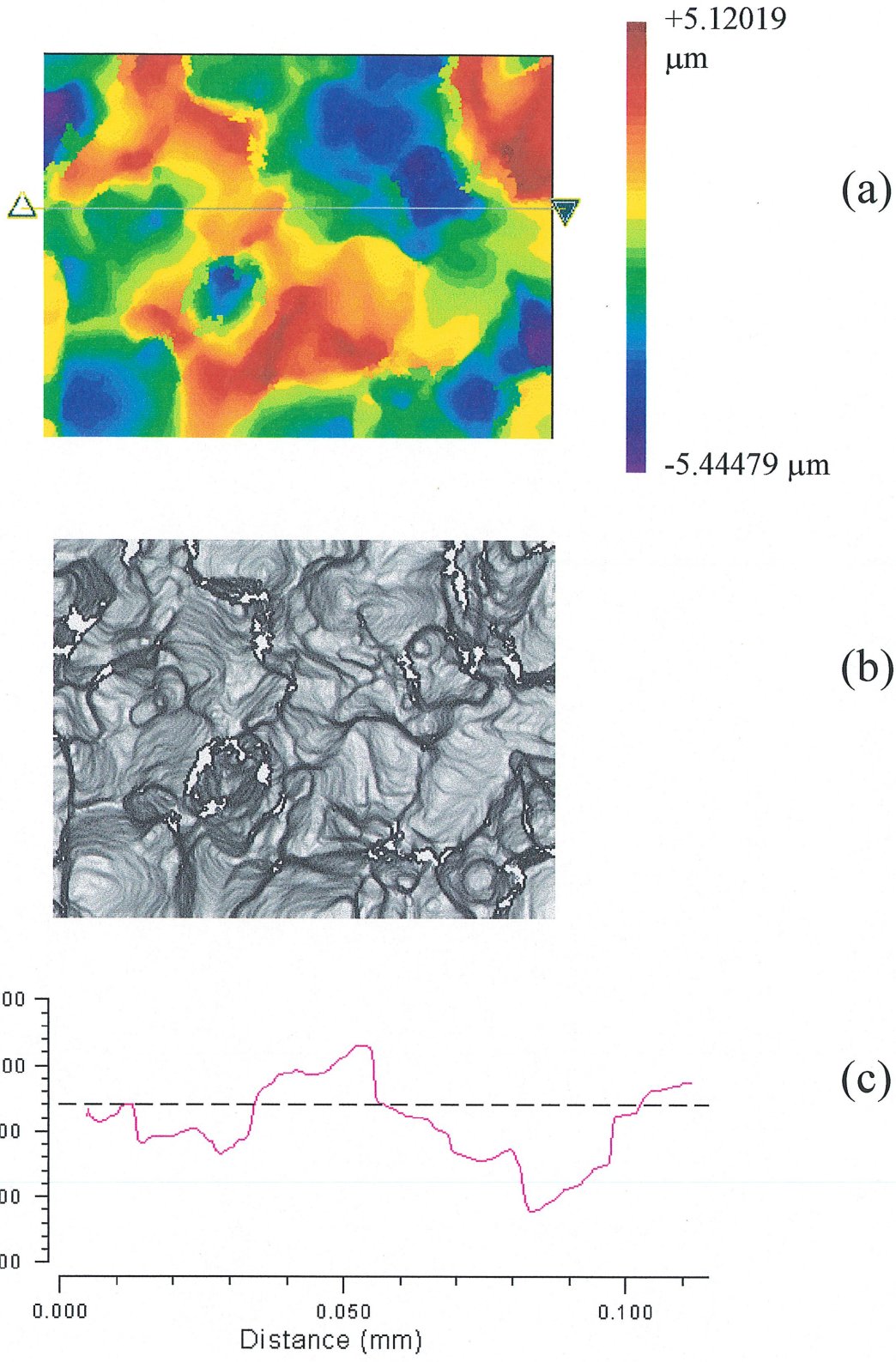

Figure 30. New View 5000 3D Optical Microscopy analysis of the 60 V_{AC} colored passive layer on Ti formed in aq. 7.5 wt. % NH_4BF_4, T = 298 K, t = 10 s. (a) Filled plot, (b) Solid plot, (c) Profile plot, at the magnification 1000 ×; working distance 3.4 mm, lateral resolution 0.64 µm, field of view 0.14 x 0.11 mm.

e) The morphology of the passive layers formed at 40 V_{AC} (Figs. 31E and 32E) and 50 V_{AC} (Figs. 31F and 32F) is similar; albeit the growth of the passive layer occurs across the entire samples, its thickness at the grain boundaries is greater with respect to the grains;

f) The morphology of the passive layers formed at 60 V_{AC} (Figs. 31G and 32G) and 70 V_{AC} (Figs. 31H and 32H) presents a new feature: step-like features on grains. Despite the decrease of the surface roughness caused by the passive layer formation and the step-shaped features, we do not observe any visible cracks or fractures that could be associated with the colored layer formation. These results indicate that the colored layers are compact and well protect the underlying metallic Ti. This observation is of importance with respect to possible applications of the colored layers, since it is essential that the Ti substrate not be exposed to a new liquid or gaseous medium.

4.4 Atomic force microscopy analysis of titanium and titanium passive layers

In order to get more information about the surface morphology and characteristics of Ti passive layers, an AFM analysis of our samples was done. Fig. 33 represents results for two Ti passive layers (formed at 15 and 25 V_{AC}) whereas Fig. 34 shows the morphology of passive layers formed at 35 and 45 V_{AC}. The general conclusion that may be drawn is that there are no fractures or cracks formed upon the AC polarization. The fact that it was impossible to etch all the samples absolutely equally, can explain some differences in the surface morphology of different samples. However, it was observed that as we increased the applied AC voltage, the surface roughness decreased.

The AFM results further support the SEM and optical microscopy ones pointing out a lack of cracks or fractures in the colored passive layerson Ti. The morphology analysis data consistently demonstrate that the colored surface layers well protect the underlying Ti substrate.

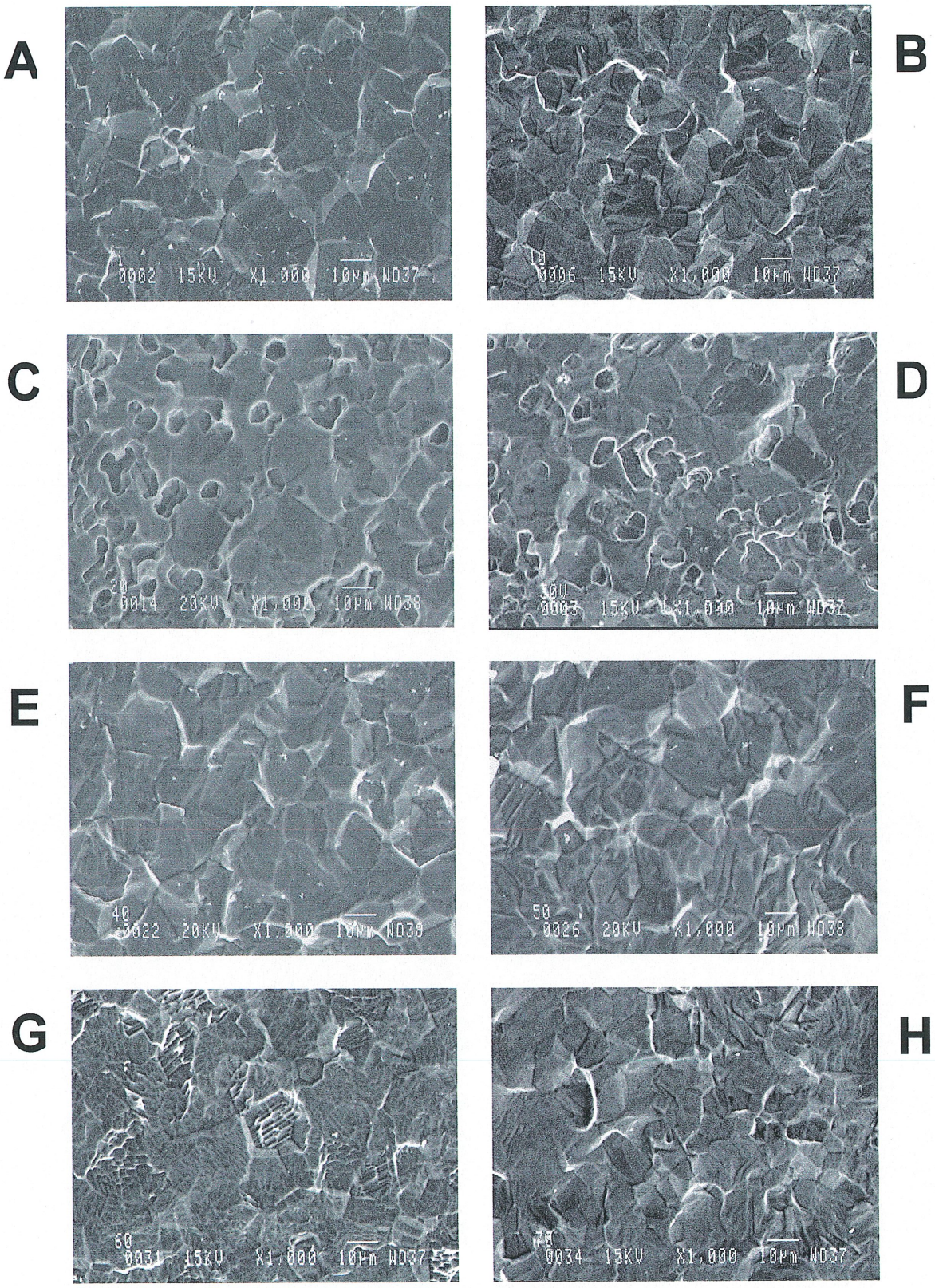

Figure 31. SEM analysis (1000 ×) of Ti and 7 Ti passive layers (10-70 V_{AC}) formed in aq. 7.5 wt. % NH_4BF_4, T = 298 K, t = 10 s.

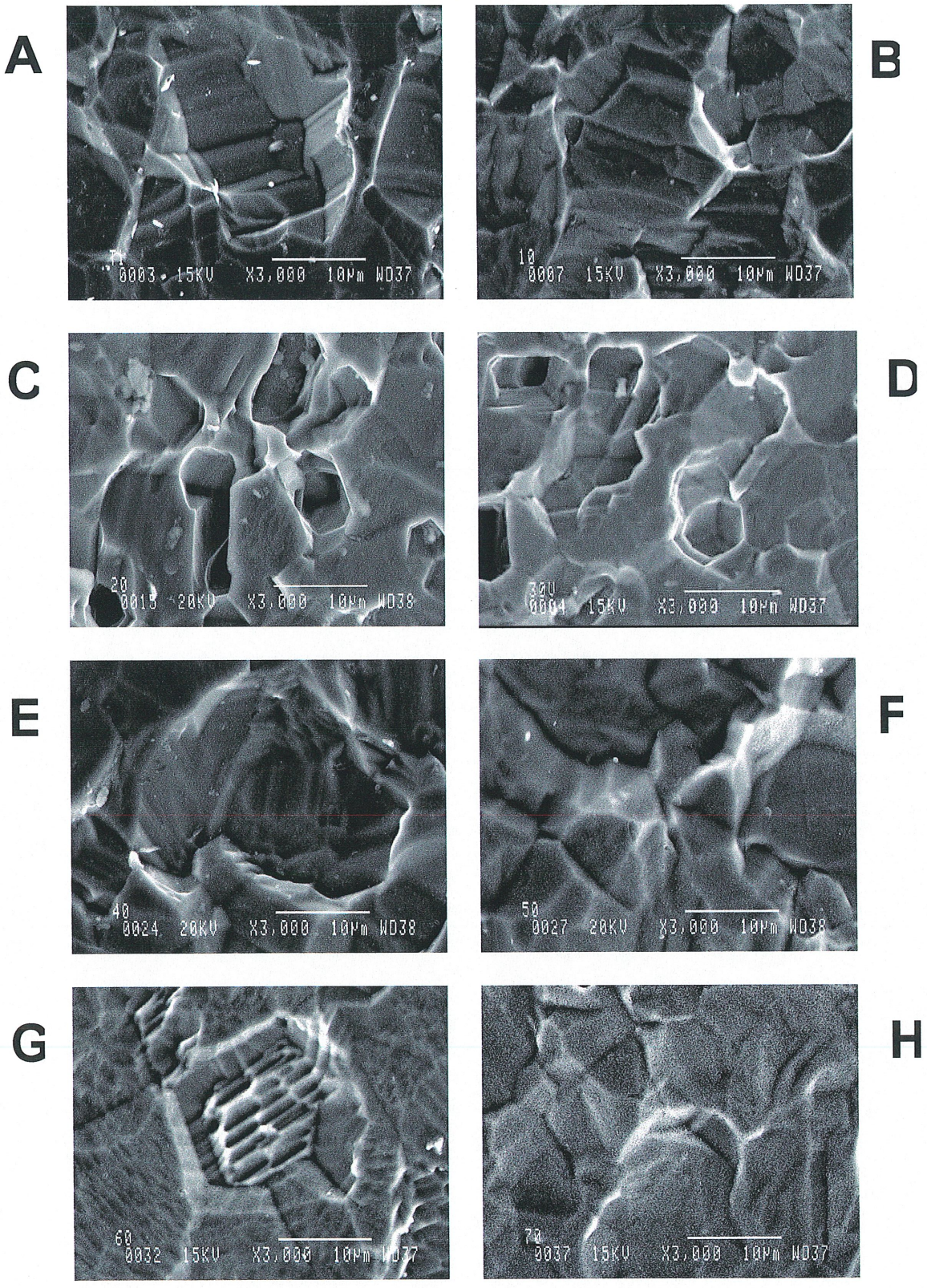

Figure 32. SEM analysis (3000 ×) of Ti and 7 Ti passive layers (10-70 V_{AC}) formed in aq. 7.5 wt. % NH_4BF_4, T = 298 K, t = 10 s.

4.5 XPS characterization and depth profile analysis of the colored Ti passive layers

XPS measurements were performed on five colored Ti passive films formed at 15, 25, 35, 45 and 55 V_{AC} transferred via air and then after consecutive sputter cycles. In Figs. 35(a), 36(a), 37(a), 38(a), and 39(a), we show XPS survey spectra for the brown (15 V_{AC}), the dark-blue (25V_{AC}), light-blue (35V_{AC}), olive-green (45V_{AC}), and pink (55 V_{AC}) layers. An XPS surface analysis of the as-received samples reveals presence of Ti, O, F, C, Ca, and N. Ti, O and F are the main constituents of the passive layers whereas C, Ca and N are surface contaminants that originate from the via-air transfer; they are not observed already after one Ar^+-ion sputter cycle. Interestingly, the surface chemical composition of the outer-most layer of the five samples is practically the same and as follows (in atomic %): Ti 17-19, O 47-48, C 28-31, F 3-4.5, N 0.3-1.1, and Ca 0.1-0.4. Figs. 35 (b) – 39 (b) show XPS depth profiles for the brown (15 V_{AC}), dark-blue (25V_{AC}), light-blue (35V_{AC}), olive-green (45V_{AC}), and pink (55 V_{AC}) layers. The spectra consist of four contributions: O, Ti, F, and C. In order to assess the chemical state of Ti on the surface of the sample and across the passive layer, we examined the chemical shift of Ti bound to O and F (ΔTi (2p)) as well as evaluated the value of the ΔBE_1 parameter (71), where ΔBE_1 is the difference in the binding energy of O (1s) and Ti (2p) bands, ΔBE_1 = O (1s) - Ti (2p). We also examined the chemical shift of the O (1s) and F (1s) bands which were found to be -1 eV and -0.5 eV, respectively, were characteristic of O^{2-} and F^-. In general, simultaneous analysis of the values of ΔTi (2p) and ΔBE_1 as well as of the O/Ti atomic ratio allow us to determine beyond any doubt the nature of the Ti oxide and Ti fluoride constituting the colored layer (60,71). In performing the quantitative XPS analysis, the Ti XPS spectra were deconvoluted into two components, one assigned to Ti^{z+} (bound to O and F) and one to Ti^0 (metallic substrate). The value of ΔTi (2p) prior to the first sputter cycle was 5.5 eV and that of ΔBE_1 was 71.5 eV, thus characteristic of TiO_2 (the outer-most layer) (38). However, their values changed upon the consecutive sputter cycles and were ΔTi (2p) = 1 - 1.5 eV and ΔBE_1 = 73.6 - 75.1 eV, thus characteristic of Ti_2O_3 or TiO respectively. Clearly, the chemical composition of the inner layer was different from the outer one.

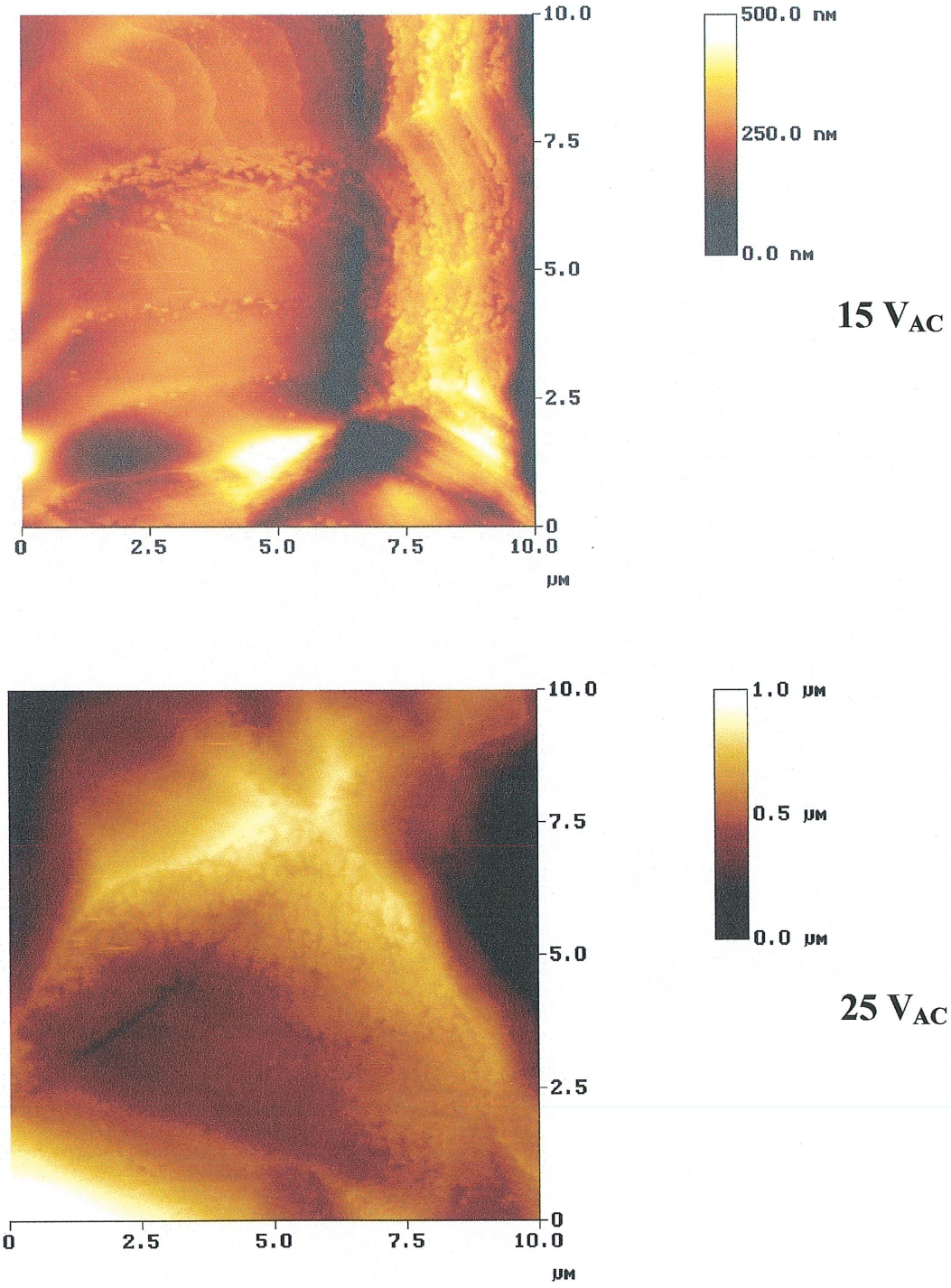

Figure 33. AFM analysis (contact mode) of the Ti passive layers formed at 15 and 25 V_{AC} in aq. 7.5 wt. % NH_4BF_4, T = 298 K, t = 10 s.

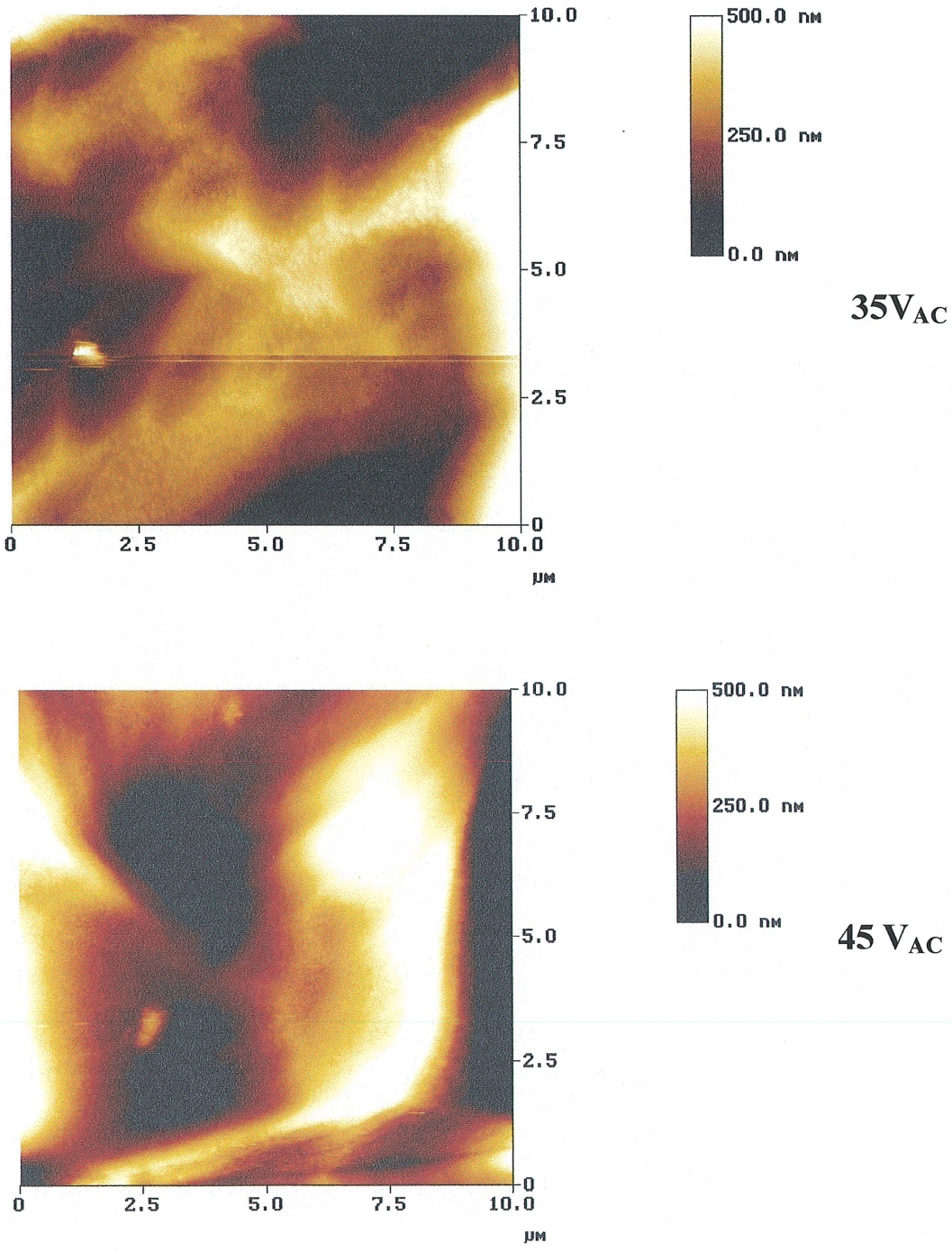

Figure 34. AFM analysis (contact mode) of the Ti passive layers formed at 35 and 45 V_{AC} in aq. 7.5 wt. % NH_4BF_4, T = 298 K, t = 10 s.

It should be stressed that in assigning the amount of Ti bound to O (the O/Ti atomic ratio), we subtracted the respective amount of Ti bound to F in the form of TiF_x, where x = 2 or 3 depending on the oxidation state of Ti within the passive layer (%F/x = %Ti att. to F). It could be concluded that TiO_2 present on the outer-most surface do not originated not from the preparation procedure but from the interaction of the lower oxide (Ti_2O_3 or TiO) with molecular oxygen during the transfer via air. At last, it should be stated that the shape of the C (1s) band was typical of graphitic C; thus we conclude that the presence of C on the surface did not lead to the formation of a surface layer of Ti carbide. This is an important observation since TiC has different electronic properties from TiO or Ti_2O_3. An inspection into the XPS depth compositional profiles reveals that in all cases F tends to accumulate at the inner metal/passive layer interface but its distribution across the latter as well as its maximal atomic concentration are a function of the applied AC voltage. In the case of the lowest voltage (15 V_{AC}), the F concentration profile is rather narrow whereas in the case of the highest voltage (55 V_{AC}) the F profile is very broad. The maximal atomic concentration of F is also a function of the applied voltage and it is found to be 10% for the 15 V_{AC} layer, 14% for the 25 V_{AC}, 18% for the 35 V_{AC} one, 16% for the 45 V_{AC} and 12% for the 55 V_{AC} ones. In the first XPS analysis of the colored Ti passive layers, Jerkiewicz and al. (15) did not report this behavior because they were not able to observe it due to experimental limitations. However, the unique XPS instrumentation utilized in the present study and comprising the Zalar Rotation™ system allowed us to divulge new compositional characteristics. The XPS compositional depth analysis led us to determine the thickness (d/nm) of the colored passive layers related to the applied AC voltage. In performing this analysis, it was assumed that the film terminated at the point at which the XPS signals of O (1s) and F (1s) dropped to half of their respective maximal intensities. The results of this analysis are shown in Fig. 40 where the relation between the thickness of the colored passive layers and the applied AC voltage is presented. There is almost a perfectly linear relation between the thickness of the colored Ti passive layers and the AC voltage (other parameters such as NH_4BF_4 concentration, temperature and polarization time being constant). The thickness varies from 78 nm for light-brown passive layer formed at 15 V_{AC} up to 291 nm for the pink passive layer formed at 55 V_{AC}.

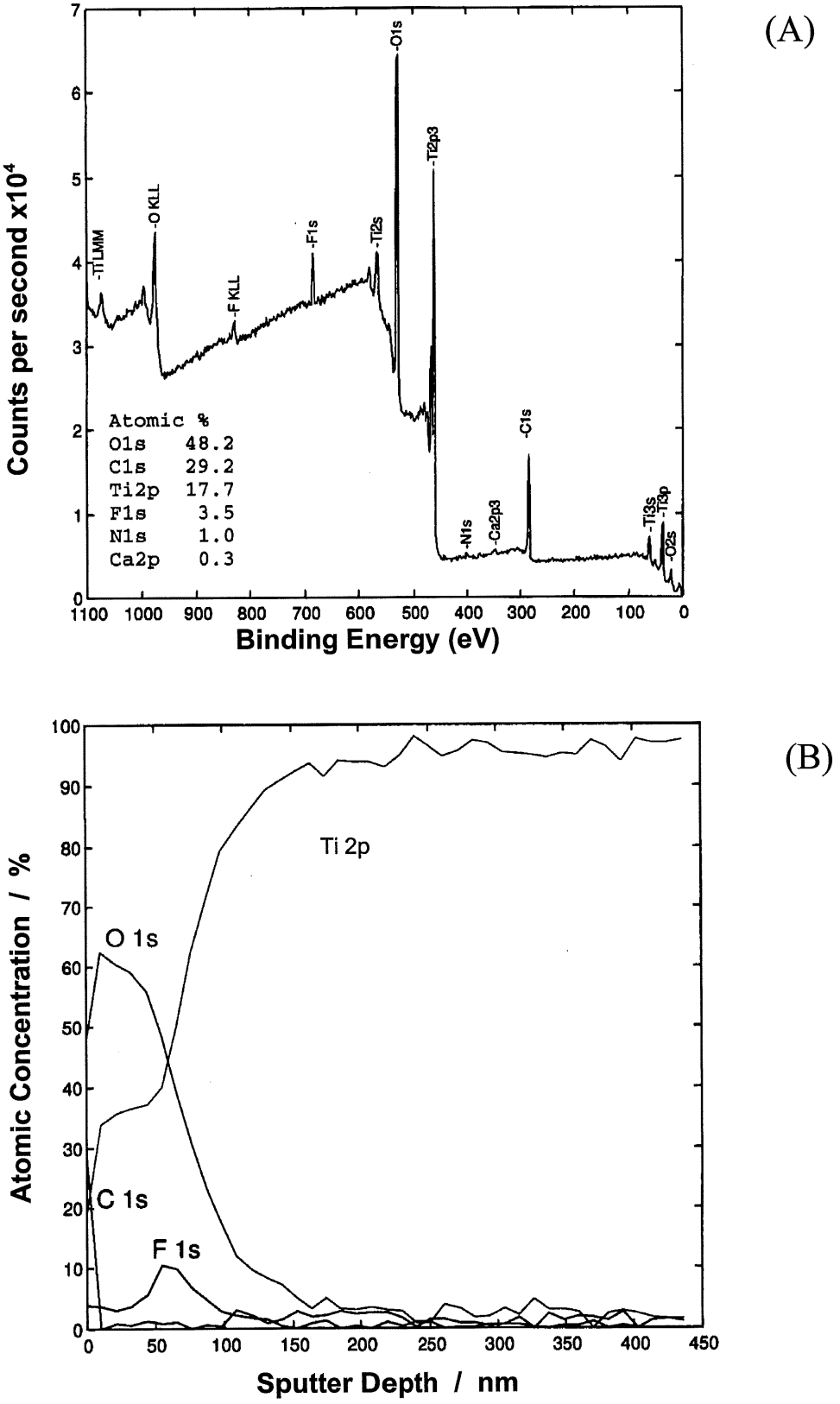

Figure 35. XPS survey spectrum (A) and XPS depth profile (B) for the brown layer formed at 15 V_{AC} in aq. 7.5 wt. % NH_4BF_4, T = 298 K, t = 10 s.

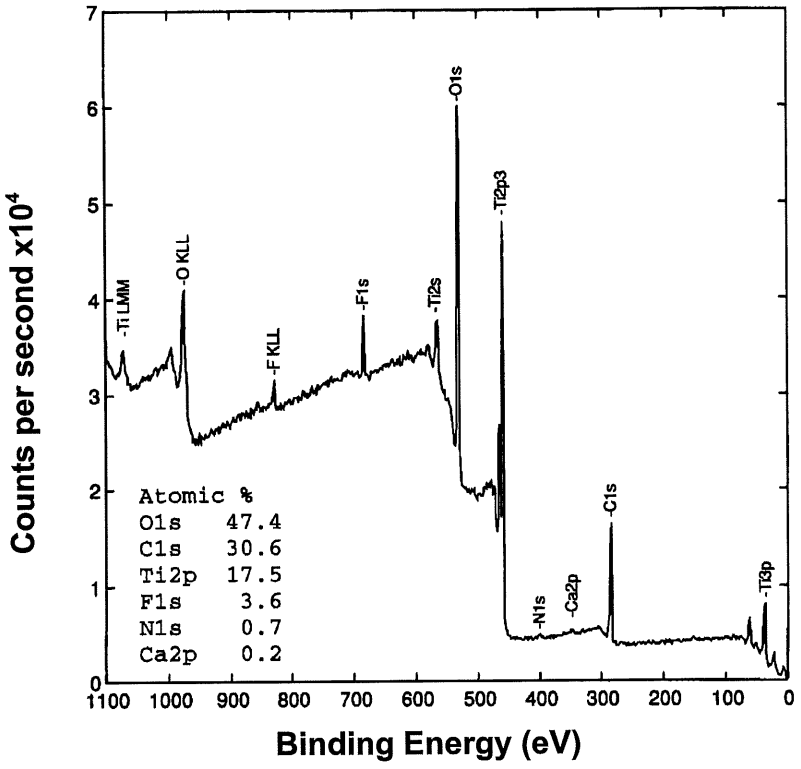

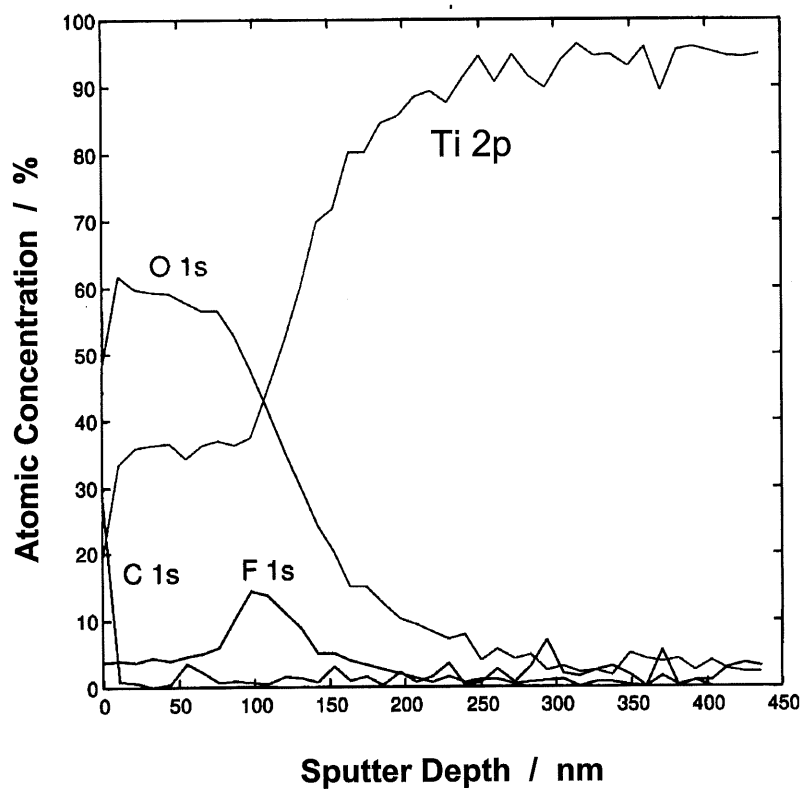

Figure 36. XPS survey spectrum (A) and XPS depth profile (B) for the dark-blue layer formed at 25 V_{AC} in aq. 7.5 wt. % NH_4BF_4, T = 298 K, t = 10 s.

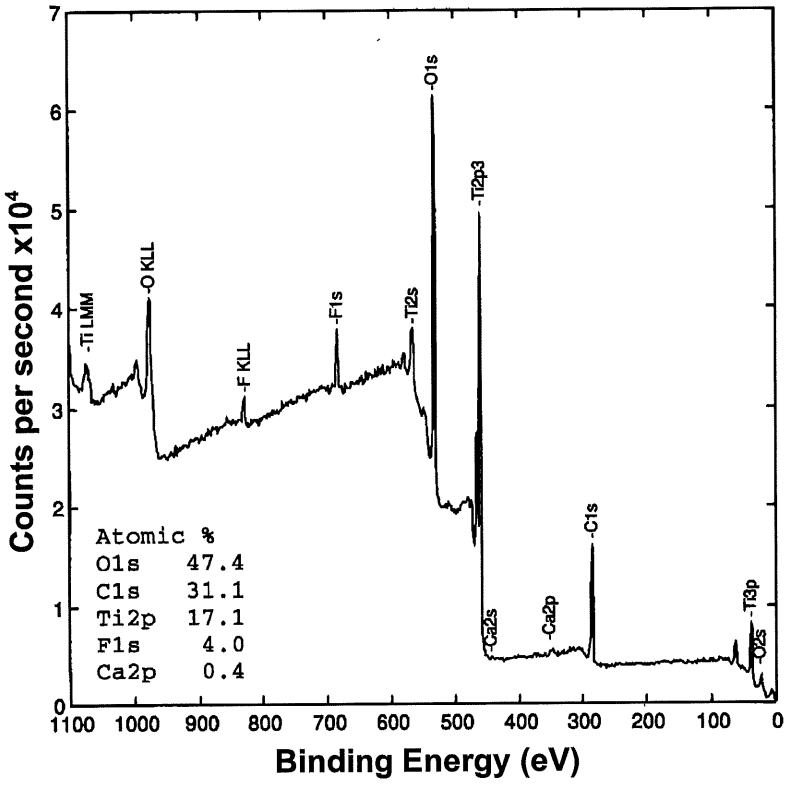

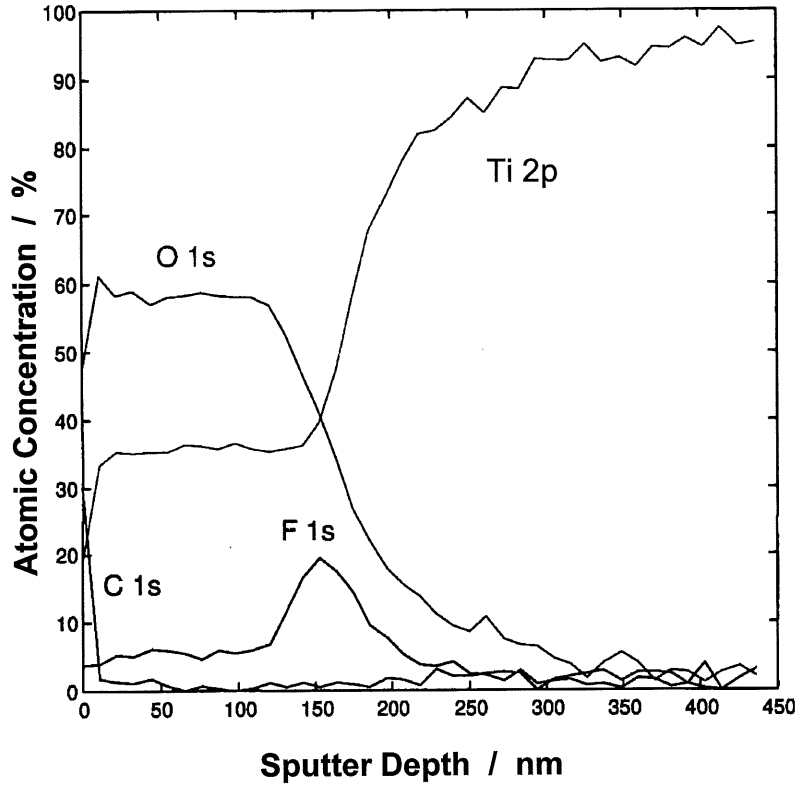

Figure 37. XPS survey spectrum (A) and XPS depth profile (B) for the light-blue layer formed at 35 V_{AC} in aq. 7.5 wt. % NH_4BF_4, T = 298 K, t = 10 s.

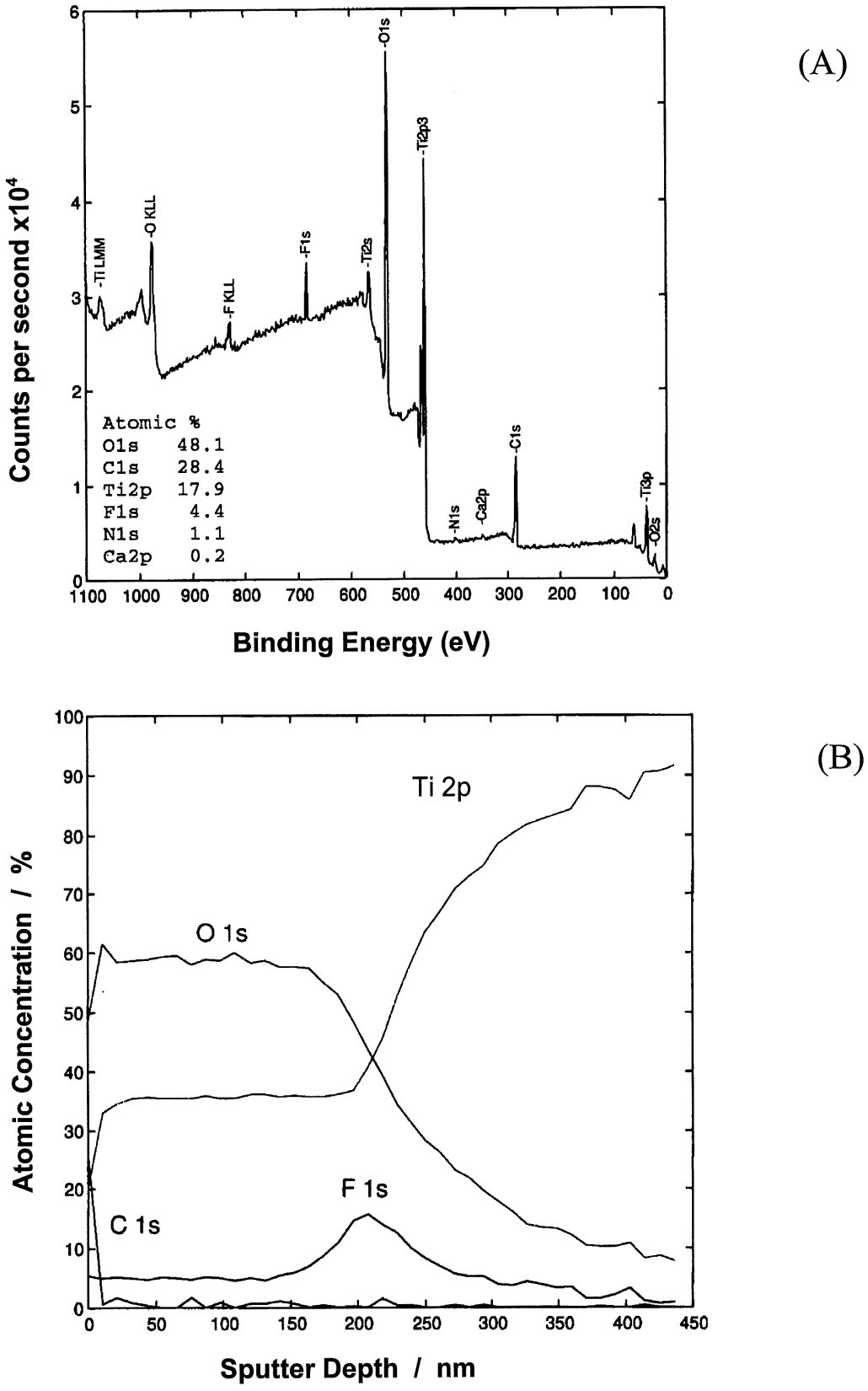

Figure 38. XPS survey spectrum (A) and XPS depth profile (B) for the olive-green layer formed at 45 V_{AC} in aq. 7.5 wt. % NH_4BF_4, T = 298 K, t = 10 s.

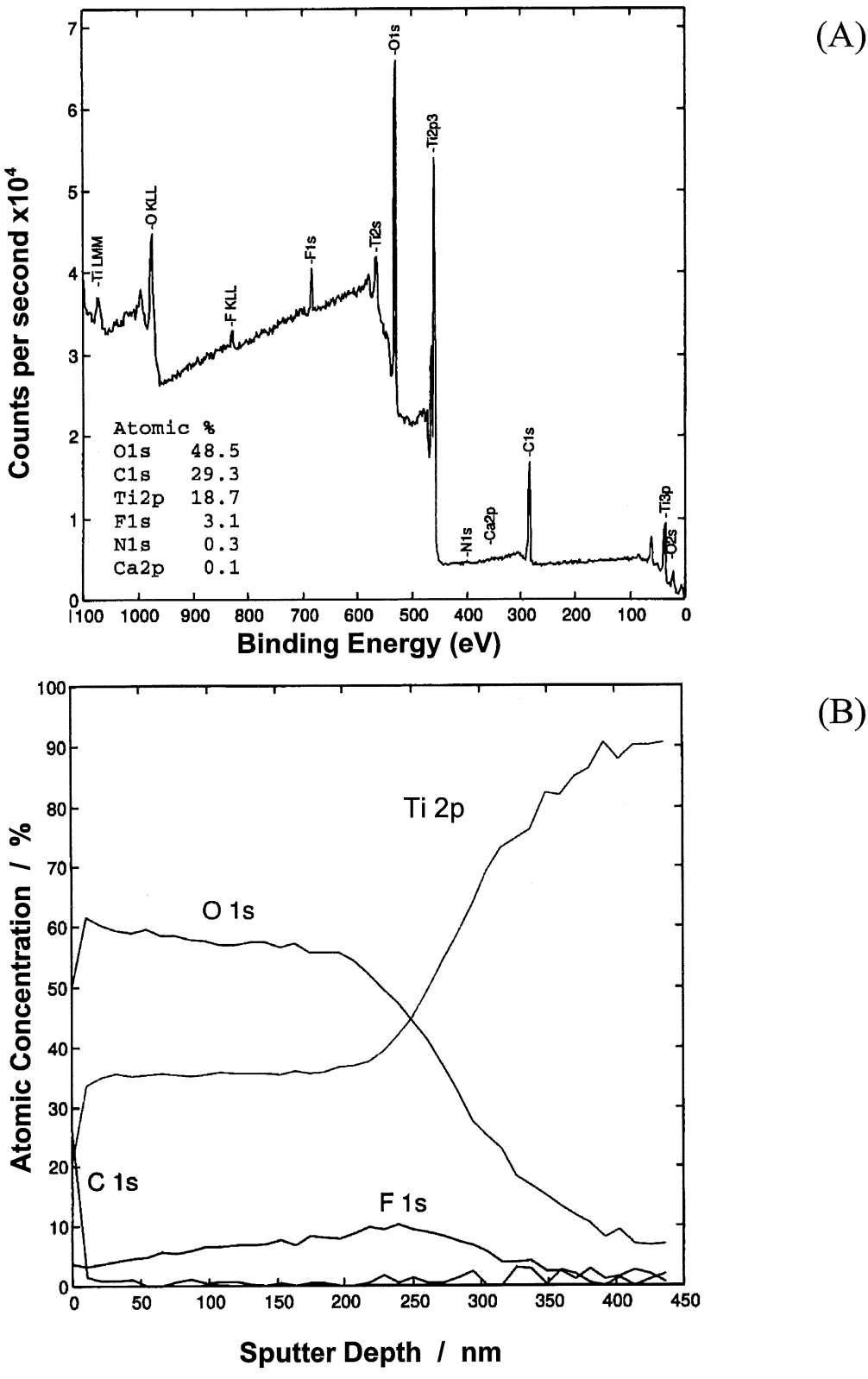

Figure 39. XPS survey spectrum (A) and XPS depth profile (B) for the pink layer formed at 55 V_{AC} in aq. 7.5 wt. % NH_4BF_4, T = 298 K, t = 10 s.

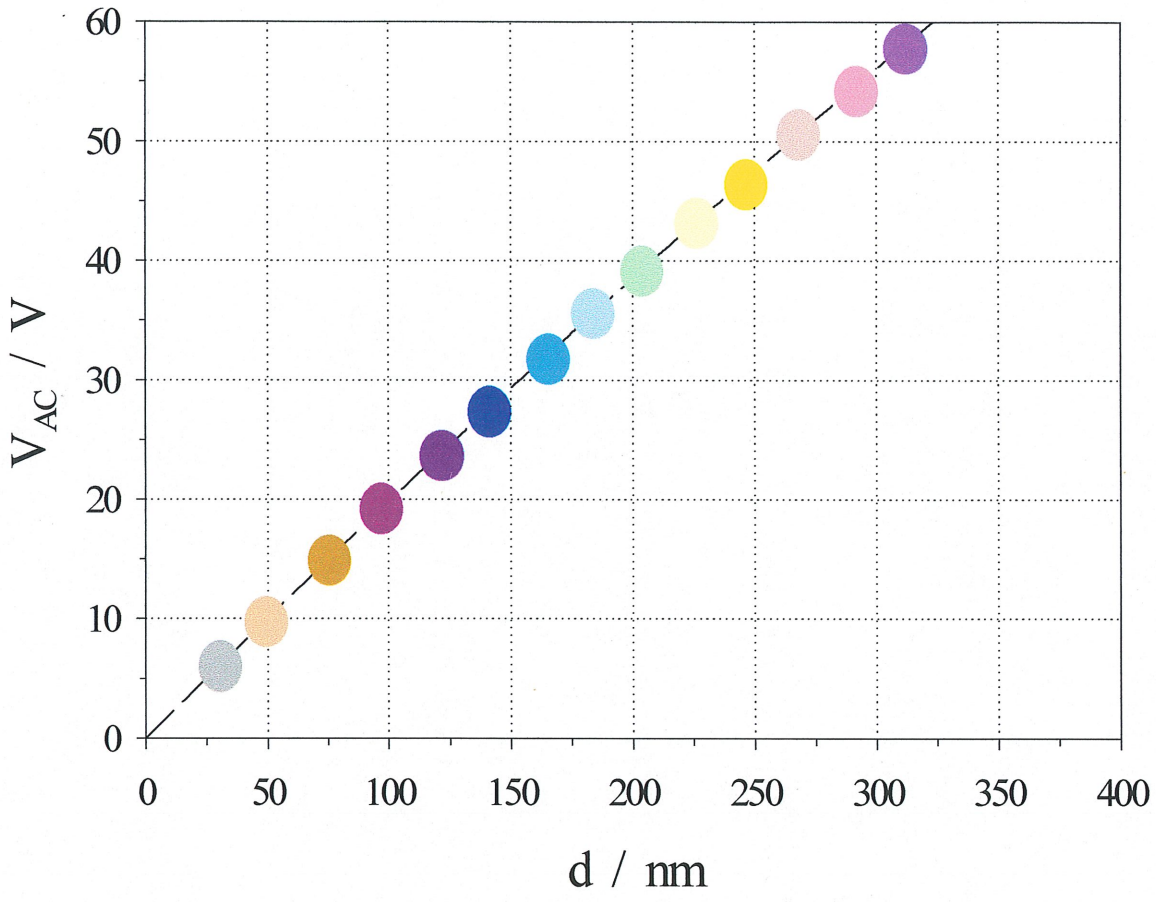

Figure 40. Relation between the thickness of the colored passive layers and the applied AC voltage in aq. 7.5 wt. % NH_4BF_4, T = 298 K, t = 10 s.

CHAPTER 5

ELECTROCHEMICAL CHARACTERIZATION OF TITANIUM AND ITS COLORED PASSIVE LAYERS

5.1 Electrochemical behavior of Ti and the colored Ti passive layers under open-circuit conditions

Firstly, we examined the open-circuit behavior of the colored titanium passive layers in the native electrolyte, thus the solution that was used for preparation of the multicolored passive films. The fact that the BF_4^- anion is very aggressive and corrosive for Ti and its colored layers (53) is confirmed in Fig. 41 which shows the corrosion potential (E_{corr}) measured vs. pure Ti (a quasi-reference electrode) in open-circuit conditions as a function of time. The potential of a corroding surface in an electrolyte, relative to a reference electrode is the corrosion potential. E_{corr} is also called rest potential, open circuit potential, or freely corroding potential (49,51).

The relatively fast dissolution (time of dissolution was from 20 to 400 sec.) of the colored passive layers in 7.5% NH_4BF_4 was observed. The colors in Fig. 41 present the real color of the titanium passive films. Right after placing the electrodes in the solution (aqueous 7.5% NH_4BF_4) the dissolution starts and the open circuit potential (measured versus freshly etched Ti electrode of the same surface area as that of the working electrodes) drops. Three different regions can be observed in the graph: (i) film stability, (ii) film dissolution, and (iii) film absence regions. Interestingly, the passive film formed on 10 V_{AC} had the longest film stability region and the dissolution of this film starts only after ca. 400 sec. As we increase the AC voltage to form the films, their stability in aq. NH_4BF_4 decreases following the order from 10 to 60 V_{AC}. This behavior means that the thickest does not possess the greatest stability. At

present, we may only speculate that this behavior can be assigned to the compact nature of the film which can allow, or not, the electrolyte to penetrate it leading to dissolution.

Open-circuit conditions were also used to record the E_{corr} vs. time profiles in the same conditions, but using a Pt electrode as reference. The results show a different shape of the curves and, naturally, different values of the open-circuit potential, yet the order of the film dissolution was found the same. On the other hand, the colored passive films were found stable in 1M aq. H_2SO_4 over the period of one week, showing excellent resistance towards sulfuric acid. The colored passive films were also found stable in aqueous chloride and perchlorate solutions upon their prolonged exposure (days or weeks).

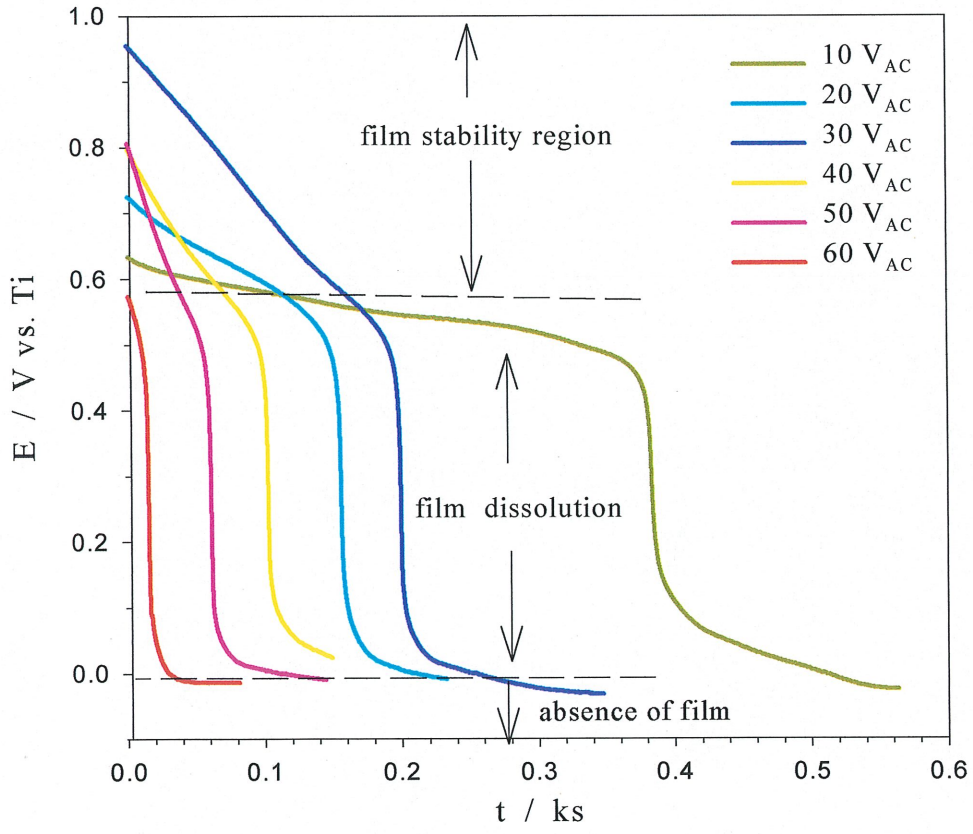

Figure 41. Open-circuit behavior of six colored passive layers in aq. 7.5 wt. % NH_4BF_4 vs pure Ti as a quasi-reference electrode. Colors represent the real film coloration.

5.2 Polarization curves of Ti and colored Ti layers

Wire-shaped electrodes of metallic Ti (to serve as a reference) and colored passive layers (10, 20,..., 60 V_{AC}) were characterized by recording polarization curves in the – 0.8 - 3.2 V potential range at the scan rate s = 1 mV s^{-1} in 1.0 M aqueous H_2SO_4. We focused particular attention on determination of the following parameters: (i) the corrosion potential and current density, E_{corr} and i_{corr}, (ii) the critical potential and current density, E_{cr} and i_{cr}, (iii) the extent of surface passivation, and (iv) modification of the polarization curve in the HER potential region (74). Figs. 42, 43, and 44 show three sets of two graphs, each comprising two polarization curves: (a) the same polarization curve for metallic Ti that serves as a reference, and (b) a polarization curve for a colored passive film formed at a given AC voltage (10, 20, ... , 60V_{AC}). An analysis of the results reveals significant changes in the HER region and the active region prior to the passive one. The current density that can be achieved in the – 0.70 - E_{corr} potential range increases with the increase of applied AC potential of the passive film formation. Only in the case of the passive films formed at 30, 40, 50 and 60 V_{AC} the current density of the HER occurring on Ti surpasses that taking place on the respective passive layer.

E_{corr} and i_{corr} were determined by linear extrapolation of the respective transients (Fig. 42) and it was examined how they varied with regard to the applied AC voltage (Fig. 45). The results reveal that as V_{AC} increases, E_{corr} shifts towards less-negative potentials; the difference of E_{corr} between Ti and the 60 V_{AC} film is ca. 190 mV. The displacement of E_{corr} towards less-negative potentials indicates that the colored passive films are more stable (more noble) than the metallic Ti. The highest value of E_{corr} shows the passive film formed on 10 V_{AC}. We do not show a relation between i_{corr} and V_{AC} because the corrosion current density was only slightly affected by the passive layer development and it remained in the 1.0×10^{-6} - 5.0×10^{-6} A cm^{-2} range. We determined the critical potential and current density, E_{cr} and i_{cr} (see inset in Fig. 42 for the applied methodology) and found that they depend on the applied AC voltage (Fig. 46). The maximum anodic current density observed in the active region for a metal that exhibits active-passive behavior is called critical current density (50). The data show that as

V_{AC} increases E_{cr} moves towards less-negative potentials; the difference of E_{cr} between Ti and the 10 V_{AC} film is ca. 80 mV. We examined the relation between i_{cr} and V_{AC} and observed that the critical current density varied little as a result of the passive film formation. Its values were found to fall in the 50×10^{-6} - 100×10^{-6} A cm^{-2} range. In the case of the 50 and 60 V_{AC} films (see Fig. 44), we observed the emergence of a secondary active-passive transition (50). At present, we are unable to assign this feature to any specific titanium oxide formation, although we may say that it corresponds to a transition of a lower oxide to a higher one. This behavior has not been reported in the literature.

5.3 Tafel plots in the HER region

Since one of the objectives of the research project was to develop Ti-based cathodic materials, we examined the activity of the colored Ti passive films towards the HER. The activity examination was accomplished by recording Tafel polarization curves (75) between 0.00 and (- 0.80) V vs. RHE, in 1.0 M aq. H_2SO_4. The selection of the pre-treatment conditions as well as the program used to obtain reproducible and meaningful steady-state Tafel polarization curves is essential (76, 77). In the course of research, we applied the so-called rectangular program (Fig. 47) to obtain cathodic polarization curves. The program comprised the initial conditioning at E_{cond} = - 0.80 V vs. RHE, for t_{cond} = 60 s. Following the conditioning, a given negative overpotential, η, was applied for a period of time sufficiently long for a steady-state current density, i_{ss}, to become established, here Δt = 60 s (see inset in Fig. 47). Once i_{ss} had been determined, the electrode was conditioned at E_{cond} = 0.00 V for Δt = 60 s and then a new negative over potential (increased by $\Delta\eta$ with respect to η, Fig. 47) was applied and the new steady-state current density was measured.

Figs. 48, 49, and 50 show three sets of two graphs, each comprising two steady-state Tafel plots: a Tafel plot for the metallic Ti to serve as a reference, and a Tafel plot for a colored passive film formed at a given AC voltage (10, 20, … , 60 V_{AC}).

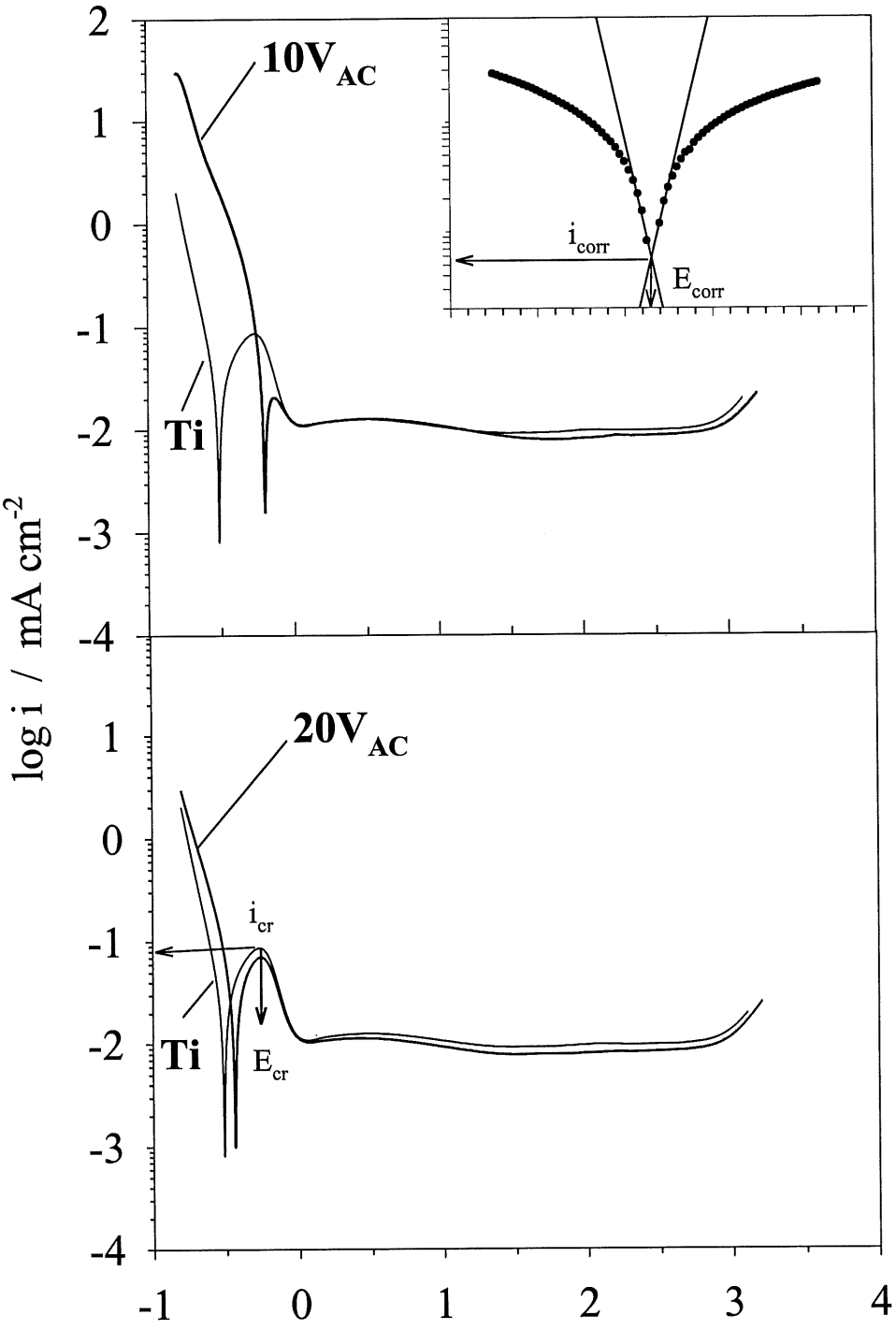

Figure 42. Two sets of two polarization curves, one for Ti (reference) and one for the passive films (formed at 10 and 20 V_{AC} in aq. 7.5 wt. % NH_4BF_4, T = 298 K, t = 10 s) in 1 M aq. H_2SO_4 (T = 298 K, s = 1 mV s^{-1}).

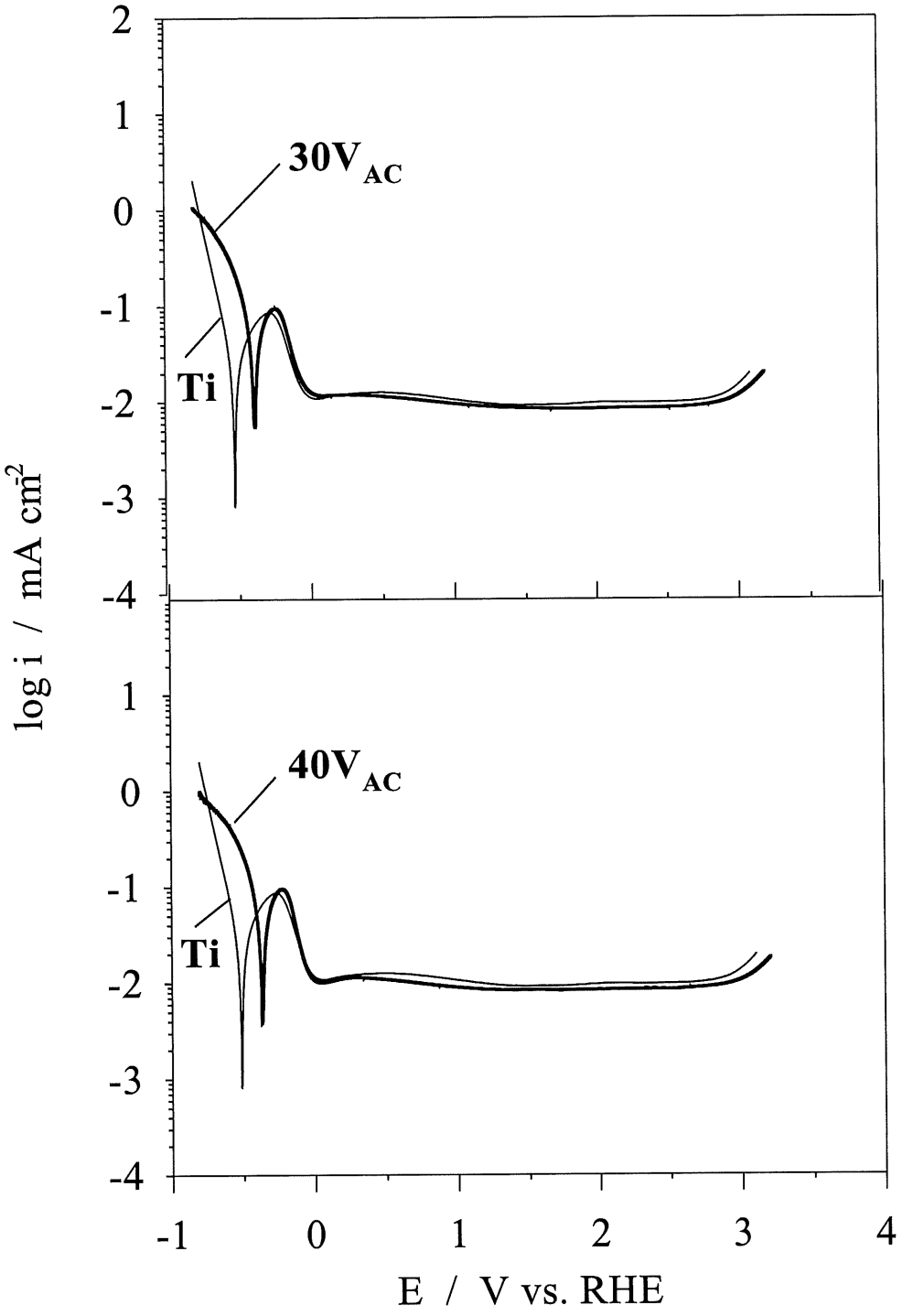

Figure 43. **Two sets of two polarization curves, one for Ti (reference) and one for the passive films (formed at 30 and 40 V_{AC} in aq. 7.5 wt. % NH_4BF_4, T = 298 K, t = 10 s) in 1 M aq. H_2SO_4 (T = 298 K, s = 1 mV s^{-1}).**

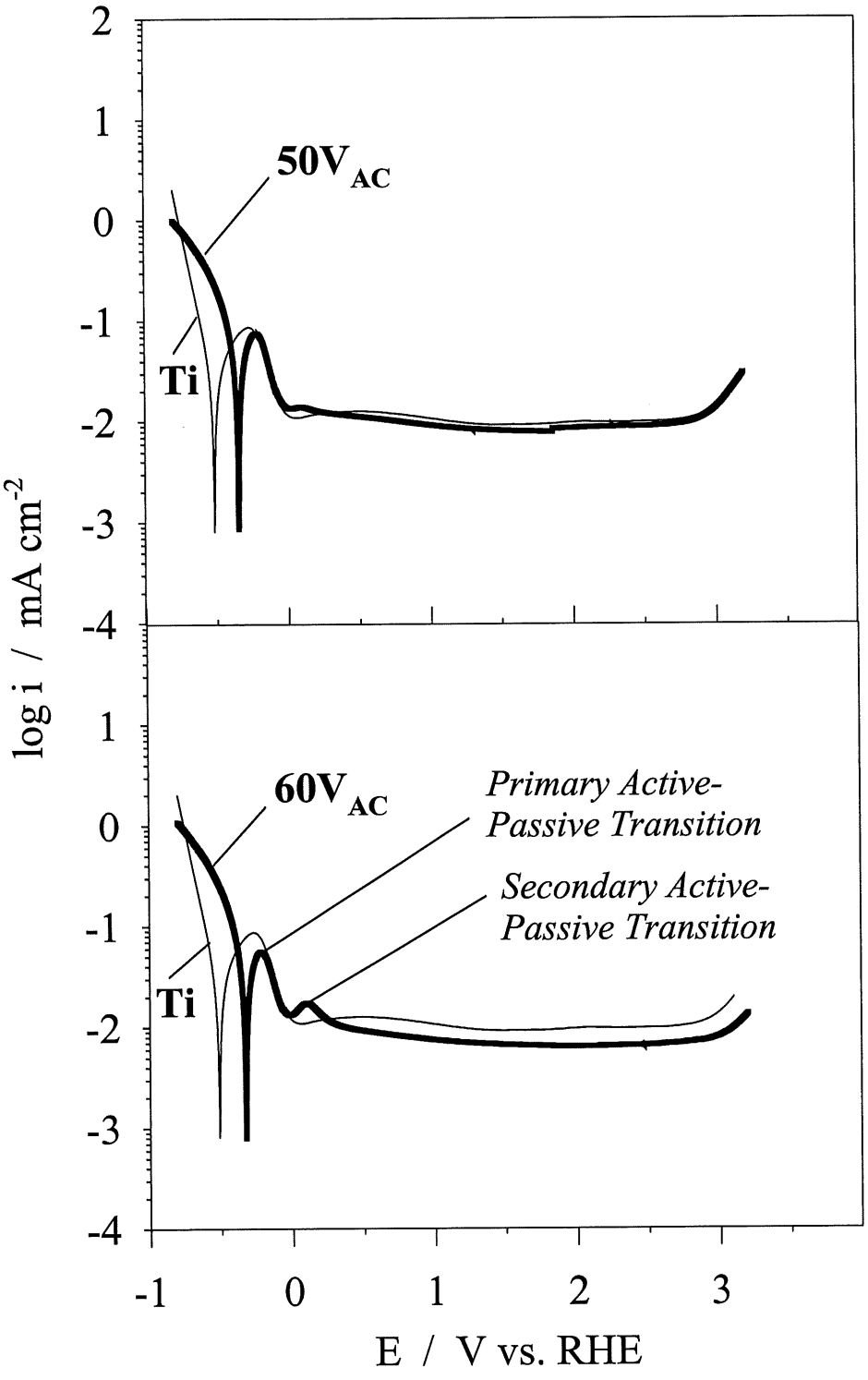

Figure 44. **Two sets of two polarization curves, one for Ti (reference) and one for the passive films (formed at 50 and 60 V_{AC} in aq. 7.5 wt. % NH_4BF_4, T = 298 K, t = 10 s) in 1 M aq. H_2SO_4 (T = 298 K, s = 1 mV s^{-1}).**

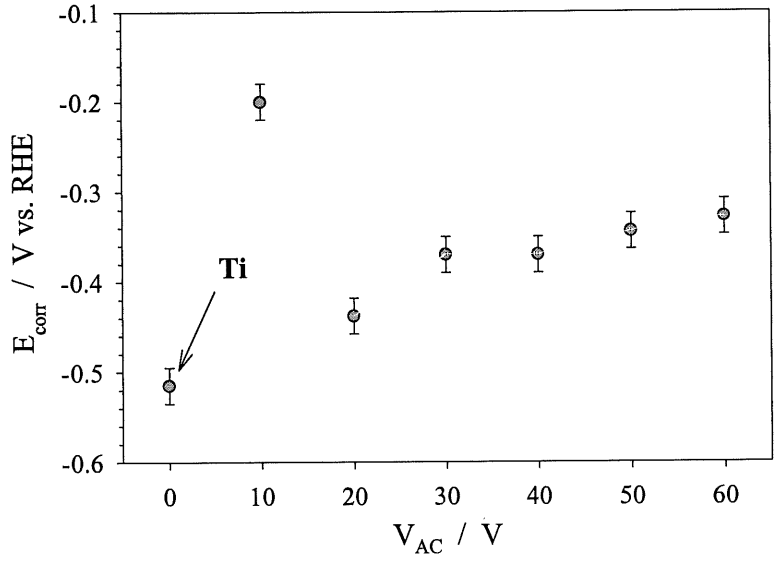

Figure 45. Relation between E_{corr} and V_{AC}. E_{corr} shifts 190 mV towards less negative potentials upon the colored layer formation.

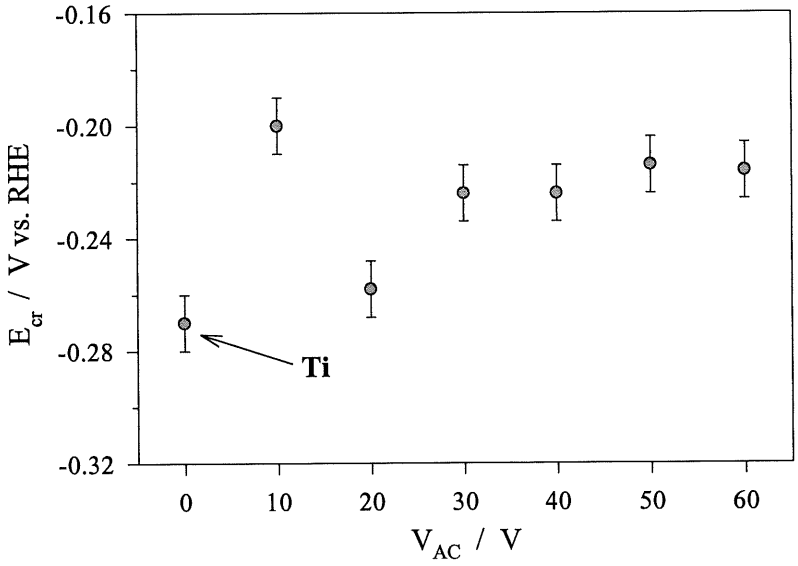

Figure 46. Relation between E_{cr} and V_{AC}. E_{cr} shifts 60 mV towards less-negative potentials upon the colored layer growth.

The Tafel polarization curve for pure Ti reveals two minima, one at ca. -0.20 V and the second one at ca. - 0.35 V vs. RHE. This behavior can be associated with two phenomena occurring simultaneously with the HER:

(i) the breakdown or partial reduction of the thin native passive film on Ti (TiO_2) that forms upon the pretreatment of Ti in aqueous solutions during etching and rinsing (at – 0.20 V vs. RHE); and

(ii) the onset of Ti hydride development as significant amounts of H become absorbed at more negative overpotentials (at – 0.35 V vs. RHE).

In the case of the colored passive layers on Ti, the Tafel polarization curves do not show a sharp, local minimum but rather a smooth transition from higher current densities towards lower ones. This local minimum is hardly visible in the case of the 10 or 20 V_{AC} passive layers, however, it becomes a well-defined feature for the $V \geq 30$ V_{AC} films. The Tafel plots show that this local minimum displaces towards more-negative overpotentials as we increase the AC voltage applied the form a given passive film. Finally, we observe that the current density that can be obtained at a given overpotential is significantly greater in the case of any passive layer than in the case of Ti (the only exception being the 60 V_{AC} film at very high overpotentials). Albeit the current densities that can be accomplished for the colored layers are much lower than those for other transition metals such as Pt, Ni, or Ni alloys, they are still greater than the current densities for metallic Ti. The data indicate that the increased activity of the colored layers (with respect to Ti) can be assigned to a lower charge transfer barrier imposed by the colored layer than the barrier associated with the native oxide (TiO_2) always present on Ti. Thus, it may be concluded that the passive layers are more active towards the HER than the metallic Ti, yet less active than other transition metals of the Group VIIIA.

The results of the electrochemical characterization of the colored Ti passive films demonstrate that they possess different properties from the metallic titanium in the negative potential range

and they show a certain resistance to H absorption. The latter behavior could be associated with formation of an internal interface that comprises a low Ti oxide state and Ti fluoride. This important conclusion could be drawn only on the basis of experimental data achieved using state-of-the-art surface-science tools such as XPS and AFM together with electrochemical techniques. The encouraging data presented above constitute a solid base for development of Ti-based cathodic materials that comprise the metallic Ti substrate, a colored layer and a catalytically active deposit of RuO_2 or/and IrO_2.

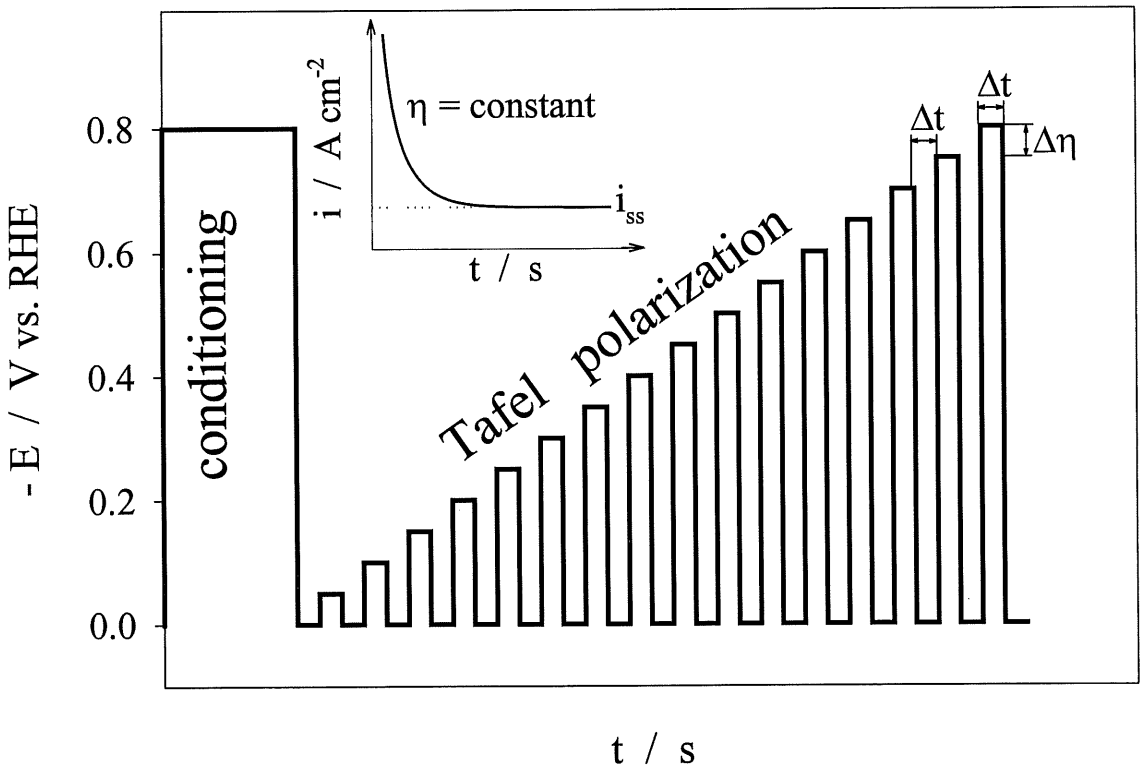

Figure 47. Program applied to obtain steady-state Tafel polarization curves for Ti and colored passive films. $\Delta\eta$ refers to the successive increment of the overpotential, η, and Δt refers to the polarization time and the conditioning time. The inset shows a typical current density, i, versus t transients until a steady-state current density, i_{ss}, becomes established.

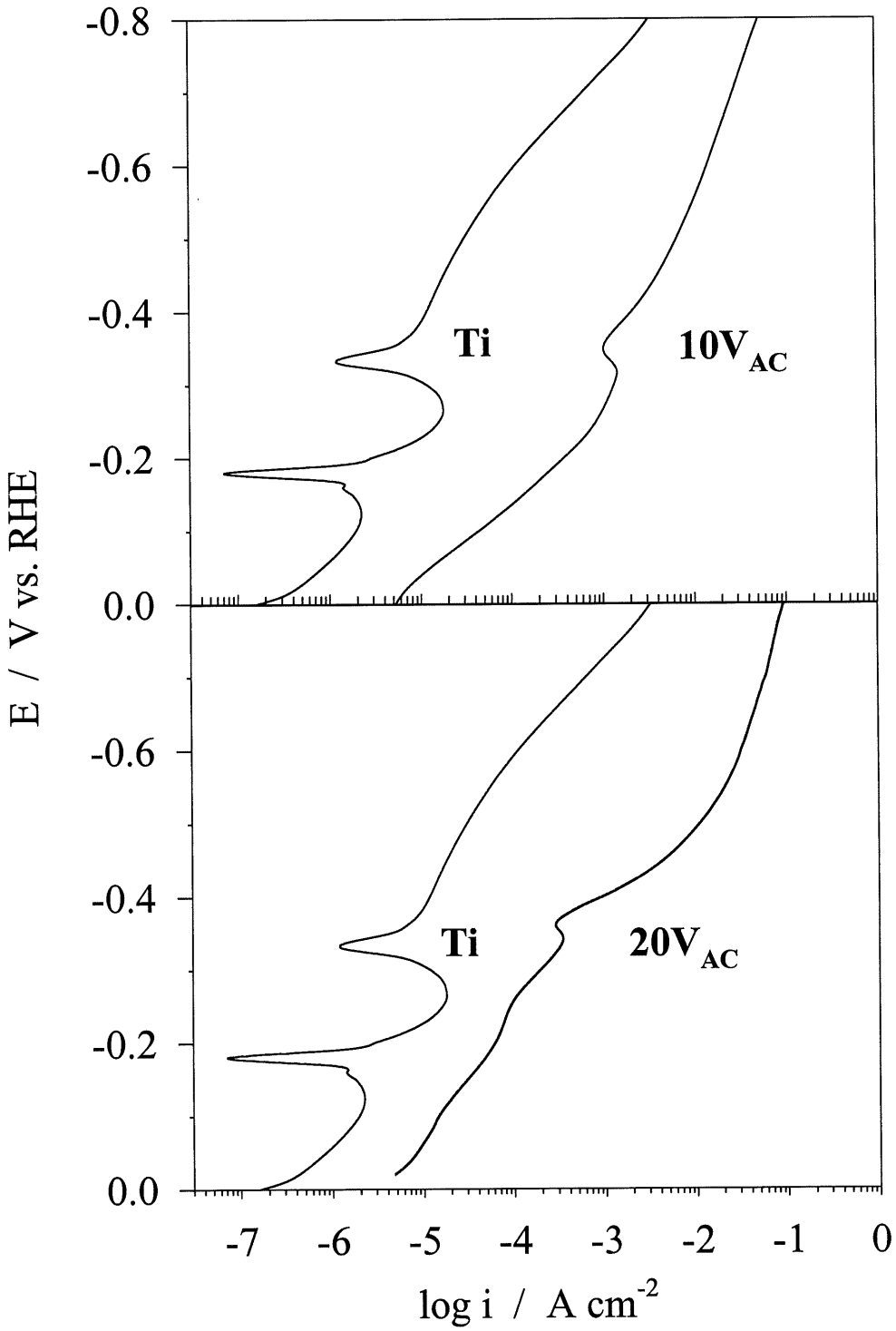

Figure 48. Steady-state Tafel polarization curves (E versus log i) for E from 0.00 V to -0.80 V vs. RHE, for Ti (reference) and two colored passive films (formed at 10 and 20 V_{AC} in aq. 7.5 wt. % NH_4BF_4, T = 298 K, t = 10 s) recorded in 1 M aq. H_2SO_4 (T = 298 K, s = 1 mV s^{-1}).

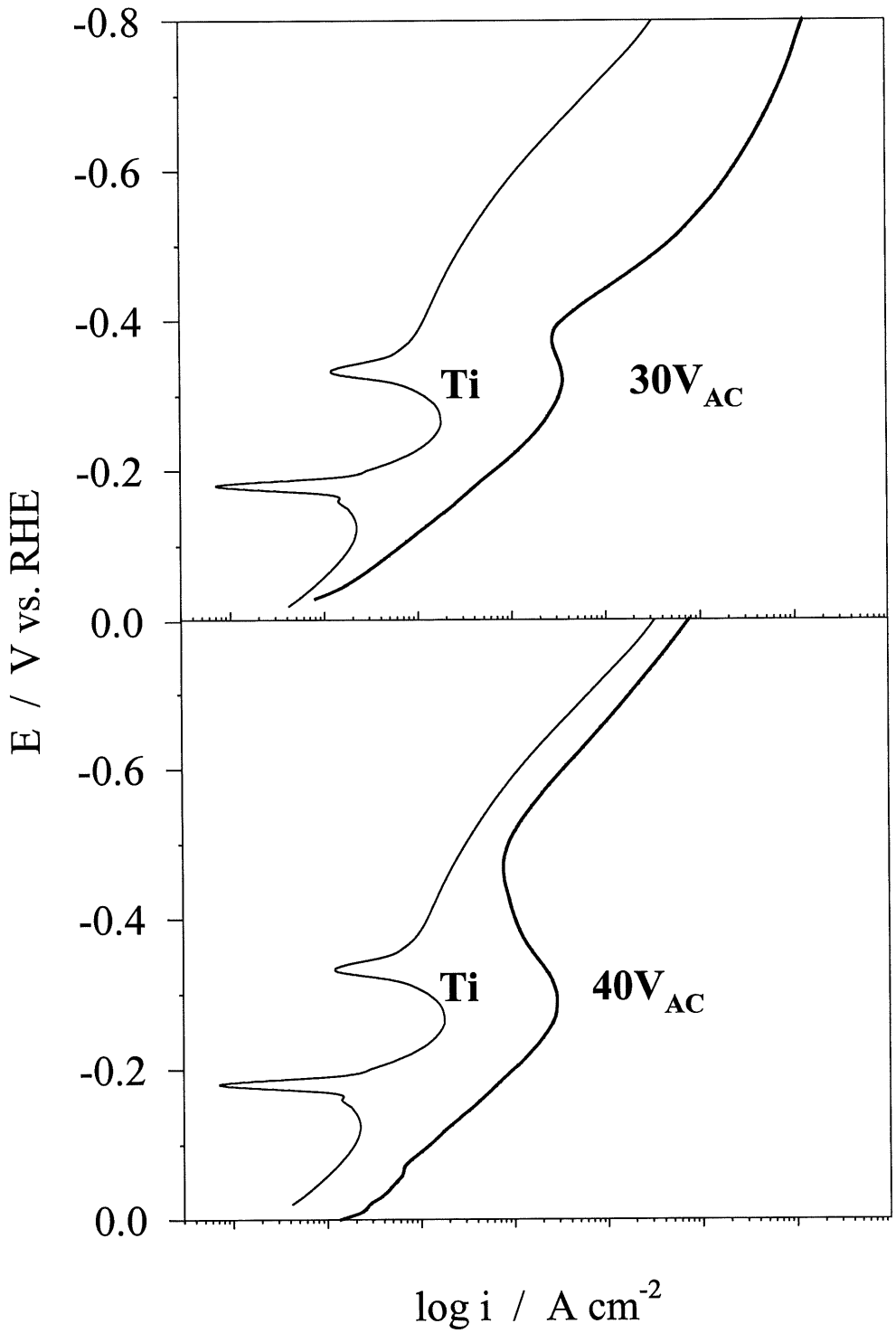

Figure 49. Steady-state Tafel polarization curves (E versus log i) for E from 0.00 V to -0.80 V vs. RHE, for Ti (reference) and two colored passive films (formed at 30 and 40 V_{AC} in aq. 7.5 wt. % NH_4BF_4, T = 298 K, t = 10 s) recorded in 1 M aq. H_2SO_4 (T = 298 K, s = 1 mV s^{-1}).

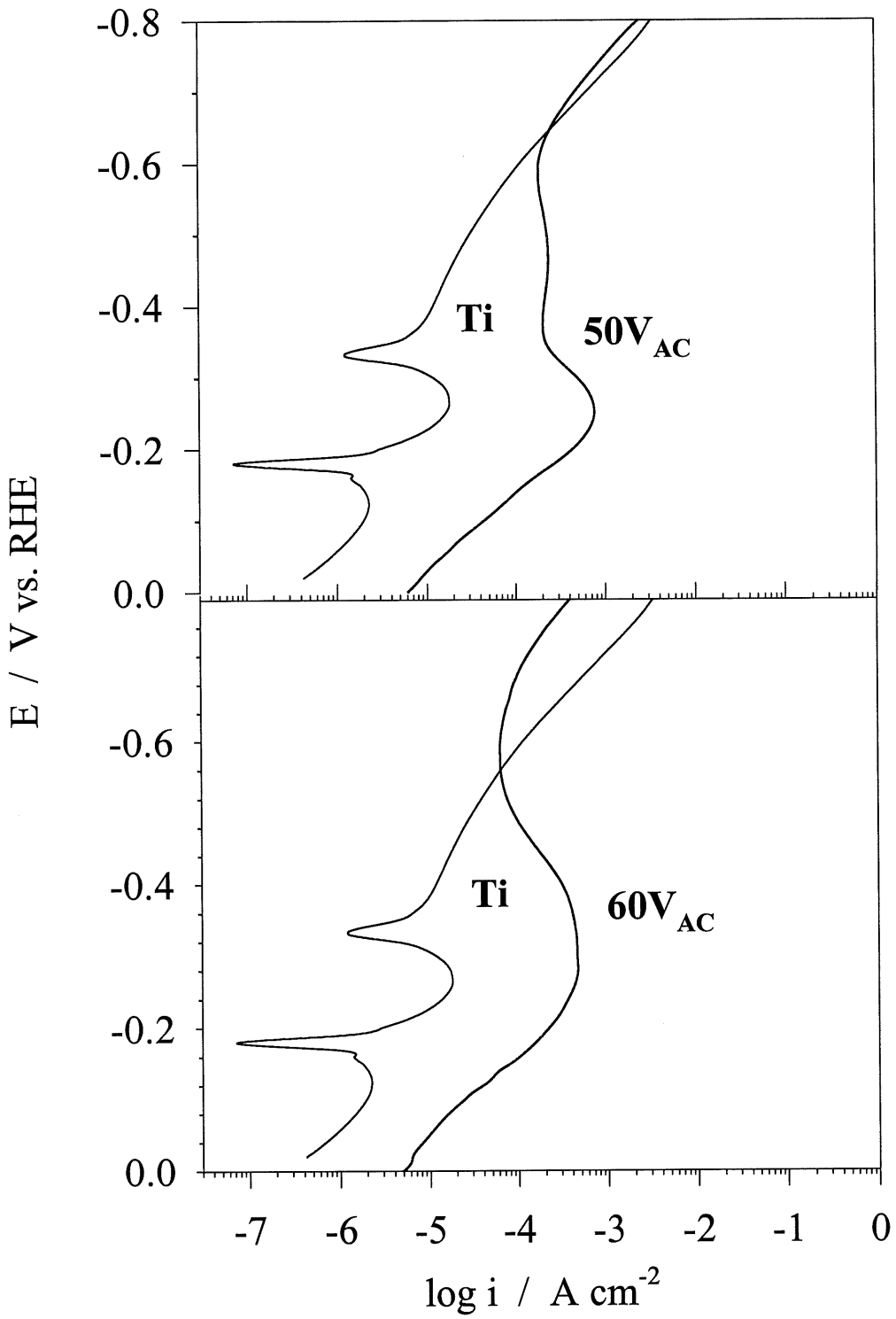

Figure 50. Steady-state Tafel polarization curves (E versus log i) for E from 0.00 V to -0.80 V vs. RHE, for Ti (reference) and two colored passive films (formed at 50 and 60 V_{AC} in aq. 7.5 wt. % NH_4BF_4, T = 298 K, t = 10 s) recorded in 1 M aq. H_2SO_4 (T = 298 K, s = 1 mV s^{-1}).

5.4 Influence of prolonged cathodic polarization on morphology and electrochemical behavior of titanium

In order to examine the resistance of titanium towards hydrogen embrittlement, we applied a constant negative current (-100 mA cm^{-2}) to a Ti electrode for different periods of time using a Hewlett Packard 6034A power supply. After each period of cathodic polarization, the electrode's morphology was examined by SEM and a polarization curve was recorded in order to analyze the changes in the electrochemical characteristics of titanium.

In Fig. 51, we show the results of SEM morphology analysis of the titanium electrode after the cathodic polarization. Fig. 51A refers to the Ti electrode freshly prepared and etched. The polycrystalline Ti structure with grains and grain boundaries with fairly uniform and non-destructed surface can easily be observed. After 1 hour of cathodic polarization (Fig. 51B), the morphology changes such as the appearance of pores and cracks along grain boundaries can be observed. Even by a naked eye, we noticed changes in the color of the electrode, which becomes dark-gray. After 4 additional hours of cathodic polarization (5 hrs in total), we observe (Fig. 51C) a progress in the cracking of titanium. The cracks becomes more pronounced and numerous. Moreover, the appearance of black points can represent the pitting of titanium (1) after 5 h of negative current application. Fig. 51D shows the black-grayish titanium hydride surface with clearly visible mechanical failure pits, cracks and inclusions produced after 10 h of cathodic polarization. Thus, the SEM analysis absolutely confirmed some previous results (49,52).

Not only mechanical properties but also electrochemical behavior of cathodicaly charged titanium electrodes were examined. The results show some unexpected and interesting behavior, such as the shift of the corrosion potential towards less negative values as we increase the time of cathodic polarization.

Fig. 52 shows polarization curves for pure and fresh Ti and Ti after the application of negative current density (cathodic polarization) for 3 h, 5 h, and 15 h. The corrosion parameters were determined the same way as in the case of the colored passive layers (see Section 5.2). We observe that upon an increase of the time of cathodic polarization, E_{corr} shifts from –0.48 V (RHE) for pure Ti, to – 0.41 V after 3 h of cathodic charging, and to – 0.35 V upon 5 h of cathodic charging. Finally, the corrosion potential stabilizes at – 0.33 V after 15 h of cathodic polarization. This shift of E_{corr} towards less negative values upon prolonged cathodic polarization does not mean that Ti becomes more noble with the hydrogen penetration,. Finally, the outcome of mechanical disintegration and corrosion of Ti caused by hydrogen penetration is clearly shown on Fig. 51.

The other electrochemical parameters such as E_{cr} , i_{cr}, and i_{corr} follow the overall tendency, i.e. they shift towards higher values upon cathodic charging. The role of the colored Ti passive layers as a barrier towards hydrogen embrittlement is negligible in the case of the cathodic charging for several hours. However, it cannot be excluded that further chemical treatment and modification could result in layers that become an effective barrier to H interfacial transfer.

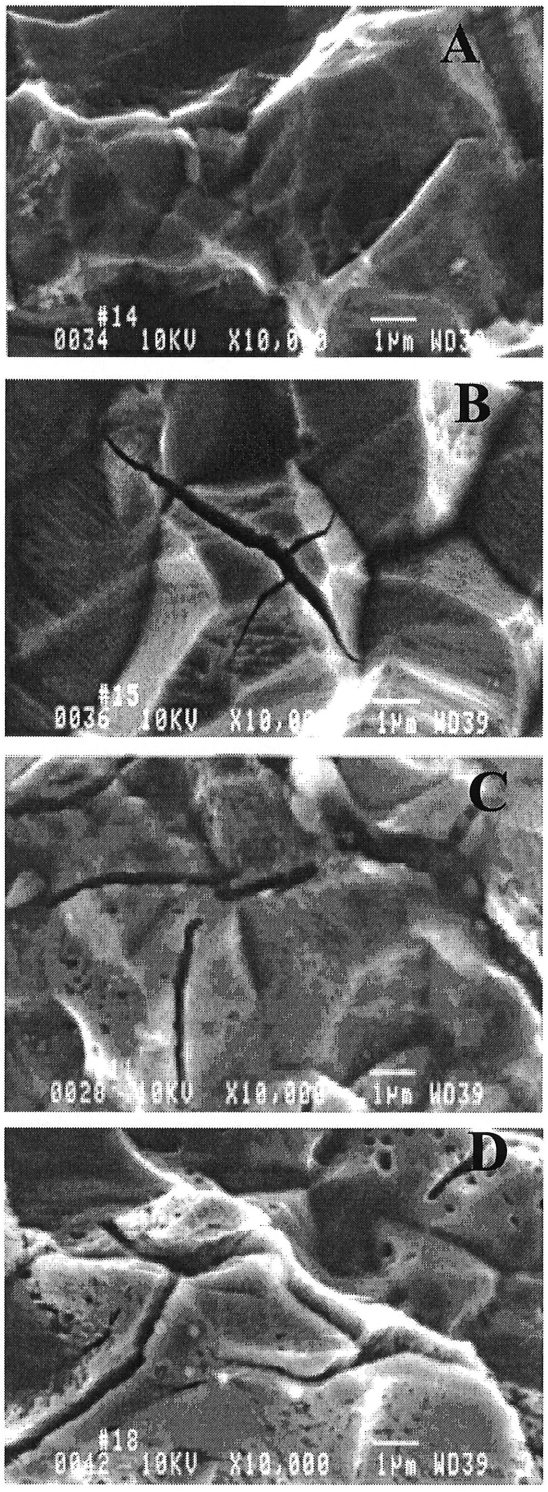

Figure 51. SEM analysis (10000 ×) of Ti electrodes after cathodic polarization at –100 mA cm^{-2} for different polarization times (A – 0 h, B – 1 h, C – 5 h, and D – 10 h) in 1 M aq. H_2SO_4 (T = 298 K).

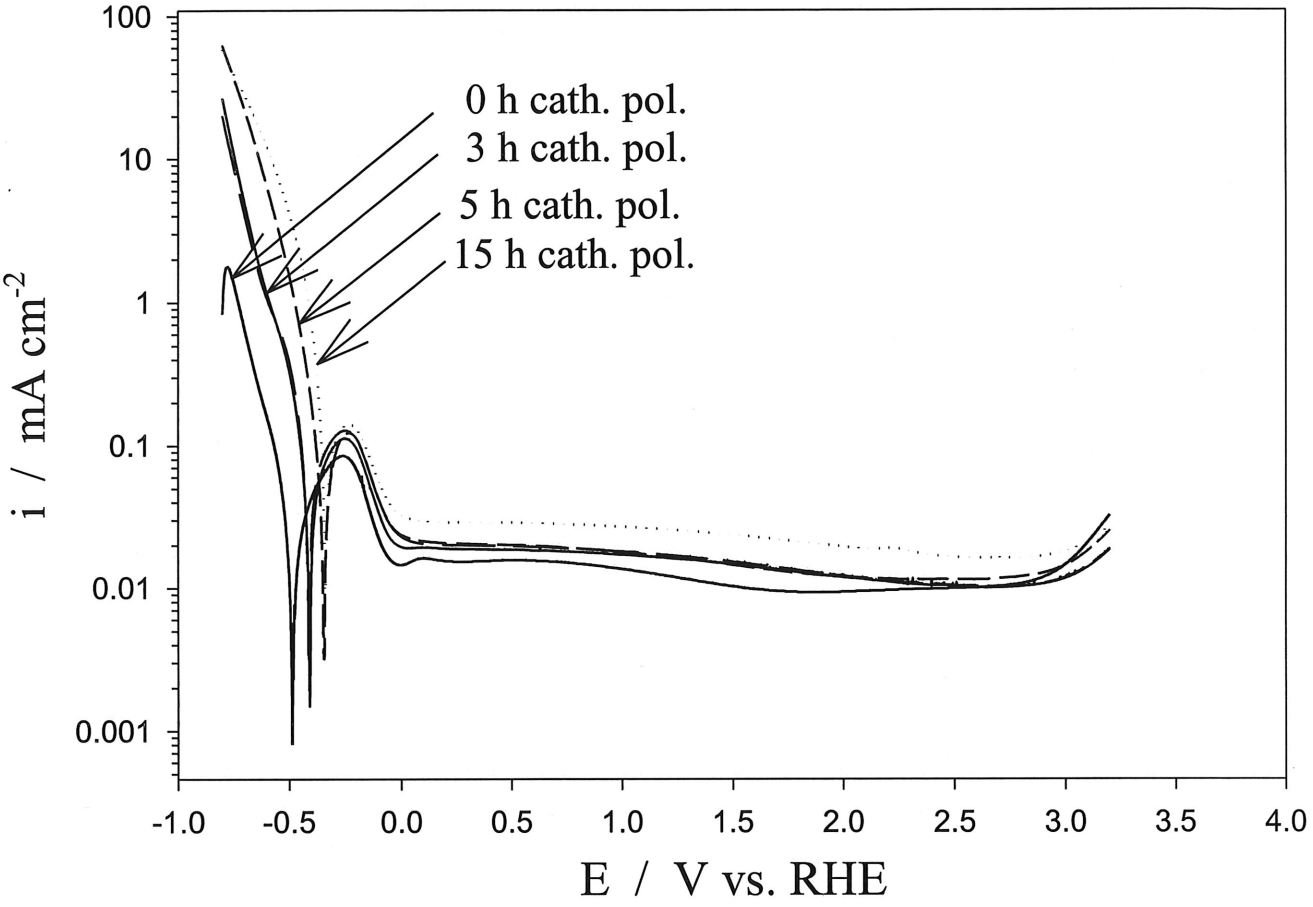

Figure 52. Impact of cathodic polarization on polarization curves of Ti after 1 h, 3 h, 5 h, and 10 h of polarization at – 100 mA cm^{-2} in 1 M aq. H_2SO_4 (T = 298 K, s = 1 mV s^{-1}).

CHAPTER 6

SURFACE CHEMICAL MODIFICATION OF THE COLORED TITANIUM PASSIVE LAYERS BY DEPOSITION OF RUTHENIUM OR/AND IRIDIUM OXIDE

Modification of the surface chemical composition and electrochemical properties of the colored titanium passive films was carried out by thermal decomposition of a respective chlorides (MCl_3, M = Ru or Ir) which result with deposition and intercalation of metal oxides (RuO_2 or/and IrO_2) on the surface of the colored layers of titanium (see Experimental). The interest in the surface modified Ti electrodes arises from the necessity to develop a suitable Ti-based cathodic material for the chlor-alkali industry where the carbon-steel electrode is unable to withstand the highly corrosive environment and has to be periodically replaced. However, its chemical stability can be enhanced through surface doping with Ru or/and Ir oxides accomplished through pyrolysis of the respective chlorides ($RuCl_3$ or $IrCl_3$). The surface-chemical modification of TiO_2 with IrO_2 or RuO_2 modifies the electronic properties of TiO_2 from semi-conducting to electronically conducting. Such prepared chemically modified mixed oxide layers reveal good catalytic properties towards the electrolytic O_2 and Cl_2 generation and are used as anode materials. Morphology of those modified layers was studied with SEM technique in order to obtain the information about surface characteristics of different noble metal oxide layers.

The objective of this work was to examine if surface-chemical modification of the colored Ti passive layers with RuO_2 or/and IrO_2 would result in catalytically active yet crack-free materials. It is well established that chemical modification of TiO_2 with RuO_2 or/and IrO_2 leads to an active but cracked and fractured layer (79,83). The presence of these structural defects makes them unsuitable as cathode materials because they do not protect the underlying Ti substrate that, eventually, becomes a subject of H embrittlement.

6.1 Morphology and chemical composition of the chemically modified layers of Ti

The morphology of the catalytic layers depends on a number of factors: (i) technique of solution spreading (immersion, brushing, spraying), (ii) solution concentration, (iii) film thickness, (iv) decomposition temperature, (v) heating rate, and (vi) atmosphere over the sample during the decomposition. Therefore, the selection of the suitable technique depends on the desired composition, morphology and cost (laboratory experiments vs. industrial production).

Fig. 53 shows SEM micrographs of three representative samples of doped Ti passive layers: RuO_2 (Fig. 53A), IrO_2 (Fig. 53B) and RuO_2+IrO_2 (Fig. 53C). These three layers are deposited on the passive film formed at 40 V_{AC}. The magnification is 2400 × for all the samples and it allows us to clearly examine the roughness and the morphology of the prepared electrode. There is a prominent difference in morphology between the RuO_2 and IrO_2 layers (Figs. 53A and 53B). The coatings obtained by thermal decomposition show a large number of interconnected microcracks that form discrete surface islands. Hence, the active surface area of the electrode has increased leading to a large capacitive charging current (see Section 6.2.4). The RuO_2+IrO_2 layer (Fig. 53C) presents mixed morphology characteristics of the RuO_2 and IrO_2 layers. Moreover, the IrO_2 and RuO_2+IrO_2 layers are cracked (29, 78), but the RuO_2 layer deposited on the 40 V_{AC} Ti passive layer is uniform, and importantly, crack-free.

In order to determine the chemical composition of the layers and to verify the applicability of the thermal treatment, an EDX analysis of the samples was performed. Fig. 54 shows the results of the EDX measurements performed on the same samples that were characterized by SEM. In order to facilitate the analysis, Fig. 54 comprises both EDX spectra and SEM micrographs. The results reveals pronounced Ru+Ti, Ir+Ti, and Ru+Ir+Ti signals showing that the thermal decomposition of the respective chlorides leads to a deposition of MO_2 (M = Ru, Ir, Ru + Ir) and its subsequent doping into the film via the solid-state diffusion (mixed solid-state mixed compound). Since EDX analysis does not reveal the presence of Cl

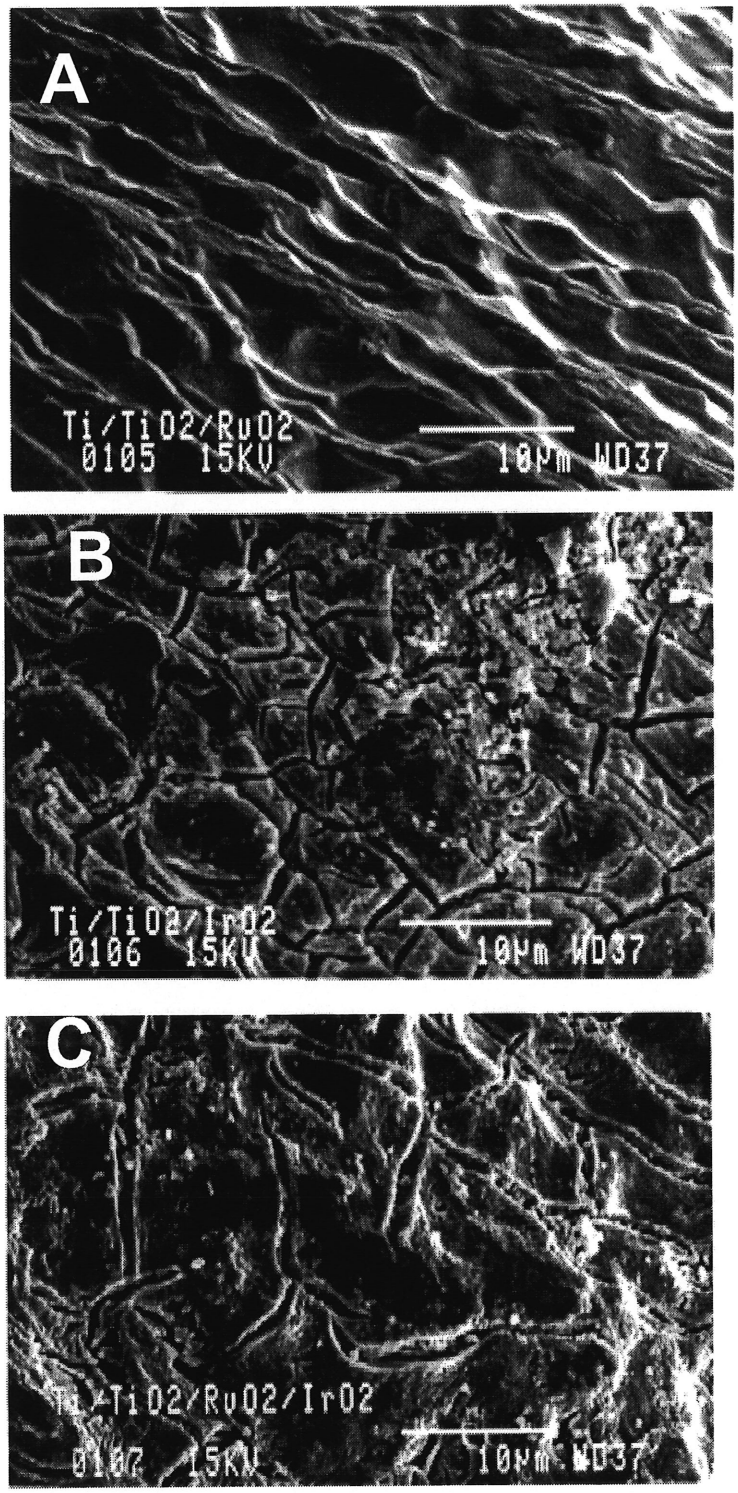

Figure 53. SEM micrographs of the chemically modified colored Ti passive layer formed at 40 V_{AC} in aq. 7.5% NH_4BF_4, t= 10 s, T = 298 K and doped with: A (RuO_2), B (IrO_2), and C (RuO_2/IrO_2).

incorporated in the doped layers, it may be concluded that they are chloride-free. Elsewhere, (33-35) it was shown that the presence of chloride led to a gradual decomposition of the film.

6.2 Electrochemical characteristics of the chemically modified passive layers

Electrochemical characterization of the modified films was accomplished by recording polarization curves, cyclic voltammetry profiles, and steady-state Tafel polarization plots in the hydrogen evolution reaction region. Important electrochemical parameters such as the Tafel slope, the exchange current density, the corrosion potential, the corrosion current density, and the extent of surface passivation were determined.

6.2.1 Polarization curves

Fig. 55 shows polarization curves of RuO_2 layer doped on: (a) pure Ti, (b) Ti passive layer formed at 20 V_{AC}, (c) Ti passive layer formed at 40 V_{AC}, and (d) Ti passive layer formed at 60 V_{AC}. The shape and corrosion parameters in the case of curves b, c, and d are similar. Only in the case of RuO_2 layer deposited directly on Ti (curve a in Fig. 55), the electrode shows lower activity towards the OER.

Fig. 56 shows polarization curves for a 40 V_{AC} passive film as well as for a 40 V_{AC} passive film chemically modified by deposition of RuO_2, IrO_2, and RuO_2+IrO_2. The transients allow us to compare their electrochemical properties. The shape of the polarization curves for doped layers is similar having the values of E_{corr} very close, between 0.65 V and 0.72 V vs. RHE. The corrosion potential for Ti passive layers formed at 40 V_{AC} is shown in Chapter 5 and its value is – 0.36 V vs. RHE. This result shows that the Ru or Ir modified layers are more noble vs. TiO_x. The doped films also show enhanced electrocatalytic activity towards the HER.

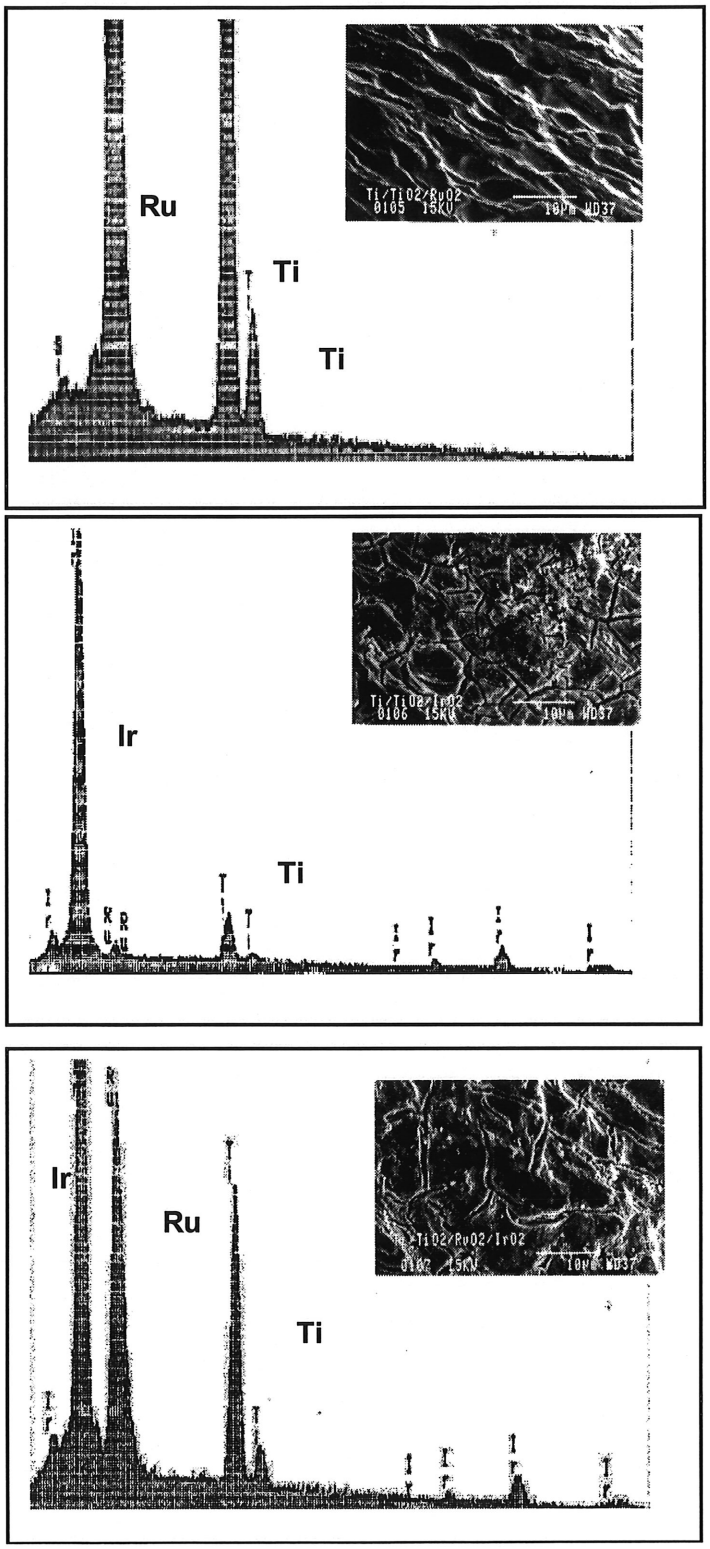

Figure 54. EDX spectra of the chemically modified colored Ti passive layer formed at 40 V_{AC} in aq. 7.5% NH_4BF_4, t= 10 s, T = 298 K : A (RuO_2), B (IrO_2), and C (RuO_2+IrO_2).

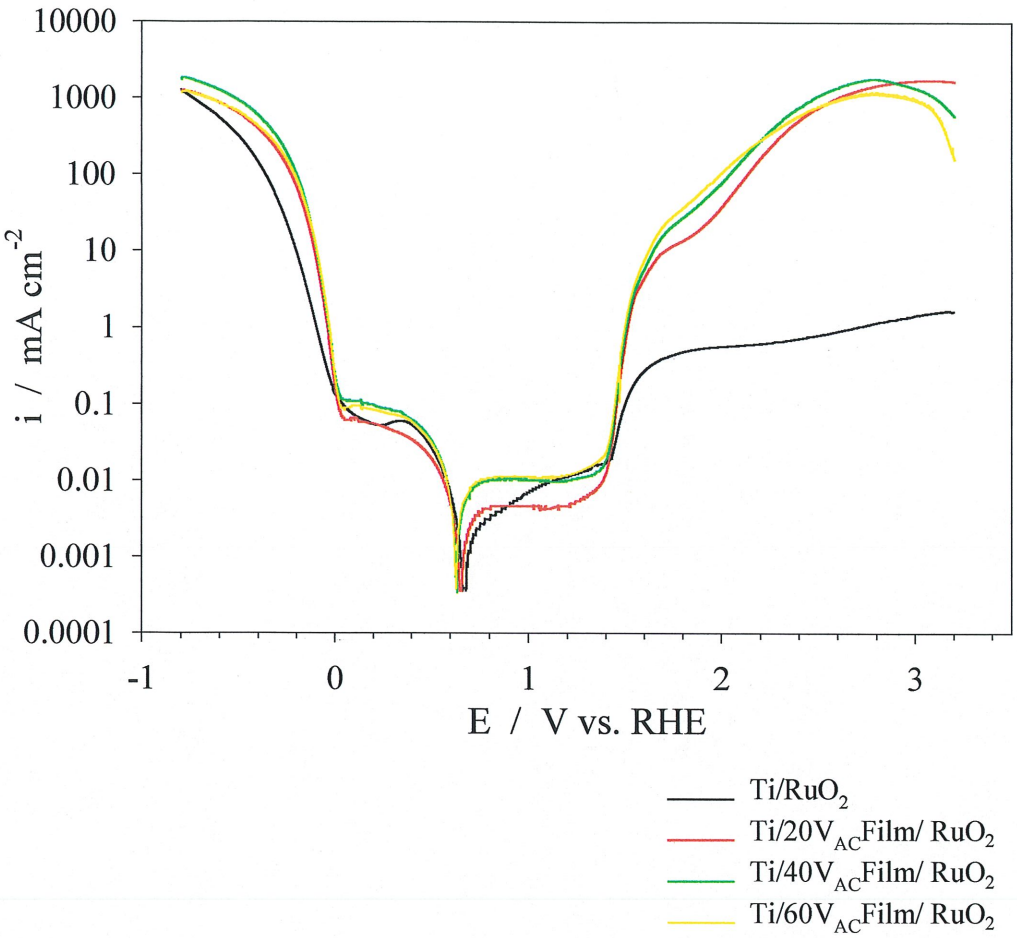

Figure 55. Set of polarization curves for the RuO_2 layer deposited on: (a) pure Ti, (b) Ti passive layer formed at 20 V_{AC}, in aq. 7.5% NH_4BF_4, t= 10 s, T = 298 K (c) Ti passive layer formed at 40 V_{AC} in aq. 7.5% NH_4BF_4, t= 10 s, T = 298 K, and (d) Ti passive layer formed at 60 V_{AC} in aq. 7.5% NH_4BF_4, t= 10 s, T = 298 K (recorded in 1M aq. H_2SO_4, T=298 K, s = 1 mV s^{-1}).

6.2.2 Impact of prolonged cathodic polarization on the chemically modified Ti passive layers

Elsewhere (see Section 5.4) it was show that cathodic polarization of Ti or colored passive layers on Ti lead to their disintegration via H embrittlement. One of the objectives of this project was to improve the resistance of the colored layers to H embrittlement through their chemical modification. In order to enhance the stability of Ti and Ti passive layers towards hydrogen penetration, we modified those films by Ru and/or Ir oxide deposition.

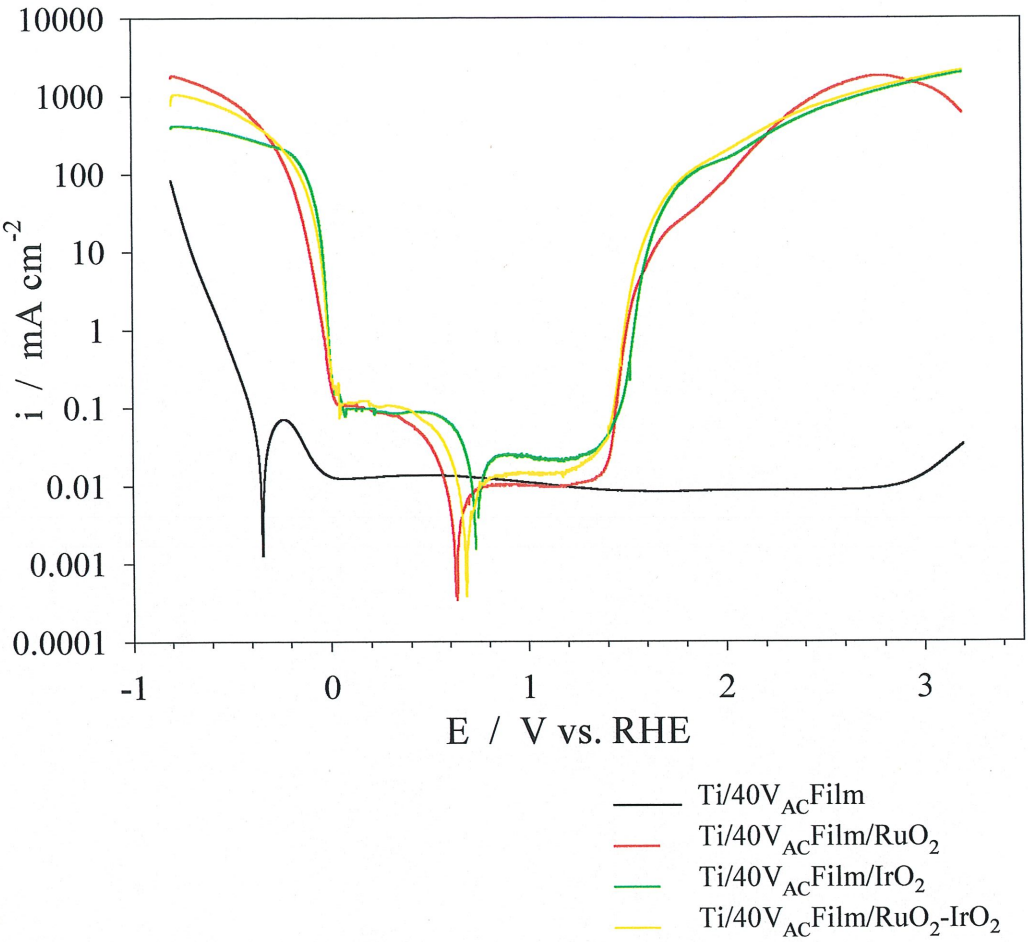

Figure 56. Set of polarization curves for: (a) the Ti passive film formed at 40 V_{AC} in aq. 7.5% NH_4BF_4, t= 10 s, T = 298 K, (b) the Ti passive film formed at 40 V_{AC} and doped by RuO_2, (c) the Ti passive film formed at 40 V_{AC} and doped by IrO_2, and (d) the Ti passive film formed at 40 V_{AC} and doped by RuO_2+IrO_2 (recorded in 1M aq. H_2SO_4 (T=298 K, s = 1 mV s^{-1}).

In Fig. 57, we show polarization curves for the RuO_2 modified film recorded every 5 hrs for the total polarization time up to 80 hrs. We selected only the RuO_2 modified layer because it was the only one that did not have crack or fractures. As it can be seen from Fig. 57, the layer is stable and unaffected during almost 20 hrs of cathodic charging. The only changes are visible in the OER region, where the electrode activity decreases upon the increase of the time of cathodic polarization. The corrosion potential, E_{corr} was constant during the initial 20 hrs of cathodic polarization (small graph in Fig. 57 presents E_{corr} vs. time of cathodic polarization).

After 35 hrs, a destruction of the electrode becomes evident and E_{corr} shifts towards negative potential values. This trend continues with the further cathodic polarization. After 80 hrs, the hydrogen damage was so prominent, that the shape of polarization curve resembled that of Ti (see Fig. 42). In conclusion the experiments show that the RuO_2 doped layers are much more resistant towards hydrogen embrittlement than pure Ti or colored passive layers on Ti. Under the same conditions, titanium was attacked by hydrogen very easily and fast. In contrast, the RuO_2 modified layer on the top of the 40 V_{AC} film was stable during almost 20 hrs of cathodic polarization. Additional efforts and improvements will be necessary to make this surface modified layer resistant towards hydrogen penetration for a period of time longer than weeks or months.

6.2.3 Open circuit potential behavior of Ti, Ti passive layers and modified Ti passive layers

In order to compare the open circuit behavior of colored Ti passive layers and the layers doped with RuO_2, IrO_2 and RuO_2+IrO_2, we measured the variation of E_{oc} with time in 1.0 M aq. H_2SO_4 (Fig. 58). For this experiment, three different passive films formed on 20, 40, and 60 V_{AC} as well as its films doped by RuO_2, IrO_2 and RuO_2+IrO_2 were prepared and placed in an electrochemical cell. The values obtained for the corrosion potential in open-circuit conditions for Ti, 20, 40, and 60 V_{AC} passive layers are consistent with the values of E_{corr} determined from polarization curves (see Fig. 45). The E_{corr} vs. time plot for the RuO_2, IrO_2 and RuO_2+IrO_2 modified layers is plane and smooth and they do not show any dissolution or decomposition.

The RuO_2, IrO_2 and RuO_2+IrO_2 modified layers do not show any dissolution or decomposition. Moreover, they are stable throughout the measurements keeping the values of the open circuit potential from 0.66 V for the RuO_2 modified layer to 0.70 V for the IrO_2 modified layer (the open circuit potential of the RuO_2 +IrO_2 layer is 0.69 V vs. RHE). These experiments confirm the improvement of the electrochemical properties of the colored Ti passive layers by their doping with RuO_2, IrO_2 and RuO_2+IrO_2.

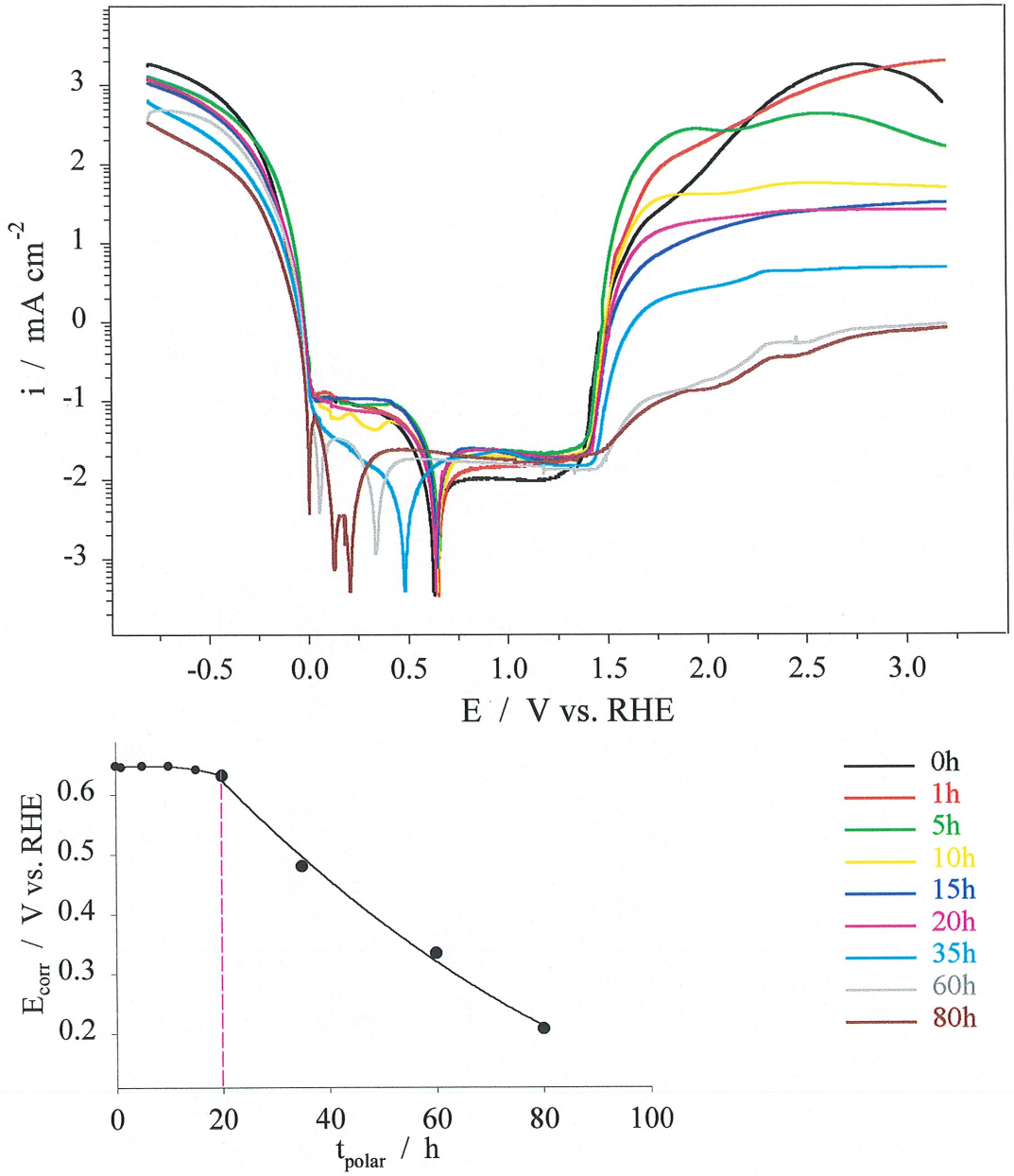

Figure 57. Impact of prolonged cathodic polarization (1 – 80 hours) at –100 mA cm^{-2} on polarization curves (upper graph) and E_{corr} (lower graph) of the colored film formed at 40 V_{AC} in aq. 7.5% NH_4BF_4, t= 10 s, T = 298 K and doped with RuO_2 (recorded in 1 M aq. H_2SO_4, T = 298 K, s = 1 mV s^{-1}).

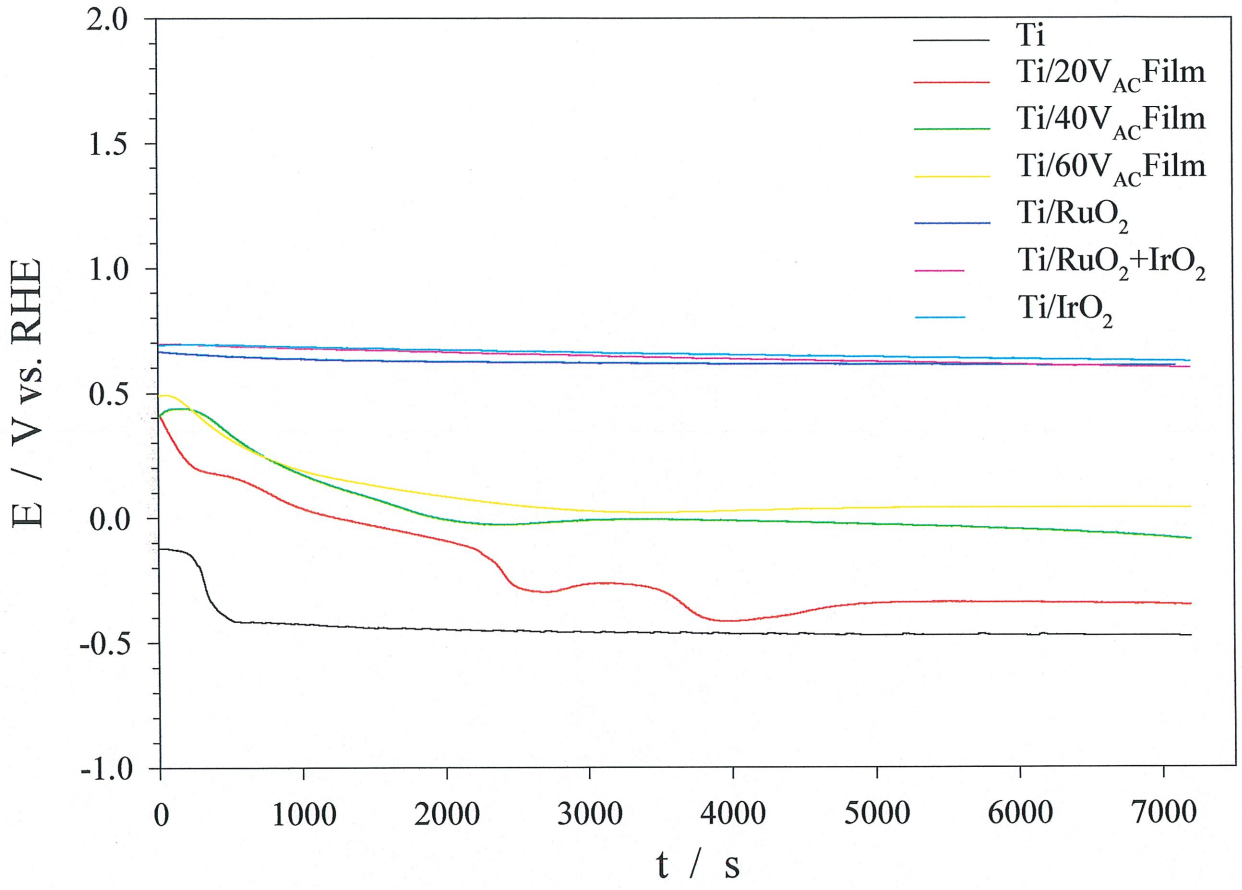

Figure 58. Ti, three colored Ti passive layers, and three modified colored Ti passive layers with RuO_2, IrO_2, and RuO_2 + IrO_2 under open-circuit conditions in 1 M aq. H_2SO_4, T = 298 K.

6.2.4 Cyclic voltammetry of surface modified Ti passive layers

Current density vs. potential (i vs. E) curves obtained using cyclic voltammetry are a good way to characterize the real surface of the modified Ti passive layers. Fig. 59 shows representative cyclic voltammograms in the double layer potential region for RuO_2, IrO_2, and RuO_2+IrO_2 doped Ti layers in 1.0 M aq. H_2SO_4 recorded at s = 100 mV s^{-1}. The upper and lower potential limits were 0.05 and 1.40 V vs. RHE, respectively. This behavior shown in Fig. 59 is typical of thermally prepared oxide layers and agrees with literature results (21, 29, 34). The broad

features are associated with a large surface heterogeneity (79). The reversible curves show that the $RuO_2 + IrO_2$ modified film has the largest real surface area, while the RuO_2-modified one has the smallest area. This observation well agrees with the SEM morphology data shown in Fig. 53.

Fig. 60 shows four cyclic voltammograms superposed for the 40 V_{AC} colored layer after chemical modification by deposition of RuO_2, IrO_2, and $RuO_2 + IrO_2$. The data indicate that the $RuO_2 + IrO_2$ modified layer has the greatest real surface area, while the RuO_2 one has the smallest one, with the IrO_2 modified layer being in between. Albeit these results coincide with those presented in Fig. 59, it is apparent that the presence of the 40 V_{AC} colored layer increases the double-layer charging current density that is a measure of the real surface area.

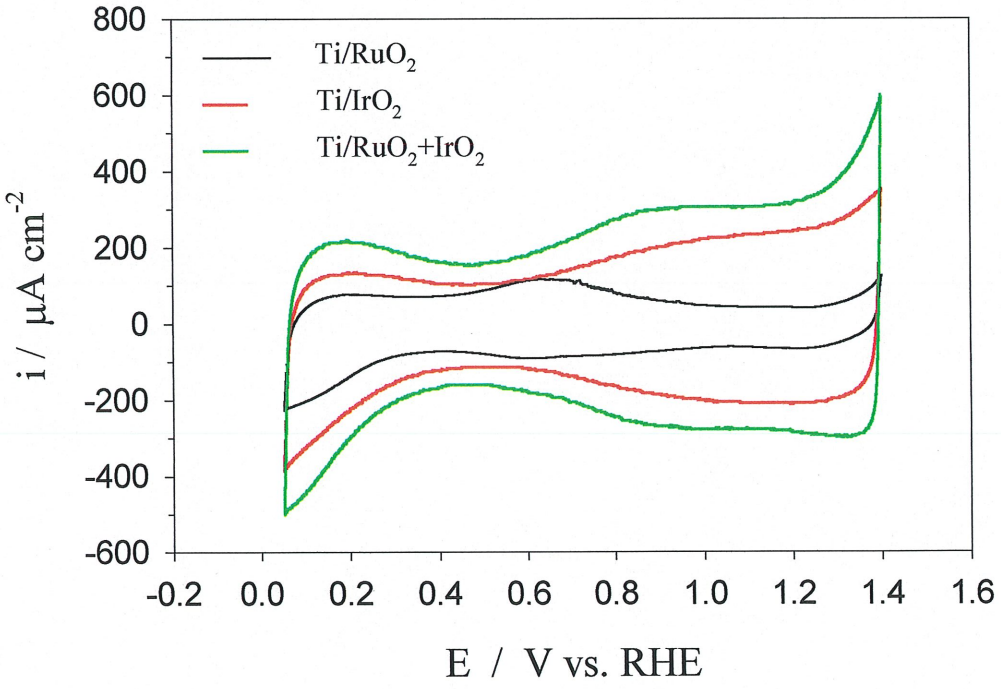

Figure 59. Cyclic voltammograms for Ti modified by deposition of RuO_2, IrO_2, and RuO_2+IrO_2 recorded in 1.0 M aq. H_2SO_4 (T = 298 K, s = 100 mV s^{-1}).

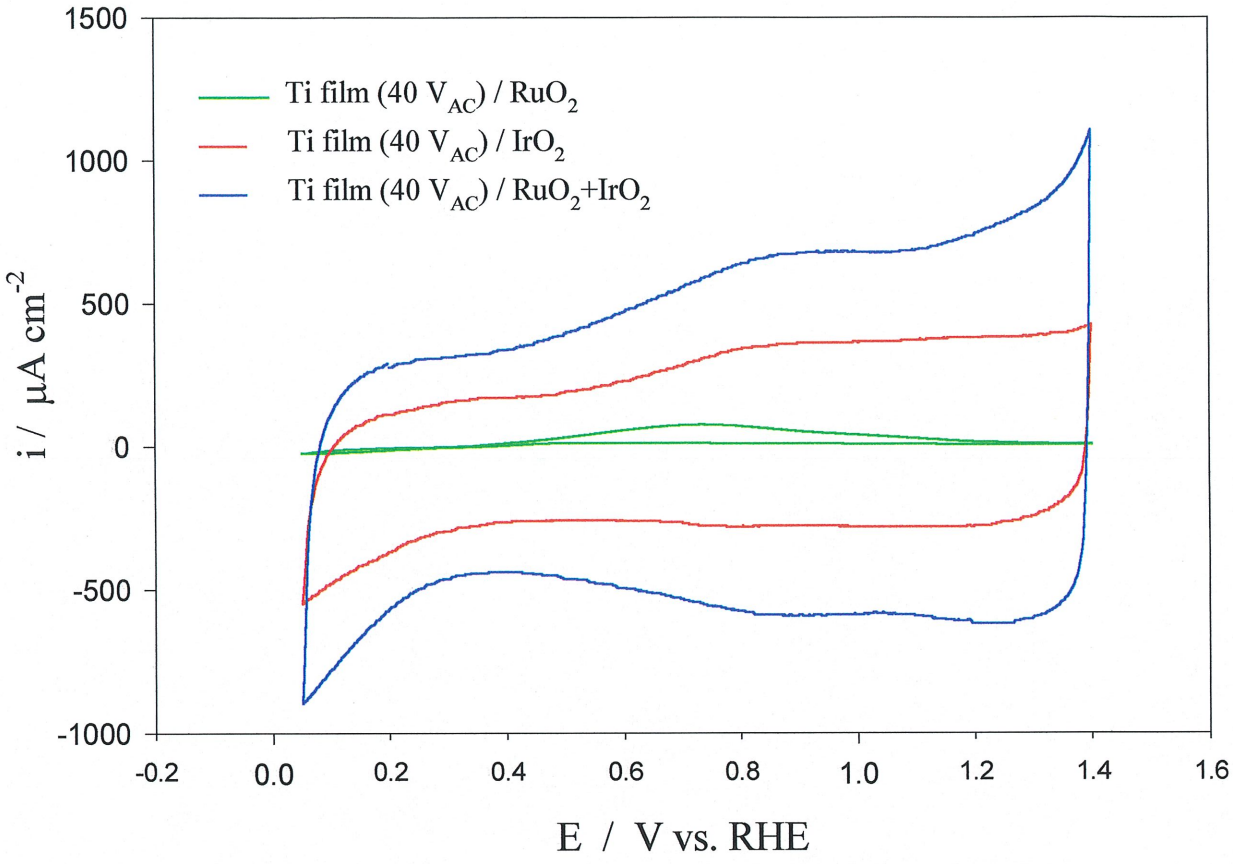

Figure 60. Cyclic voltammograms for Ti film formed at 40 V_{AC} in aq. 7.5% NH_4BF_4, t = 10 s, T = 298 K and doped with RuO_2, IrO_2, and RuO_2 + IrO_2 (recorded in 1.0 M aq. H_2SO_4, T = 298 K, s = 100 mV s^{-1}).

The impact of the scan rate on the cyclic voltammetric behavior of the 60 V_{AC} film modified with RuO_2 + IrO_2 was also examined. We selected this particular film because it exhibited the greatest real surface area and, therefore, it could become a suitable material for electrochemical supercapacitors (80). Cyclic voltammograms were recorded at various scan rates (s) between 10 and 100 mV s^{-1}. The influence of this parameter on the cyclic voltammograms is shown in Fig. 61. The current density exhibits almost a linear relationship with scan rate for the entire range investigated.

The inset in Fig. 61 shows the current density vs. scan rate relation at 0.50 V vs. RHE. The double layer capacitance C_{dl} was obtained from the slope of this relationship and its value was found to be 500 μF cm^{-2} , the value that is in good agreement with the values obtained in literature (81-84).

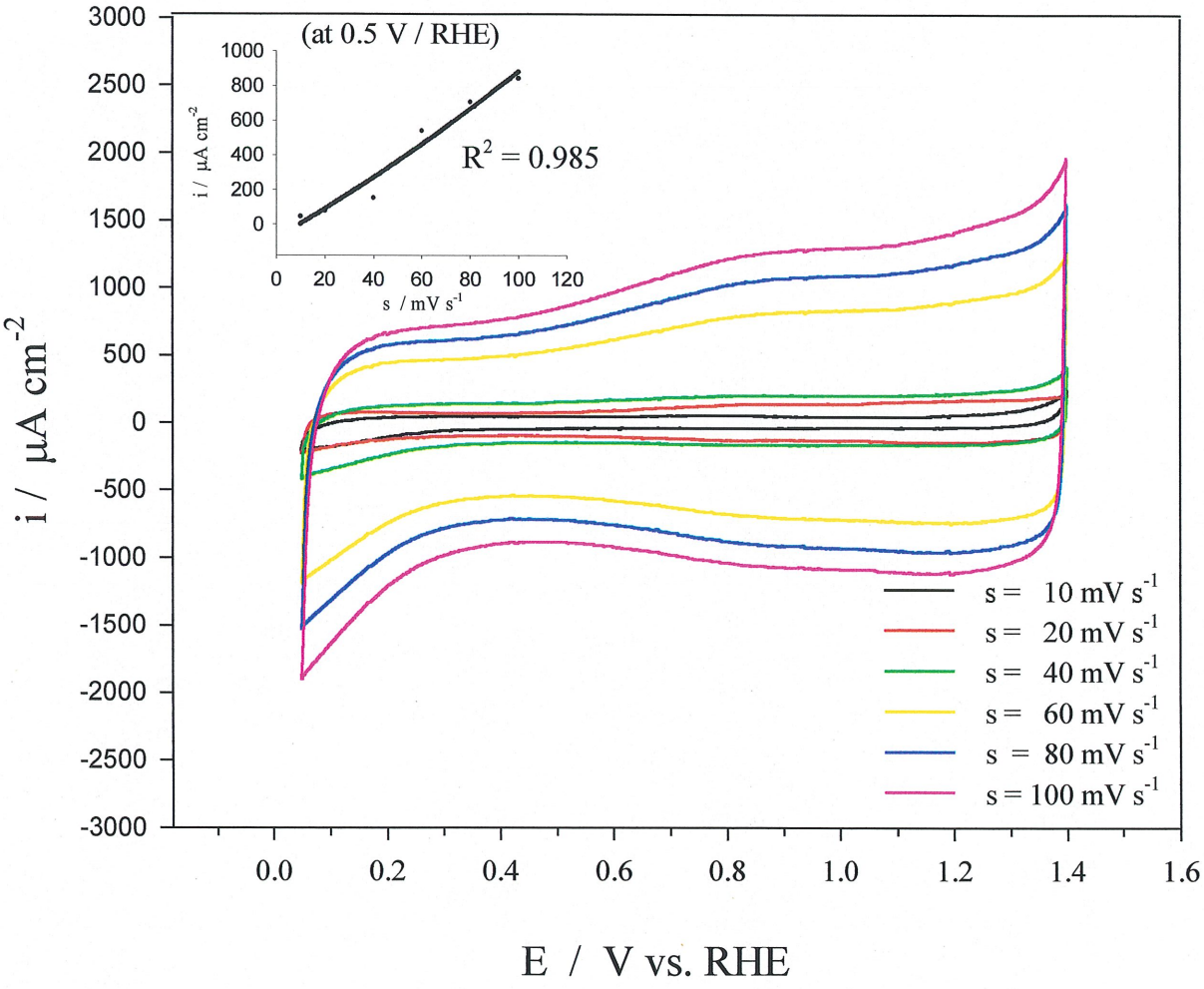

Figure 61. Cyclic voltammograms for the 60 V_{AC} film modified with RuO_2+IrO_2 recorded at different scan rates in 1.0 M aq. H_2SO_4, T = 298 K. The inset shows the current density vs. scan rate relation at 0.05 V vs. RHE.

6.2.5 HER Tafel plots for the chemically modified Ti passive layers

In order to compare the activity of the doped and undoped colored Ti passive layers towards the HER, Tafel plots were recorded between 0.00 and -0.80 V vs. RHE, in 1.0 M aq. H_2SO_4. The pre-treatment conditioning as well as the program used to obtain reproducible and meaningful steady-state Tafel polarizations were the same as those used in the Tafel plot analysis of the colored Ti passive layers (see Section 5.3). Figs. 62-65 show the steady-state Tafel polarization curves (E versus log i) for chemically modified Ti and chemically modified passive films. Tafel plots for pure Ti doped by IrO_2, RuO_2 and RuO_2+IrO_2 are shown in Fig. 62. Fig. 63 shows three Tafel plots for Ti passive layer formed at 20 V_{AC} and doped with IrO_2, RuO_2 and RuO_2+IrO_2. Tafel plots and parameters for the Ti passive layer formed at 40 V_{AC} and doped by the above mentioned oxides is presented in Fig. 64, and three passive layers formed at 60 V_{AC} and doped are presented in Fig. 65. The exchange current density (i_0) and Tafel slope (b) for each Tafel polarization curve were also determined and they are shown in a table below each Tafel plot (see Tables 1-4). Generally, all doped films are stable in the hydrogen evolution reaction region, without any breakdown or partial breakdown. The Tafel slope (b) varies from 13 mV (Ti/20 V_{AC}/RuO_2+IrO_2) to 111 mV (Ti/40 V_{AC}/RuO_2) depending on the overpotential and chemical treatment. The highest values of the Tafel slope show the 60 V_{AC} passive layer on Ti doped by IrO_2, RuO_2 and RuO_2+IrO_2. The Ti passive layer formed at 60 V_{AC} and doped by RuO_2 exhibit two values of overpotentials (low η at 70 mV and high η at 111 mV). The shape of the IrO_2 doped pure Ti or titanium passive layers (black circles in Figs. 62-65) varies from – 0.4 to – 0.6 V vs. RHE. The exchange current densities vary from 0.54 x 10^{-6} mA cm^{-2} (Ti/40 V_{AC}/RuO_2) to 110 x 10^{-6} mA cm^{-2} (Ti/20 V_{AC}/IrO_2). The comparison of Tafel behavior of Ti passive layers and doped Ti passive layers clearly shows that the current density which can be obtained at a given overpotential is significantly greater in the case of doped passive layers than undoped ones. As a conclusion for this set of experiments we may say that the surface modified Ti passive films are much more active towards the HER than the passive films on Ti or pure Ti.

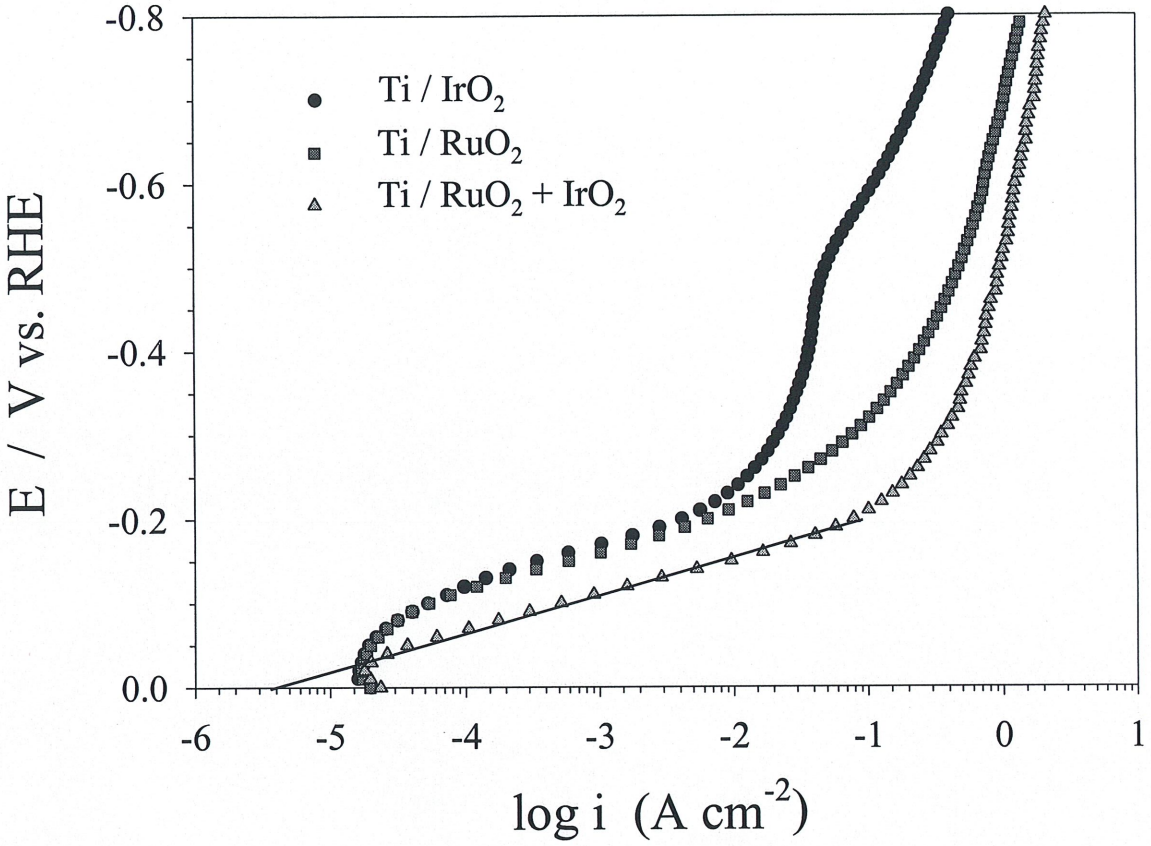

Figure 62. Steady-state Tafel polarization curves (E versus log i) for E from 0.00 V to -0.80 V vs. RHE, for Ti doped with IrO_2, RuO_2, and RuO_2+IrO_2 recorded in 1M aq. H_2SO_4 (T = 298 K).

Table 1. Tafel plot parameters: exchange current density (i_0) and Tafel slope (b) for Ti doped with IrO_2, RuO_2, and RuO_2+IrO_2.

Type of electrode	i_0 (mA cm^{-2})	b (mV)
Ti / IrO_2	$1.1 \cdot 10^{-6}$	58
Ti / RuO_2	$0.9 \cdot 10^{-6}$	57
Ti / RuO_2+IrO_2	$2.7 \cdot 10^{-6}$	43

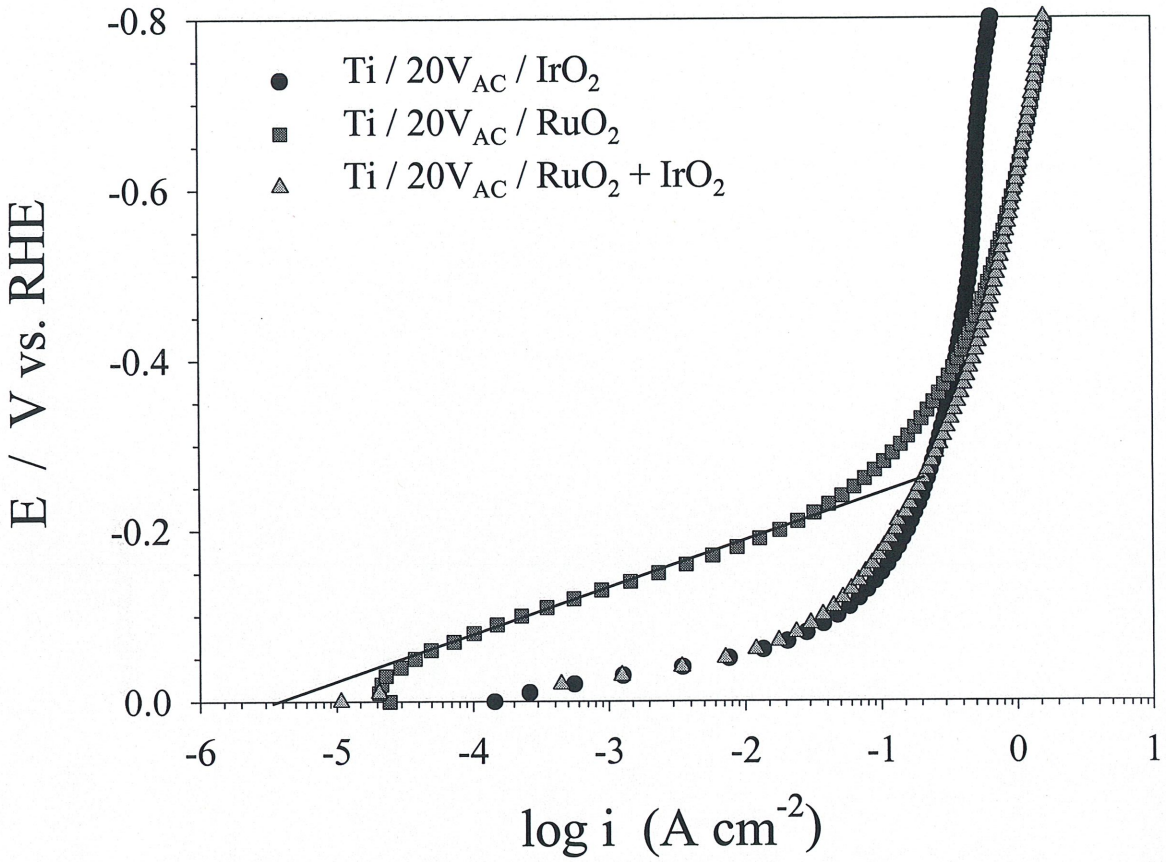

Figure 63. Steady-state Tafel polarization curves (E versus log i) for E from 0.00 V to -0.80 V vs. RHE, for Ti (20V_{AC} film) doped with IrO_2, RuO_2, and RuO_2+IrO_2 recorded in 1M aq. H_2SO_4 (T = 298 K).

Table 2. Tafel plot parameters: exchange current density (i_0) and Tafel slope (b) for Ti (20V_{AC} film) doped with IrO_2, RuO_2, and RuO_2+IrO_2.

Type of electrode	i_0 (mA cm^{-2}))	b (mV)
Ti (20V_{AC})/ IrO_2	$110 \cdot 10^{-6}$	28
Ti (20V_{AC})/ RuO_2	$3.8 \cdot 10^{-6}$	59
Ti(20V_{AC})/RuO_2+IrO_2	$4.9 \cdot 10^{-6}$	13

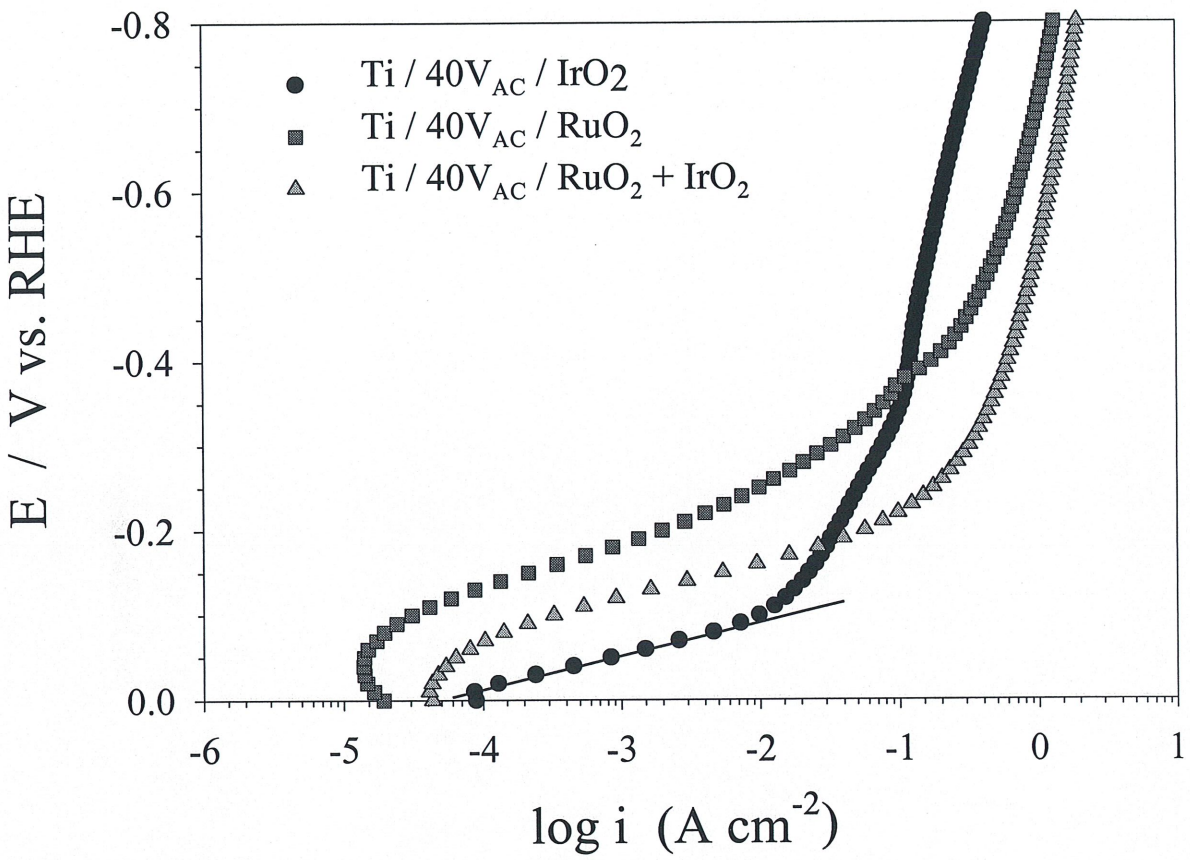

Figure 64. Steady-state Tafel polarization curves (E versus log i) for E from 0.00 V to -0.80 V vs. RHE, for Ti ($40V_{AC}$ film) doped with IrO_2, RuO_2, and RuO_2+IrO_2 recorded in 1M aq. H_2SO_4 (T = 298 K).

Table 3. Tafel plot parameters: exchange current density (i_0) and Tafel slope (b) for Ti ($40V_{AC}$ film) doped with IrO_2, RuO_2, and RuO_2+IrO_2.

Type of electrode	i_0 (mA cm^{-2}))	b (mV)
Ti($40V_{AC}$) / IrO_2	$45 \cdot 10^{-6}$	40
Ti ($40V_{AC}$)/ RuO_2	$0.54 \cdot 10^{-6}$	57
Ti ($40V_{AC}$)/ RuO_2+IrO_2	$1.6 \cdot 10^{-6}$	43

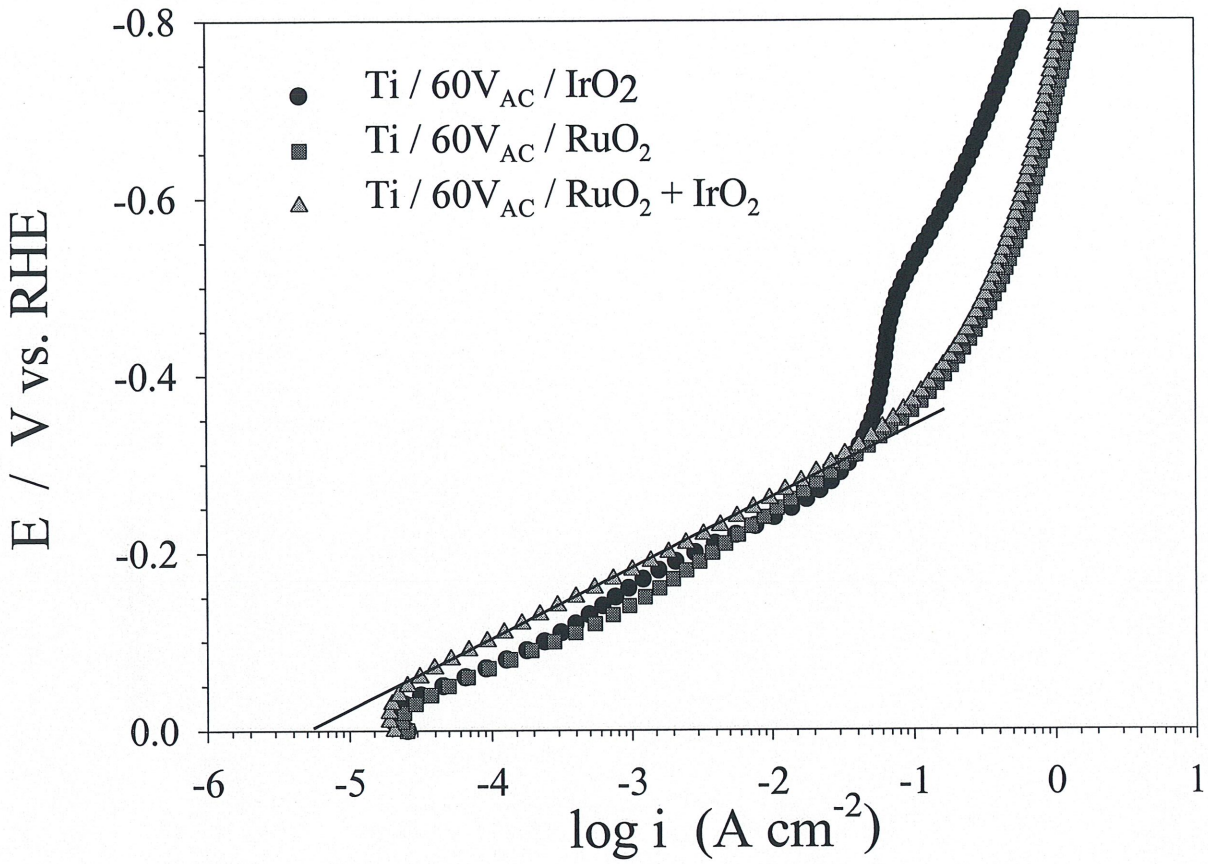

Figure 65. Steady-state Tafel polarization curves (E versus log i) for E from 0.00 V to -0.80 V. vs., RHE, for Ti ($60V_{AC}$ film) doped with IrO_2, RuO_2, and RuO_2+IrO_2 recorded in 1M aq. H_2SO_4 (T = 298 K).

Table 4. Tafel plot parameters: exchange current density (i_0) and Tafel slope (b) for Ti ($60V_{AC}$ film) doped with IrO_2, RuO_2, and RuO_2+IrO_2

Type of electrode	i_0 (mA cm^{-2}))		b (mV)
Ti($60V_{AC}$) / IrO_2	$12 \cdot 10^{-6}$		83
Ti($60V_{AC}$) / RuO_2	$9.6 \cdot 10^{-6}$	(low η)	70
	$60 \cdot 10^{-6}$	(high η)	111
Ti ($60V_{AC}$) / RuO_2+IrO_2	$1.6 \cdot 10^{-6}$		84

CHAPTER 7

MORPHOLOGY AND ELECTROCHEMICAL CHARACTERIZATION OF EBONEX® ON TITANIUM

Ebonex® is a ceramic material based on the Magneli suboxides of titanium. The main material for the production of Ebonex® is titanium dioxide which is one of the most abundant Ti materials produced by the chemical industry. The non-stoichiometric oxides are blue-black in color and electronically conductive, whilst retaining a high corrosion resistance and a low toxicity. They are electrode materials in the electrochemical industry owing to their corrosion resistance and electronic conductivity. Titanium based materials already play an important role in electrochemistry because of their high stability. The Magneli phase-Ti conductive oxides (Ti_4O_7 and Ti_5O_9) are known to have comparable conductivities (85) and therefore, they attracted much attention (86,87). Ebonex®, a conductive ceramic material, is mainly composed of the Magneli phase titanium oxides (Ti_4O_7 and Ti_5O_9) and is considered a suitable electrode material because of its bulk conductivity that matches that of carbon and graphite electrodes. It is resistant to corrosion in various aqueous electrolytes and shows no tendency to form hydride upon contact with molecular hydrogen or upon cathodic polarization. Pletcher et al. (86) have studied the kinetics of the ferro/ferricyanide couple at Ebonex® electrodes. They have also electrodeposited five metals such as Cu, Au, Ni, Pd, and Pt on Ebonex® in order to modify its properties and, then, they investigated the electrochemical characteristics of such modified electrode materials (87).

7.1 SEM analysis of Ebonex® on Ti

SEM analysis was performed at three different magnifications, namely 1 000, 3 000, and 10 000 ×, in order to bring out any surface features. Fig. 66 presents the SEM micrographs of the Ebonex® coated Ti at the magnification 1000 and 3000 ×. The Ebonex® coating does not

show any grain structure, but it shows some typical features of ceramic electrodes (pores and disordered regions between crystallites). Darker regions on the photographs represent deeper surface areas, giving us the impression of an irregular, porous surface. However, this structure shows the high roughness of the coating, which may be related to the high electrocatalytic activity of this material. No traces of titanium metal substrate we observed, indicating uniformity in the coating layer. Moreover, this morphology analysis data indicates that the electrochemical characteristics subsequently determined are characteristic of Ebonex®-Ti material.

7.2 Electrochemical characterization of Ebonex® on Ti

The instrumentation and preparation of electrodes for electrochemical characterization of the EBONEX® coating on Ti were described in Experimental. We focused our attention on the determination of the corrosion potential and current density, E_{corr} and i_{corr}, the critical potential and current density, E_{cr} and i_{cr}, the extent of surface passivation, and the potential of the onset of the OER.

7.2.1 Polarization curves

Fig. 67 shows polarization curves for pure Ti, the colored Ti passive layer formed at 60 V_{AC} and Ebonex® on Ti. These three curves are superimposed in order to compare the electrochemical parameters of the three different electrode materials. Corrosion parameters of metallic Ti were already determined (see Chapter 5) and they are as follows: $E_{corr} = -0.51$ V and $E_{cr} = -0.27$ V vs. RHE. The electrochemical parameters for the colored Ti passive layer formed at 60 V_{AC} are: $E_{corr} = -0.33$ V and $E_{cr} = -0.22$ V vs. RHE. Ebonex® on Ti exhibits even more pronounced shift of E_{corr} and E_{cr} towards less-negative potentials with respect to Ti, thus revealing its stability: ($E_{corr} = -0.24$ V and $E_{cr} = -0.09$ V vs. RHE). The overpotentials for the HER and OER are lower than for Ti or the colored passive films.

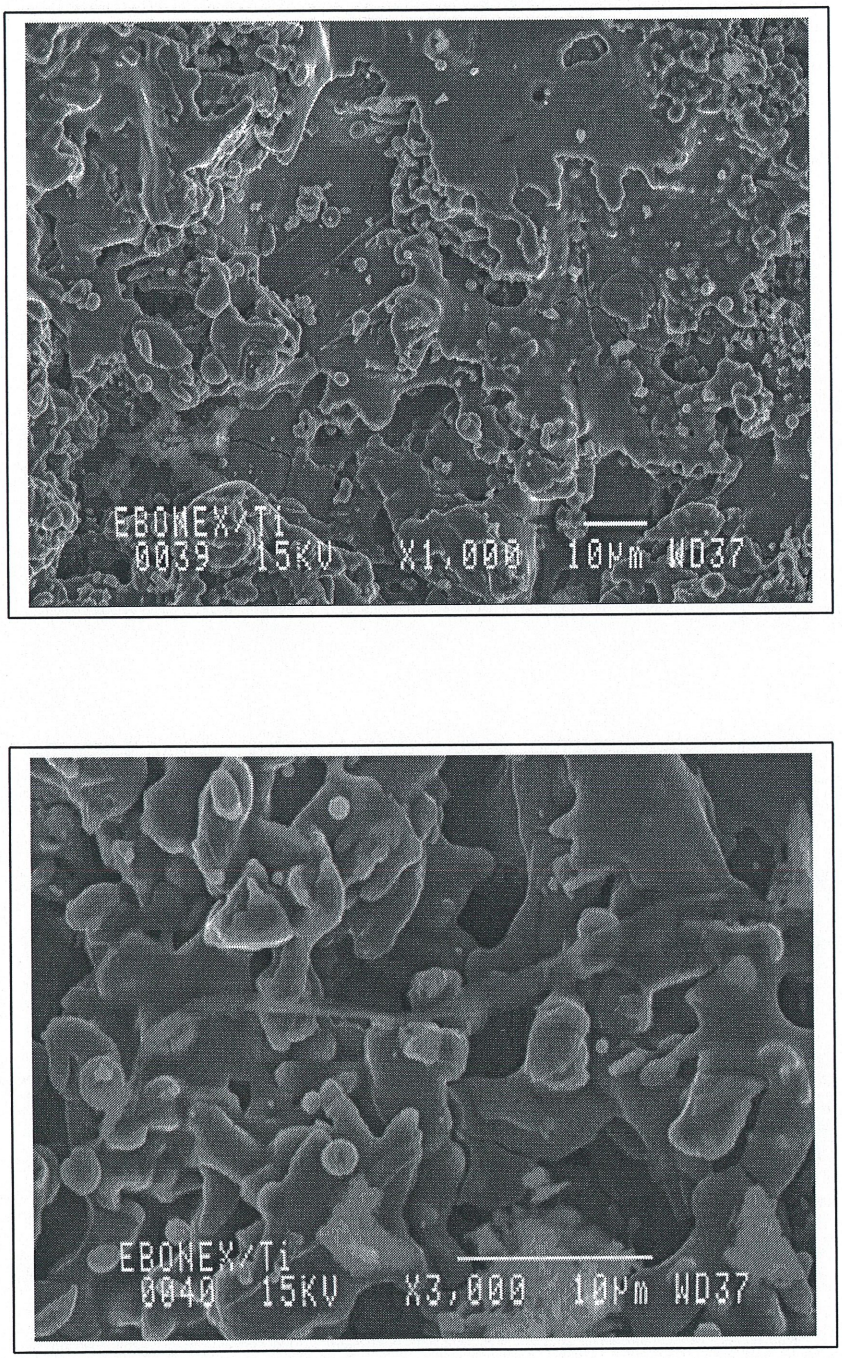

Figure 66. SEM micrographs of Ebonex® on Ti (magnification 1000 × and 3000 ×).

Fig. 68 represents the impact of the scan rate on the polarization curves for Ebonex® coated Ti at the scan rates of 1, 5, 10, 20, 40, and 60 mV s^{-1}. As can be seen in Fig. 68, the increase of the scan rate does not lead to changes of E_{corr} and i_{corr}. In the passive region, we observe only that this area becomes narrower upon the scan rate increase. The secondary passive region that commences at ca. 1.4 V vs. RHE was observed at every scan rate.

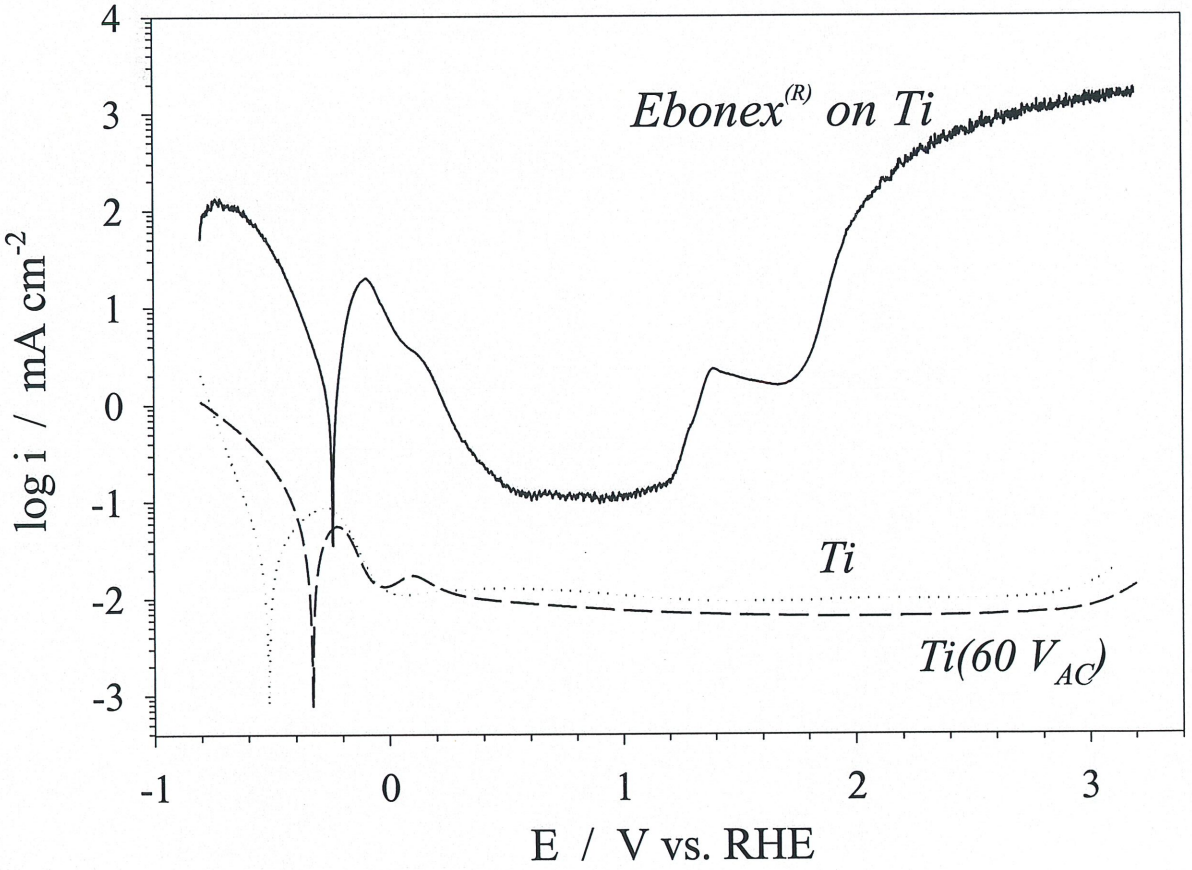

Figure 67. Comparison of polarization curves for Ti, the 60 V_{AC} colored Ti passive layer, and Ebonex® on Ti recorded in 1 M aq. H_2SO_4 (T = 298 K, s = 1 mV s^1).

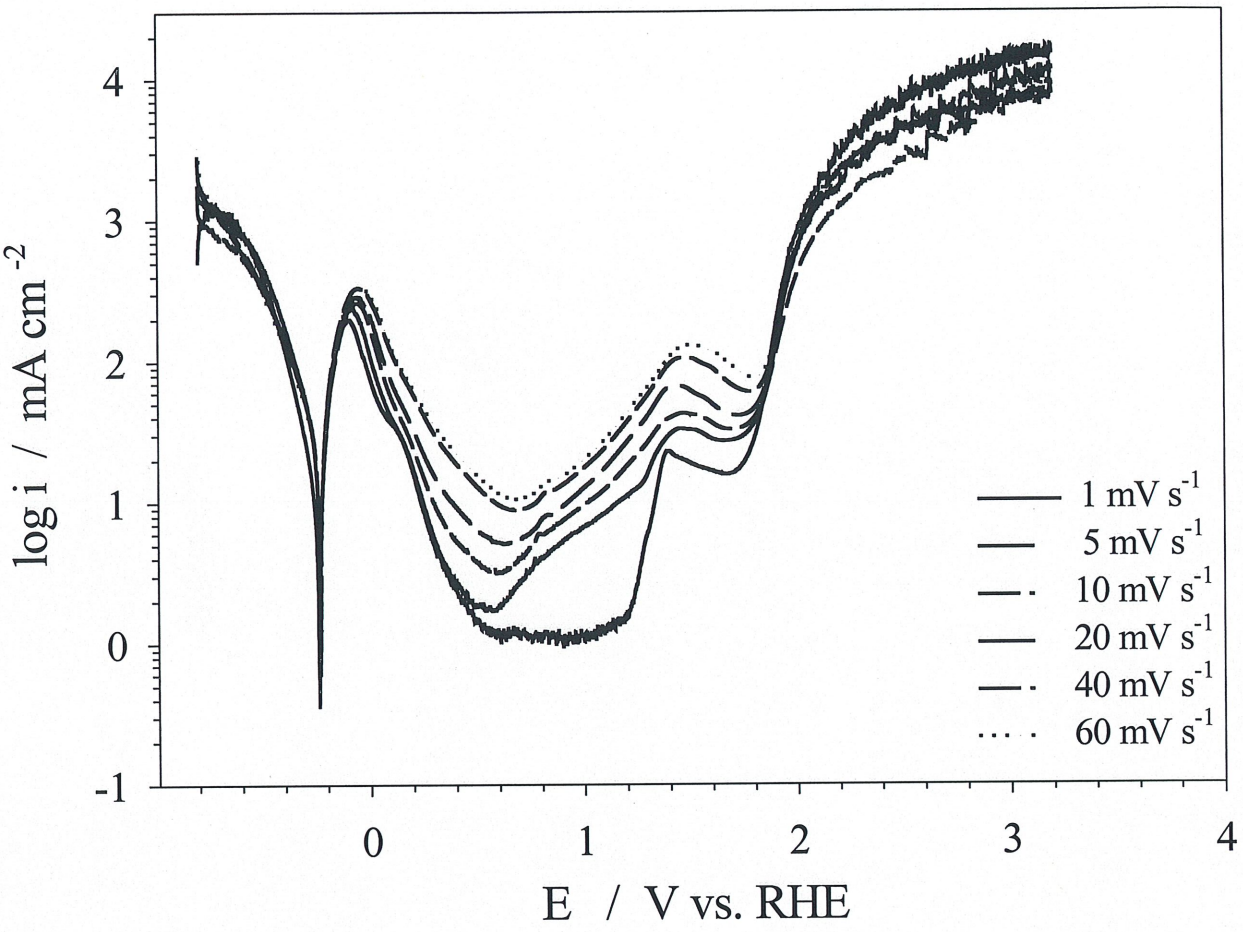

Figure 68. Influence of the scan rate on the polarization curve of Ebonex® on Ti recorded in 1 M aq. H_2SO_4 (T = 298 K, s = 1 – 60 mV s^{-1}). RHE was used as a rererence electrode and Pt grid as a counter electrode.

7.2.2 Cyclic voltammetry of Ebonex® on Ti

In Fig. 69 we show cyclic voltammograms for Ebonex® on titanium recorded in the potential region between 0.05 and 2.0 V vs. RHE at the scan rates of 20, 40, 60, 80, and 100 mV s^{-1} in 1 M aq. H_2SO_4. These CV profiles confirm the results shown in Figs. 67 and 68 as well as they reveal the presence of two passive regions, primary and secondary, that remain apparent even at high scan rates ($s \leq 100$ mV s^{-1}). The

peak current density of secondary passive region increases upon increase of the scan rate (see inset in Fig. 69). The lack of any cathodic peak over the whole potential range indicates that the surface, once oxidized anodically, cannot be reduced in this potential range. The fact that the cathodic curves are superimposable between 0.05 and 2.0 V during the negative-going scan is a clear indication of the stability of the original oxide state (Ti_4O_7 – Ti_5O_9).

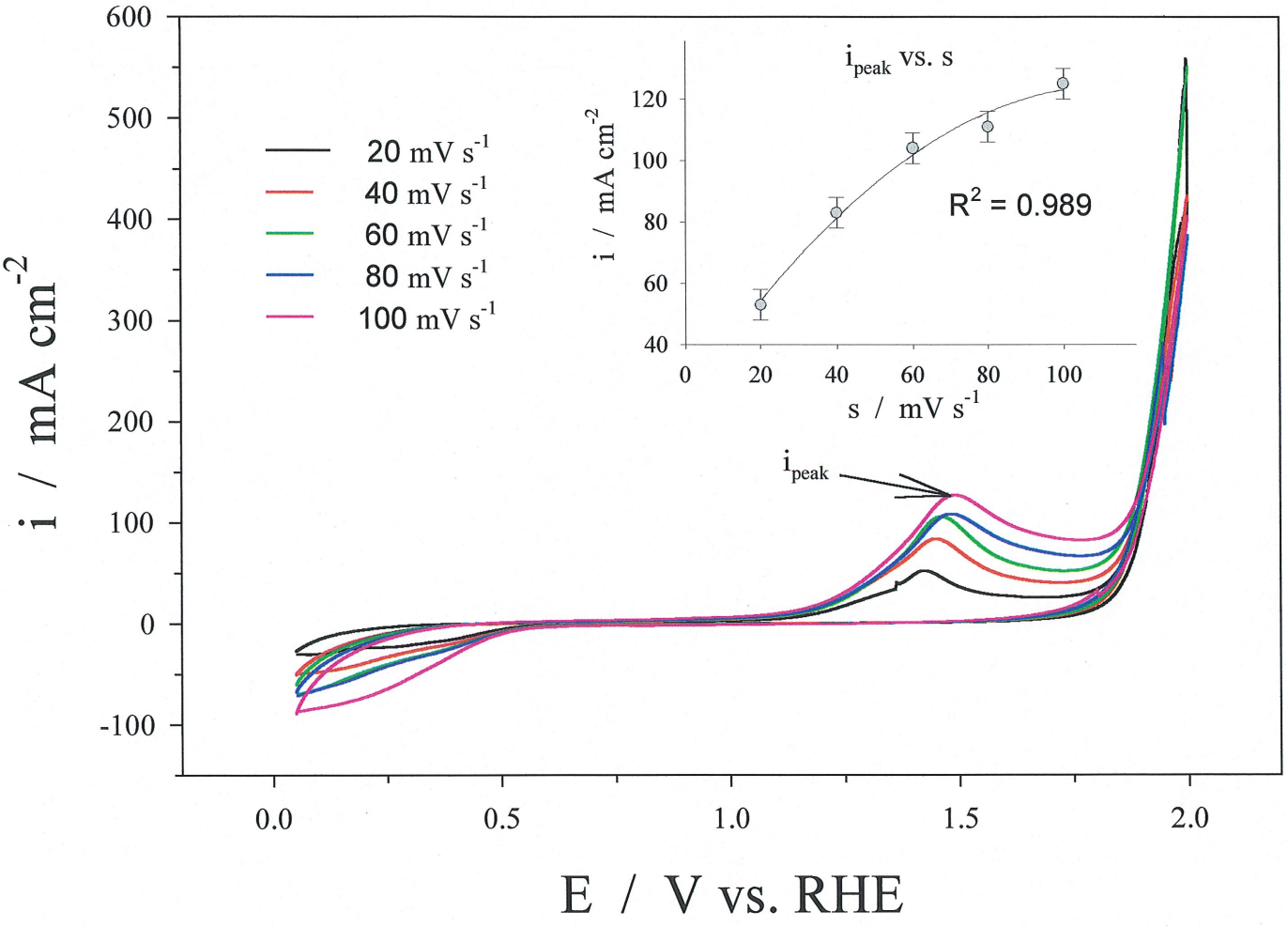

Figure 69. Cyclic voltammogram of EBONEX® on Ti in 1 M aq. H_2SO_4 between 0.05 and 2.0 V vs. RHE with various scan rates (T = 298 K). Pt grid was used as a counter electrode.

7.2.3 HER Tafel plots for Ebonex® on Ti

Tafel polarization curves were recorded in order to examine the material's activity towards the HER. The same program and experimental setup for Tafel plots were used as in the case of the characterization of the colored Ti films and modified Ti layers. Fig. 70 presents a representative Tafel plot recorded between 0.00 and – 0.80 V vs. RHE. The curve reveals two regions with a local minimum that corresponds to E_{corr} and i_{corr}. The corrosion parameters (E_{corr} and i_{corr}) were determined by the extrapolation methodology (see Fig. 42 in Chapter 5). As can be seen in Fig. 70, the value of corrosion potential (E_{corr}) was – 0.25 V vs. RHE, and the ctitical current density (i_{corr}) was 0.28 mA cm^{-2}.

7.2.4 Impact of prolonged cathodic polarization on Ebonex® on Ti

In order to examine the stability of Ebonex® on Ti we polarized cathodically our electrodes applying the current density of – 100 mA cm^{-2} (the same methodology as in the case of examination of the colored Ti films or the chemically modified layers). After application of a negative current for a given time, we recorded a polarization curve at the scan rate of 1 mV s^{-1}. Fig. 71 shows polarization curves that reveal the influence of cathodic polarization. After only 1 hr of the cathodic polarization, we observed a higher current in the HER and passivation regions. The tendency continued after an extension of the cathodic polarization for 4 more hours (5 hrs in total). During the recording of a polarization curve after 5 hrs of cathodic polarization, we observed that the Ebonex® coating became separated from the titanium substrate. There are two hypotheses that could respond to the question why Ebonex® was detached. One reason may be in the machining of electrodes, because the mechanical stress and vibrations could affect the Ebonex® coating. The other, more conceivable explanation, lies in hydrogen damage to the electrodes during the cathodic charging, hydrogen penetrates the Ebonex® coating, causing a breakdown at the Ebonex®/Ti interface. The results show that despite excellent electrochemical characteristics, Ebonex® coating on Ti, it is not stable upon prolonged cathodic polarization and as such cannot be utilized in the electrochemical industry.

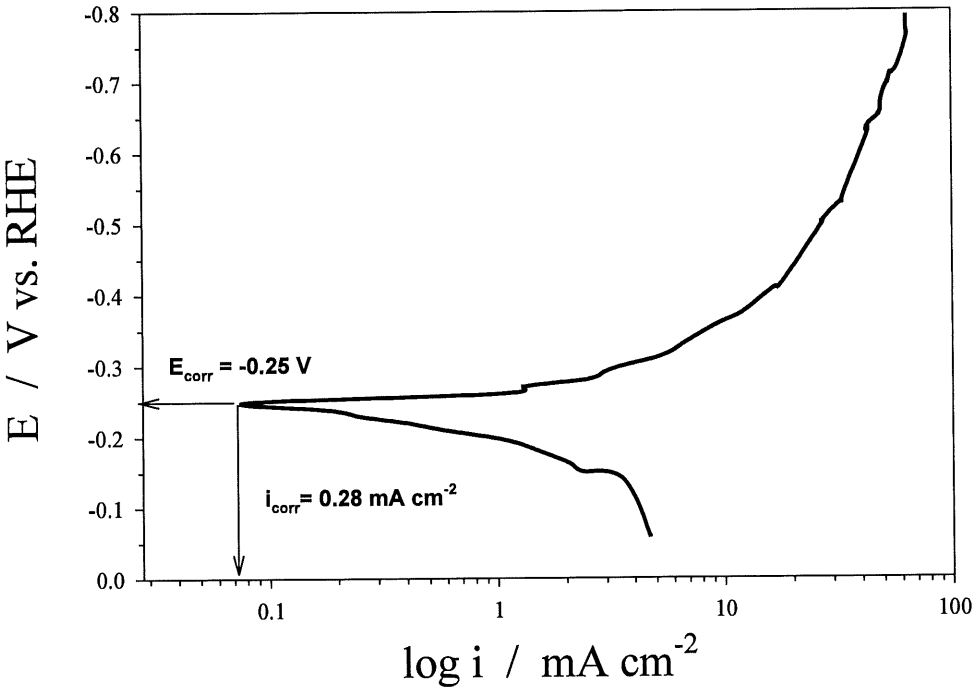

Figure 70. Tafel plot for Ebonex® on Ti in the HER region between 0.0 V and - 0.80 V vs. RHE recorded in aq. 1 M H_2SO_4 (T = 298K). Pt grid was used as a counter electrode.

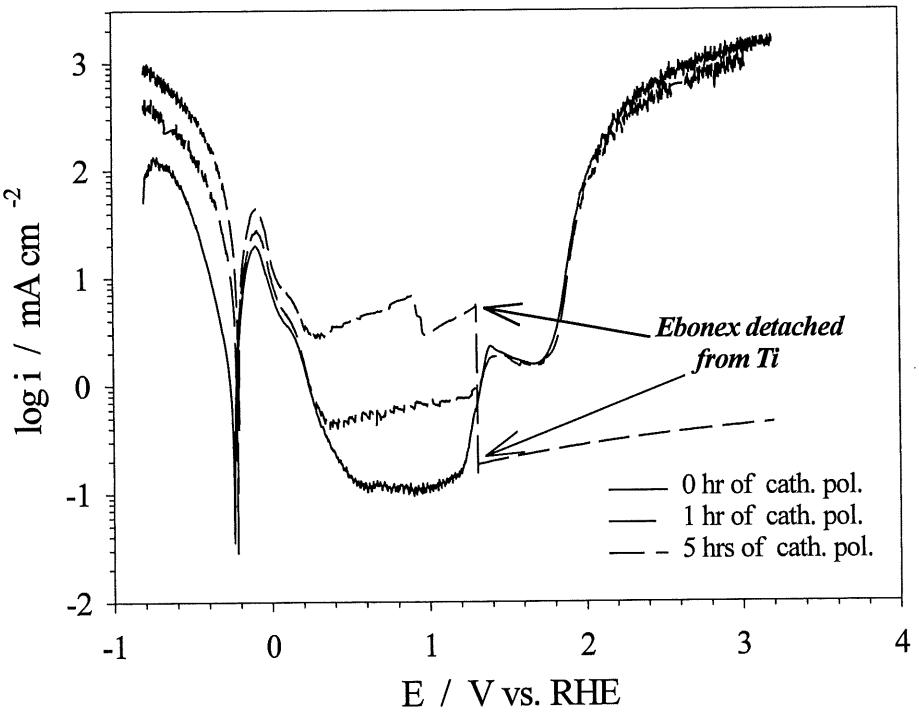

Figure 71. Impact of cathodic polarization on Ebonex® on Ti recorded in aq. 1 M H_2SO_4 (T = 298K, s = 1 mV s^{-1}). Pt grid was used as a counter electrode.

CONCLUSIONS

In this study, a new procedure of preparing colored passive layers on titanium by application of AC polarization in aq. NH_4BF_4 was developed. This methodology gives a wide spectrum of well-defined and brightly colored layers. Therefore, we conclude that the unique results that were obtained in aqueous NH_4BF_4 are directly related to experimental methodology. The examination of the influence of different experimental parameters on the surface coloration (electrolyte pH, concentration, time of the polarization), guide us to the bright and uniform colors on titanium.

A combination of the electrochemical coloration of Ti by AC polarization with masking techniques used in the semiconductor industry allows us to develop a method of pattern design on Ti that we refer to as electrochemical lithography. It can be effectively use for decorative purposes and surface finishing.

The morphology of the colored passive films was studied by application of optical microscopy, scanning electron microscopy, and atomic force microscopy. The general observations are that the passive films revealed the same coloration on different grains, the surface roughness decreases upon the color film formation, and the colored passive films revealed no cracks or fractures.

The information about the surface-chemical composition and the thickness of the colored titanium passive layers was obtained using X-ray photoelectron spectroscopy. A relation between the thickness, the coloration and the applied AC voltage was established. XPS analysis of the as-received samples reveals presence of Ti, O, F, C, Ca, and N. Ti, O and F are the main constituents of the passive layers, whereas C, Ca, and N are surface contaminants that originate from the via-air transfer. The surface chemical composition of the outer-most layer of the colored titanium passive layers is practically the same and Ti, O, and F are present in the

same quantities. However, the chemical composition of the inner layer, as determined on the basis of XPS depth profiling, is not the same and it depends on the surface coloration which is a function of the experimental conditions.

Electrochemical properties of the metallic Ti and colored Ti passive layers are determined by recording polarization curves in the – 0.8 - 3.2 V vs. RHE range as well as Tafel plots in the hydrogen evolution reaction (HER) region in 1.0 M aqueous H_2SO_4. The polarization curves show that the corrosion potential of the colored passive layers shifts towards less-negative potential indicating that they are more stable than Ti under the same conditions. The passive region for the colored layers resembles that for Ti. The Tafel plots for the HER demonstrate that the passive layers have higher activity towards the HER than Ti. The Tafel relations reveal new features that can be associated with the partial breakdown/decomposition of the passive layers, H absorption and the onset of Ti hydride formation.

Modification of the surface chemical composition and electrochemical properties of multicolored titanium passive films was accomplished by deposition and intercalation of RuO_2 or/and IrO_2 through thermal oxidative decomposition of respective chlorides. Our interest in surface modified Ti electrodes arises from the necessity to develop a suitable Ti-based cathodic material for the chloro-alkali industry where the carbon-steel electrode is unable to withstand the highly corrosive environment. However, the chemical stability of Ti can be enhanced through its surface doping with RuO_2 or/and IrO_2. The surface doping of TiO_x with RuO_2 or/and IrO_2 modifies the electronic properties of the former from semi-conducting to electronically conducting. Such prepared chemically modified mixed oxide layers reveal promising catalytic properties towards the hydrogen evolution reaction and could become a new Ti-based cathode material. Surface morphology of these chemically modified layers was determined using SEM. The RuO_2 layer deposited on top of the colored Ti passive films reveals no cracks and fractures. On the other hand, the IrO_2 and RuO_2+IrO_2 layer have pronounced cracks and fractures. The RuO_2-modified catalyst well protects the underlying Ti (compact layer) as well as enhances the catalytic properties. The colored passive films

increase the adhesion of RuO_2 on Ti and effectively absorb any thermal stress that would lead to a cracked RuO_2 deposit in absence of the interfacial colored film. Therefore, it may be concluded that under such condition the colored passive layers play the role of an interfacial adhesive.

Surface morphology of Ebonex® (non-stoichiometric mixture of Ti oxides) on metallic Ti was examined by using optical microscopy and scanning electron microscopy. Electrochemical characterization of Ebonex® on Ti and its comparison with pure Ti and colored Ti passive layers, were accomplished using linear sweep voltammetry, cyclic voltammetry, Tafel plots, and prolonged cathodic polarization. Ebonex® revealed higher electrocatalytic activity than Ti or its colored passive layers. On the other hand, Ebonex® shows instability during prolonged application of a negative current that leads to its peeling off from the metallic substrate.

REFERENCES

1. R.W. SCHUTZ, Corrosion Tests and Standards-Application and Interpretation, *Edited by* R. BABOIAN, ASTM Manual series, Philadelphia, PA, 1995., Ch. 52., p. 493.
2. H. CHANDLER *in* Metallurgy for the Non-Metallurgist, *Edited by* THE MATERIAL INFORMATION SOCIETY, Ohio, USA, 1998., p. 250.
3. H. P. GODARD, W. B. JEPSON, M. R. BOTHWELL, R. L. KANE *in* The Corrosion of Light Metals, *Edited by* JOHN WILEY & SONS Inc., New York, NY, USA, pp. 315-328, (1967).
4. Corrosion Resistance of Metal and Alloys, Amer. Chem. Soc. Monograph, **158**, p. 97 and 647, (1963).
5. J. B. COTTON and B. P. DOWNING, Inst. Mar. Eng. (U.K.), **69**, 311, (1957).
6. E. E. MILLAWAY, Mater. Protect., **4** (1), (1965).
7. N. D. TOMASHOV, R. M. ALTOVSKII, and M. TAKUSHNEREV, Dokl. Akad. Nauk. (USSR), **141**, **4**, 2, (1961).
8. V. V. ANDREEVA, Corrosion, **20**, 35, (1964).
9. E. ENCE and J. MARGOLIN, J. Metals, **6**, 346, (1954).
10. P. A. JACQUET, Metal Treatment, **18**, 176, (1951).
11. C. MA and E. M. PERES, Ind. Eng. Chem., **43**, 675, (1951).
12. D.A. McLEAN, N. SCHWARTZ, J. K. WERNER, and M. GRESH, *in* Bell Tel. Labs. Rpt. AD-232-690, pp. 14-15. (1960).
13. E. WAINER, U.S. Pat. 2, **874**, 102, (1959).
14. M. E. SILBERT, J. Electrochem. Soc., **110**, 65, (1963).
15. G. JERKIEWICZ, H. STRZELECKI, and A. WIECKOWSKI, Langmuir, **12**, 1005, (1996).
16. G. WYSZNECKI, and W.S. STYLES, Color Science: Concepts and Methods,

Quantitative Data and Formulae, Wiley-Interscience, New York, (1982).

17. K. MASSAU, The Physics and Chemistry of Colors, Wiley-Interscience, New York, (1983).
18. A. HAGFELDT, N. VLACHOPOULOS, AND M. GRÄTZEL, J. Electrochem. Soc., **141**, 82, (1994).
19. W. A. SEELEY, M.Sc. Thesis, University of Kanzas, USA, (1970).
20. M. KODINTSEV and S. TRASSATTI, Electrochim. Acta, **39**, 1803, (1993).
21. V.A. ALVES, L.A. DA SILVA, J.F.C. BOODTS and S. TRASSATTI, Electrochim. Acta, **39**, 1585, (1993).
22. L. TOMCSÁNYI, F. MOLNÁR, J. LISZI and A. DE BATTISTI, Electrochim. Acta, **39**, 1923, (1994).
23. P.C.S. HAYFIELD, Platinum Metals Rev., **42**, 46, (1998).
24. CH. COMNINELLIS and G.P. VERCESI, J. Appl. Electrochem., **21**, 136, (1991).
25. R. KÖTZ and S. STUCKI, Electrochim. Acta, **31**, 1311, (1986).
26. C. IWAKURA, K. HIRAO and H. TAMURA, Electrochim. Acta, **22**, 335, (1977).
27. K. FUKUDA, C. IWAKURA and H. TAMURA, Electrochim. Acta, **23**, 613, (1978).
28. K. FUKUDA, C. IWAKURA and H. TAMURA, Electrochim. Acta, **24**, 363, (1979).
29. S. TRASATTI, Electrochim. Acta, **29**, 1503, (1984).
30. F.I. MATTOS-COSTA, P. DE LIMA-NETO, S.A.S. MACHADO and L.A. AVACA, Electrochim. Acta, **44**, 1515, (1998).
31. H. SCHMIDT, *in* Chemistry, Spectroscopy and Applications of Sol-gel Glasses, *Edited by* R. REISFELD and C.K. JØRGENSEN, Springer-Verlag, Berlin, 1992. p.119.
32. S. SAKKA and T. YOKO, *in* Chemistry, Spectroscopy and Applications of Sol-Gel Glasses, *Edited by* R. REISFELD and C. K. JØRGENSEN, Springer-Verlag, Berlin, 1992. p. 89.

33. J.L. FERNÀNDEZ, C.A. MAROZZI, M.R. GENNERO DE CHIALVO, and A.C. CHIALVO, J. Electroanal. Chem., **457**, 109, (1998).

34. C.L.P.S. ZANTA, A.R. DE ANDRADE, and J.F.C. BOODTS, Electrochim. Acta, **44**, 3333, (1999).

35. C. ANGELINETTA, S. TRASATTI, Lj.D. ATANASOSKA, R.T. ATANASOSKI, J. Electroanal. Chem., **214**, 535, (1986).

36. R. KÖTZ, S. STUCKI, Electrochim. Acta, **31**, 1311, (1986).

37. CH. COMNINELLIS, G.P. VERSECI, J. Appl. Electrochem., **21**, 136, (1991).

38. G. JERKIEWICZ, S. HRAPOVIC, G. VATANKHAH, B.L. LUAN, *in* Proceedings of the Symposium on Environmental Degradation of Metals and Corrosion Control of Metals, *Edited by* M. ELBOUJDAINI, E. GHALI, METSOC, Quebec, (1999).

39. S. JIN, A. VANNESTE, E. GHALI, S. BOILY, R. SCHULTZ, J. Electrochem. Soc., **144**, 4272, (1997).

40. S.H. YIP, D. GUAY, S. JIN, E. GHALI, A. VANNESTE, R. SCHULTZ, J. Mater. Res., **13**, 1171, (1998).

41. J.-L. DEPLANCKE, M. SUN, T.J. O'KEFFE, R. WINAND, Hydrometallurgy, **23**, 46, (1989).

42. J.-L. DEPLANCKE, M. SUN, T.J. O'KEFFE, R. WINAND, Hydrometallurgy, **24**, 179, (1990).

43. J. PRZYLUSKI and K. KOLBRECKA, J. App. Electrochem., **23**, 1063, (1993).

44. J.R. SMITH and F. C. WALSH, J. Appl. Electrochem., **28**, 1021, (1998).

45. W.J. MACKLIN and R.J. NEAT, Solid State Ionics, **53**, 694, (1992).

46. M. MAYR, W. BLATT, B. BUSSE and H. HEINKE, 4th International Forum on Electrolysis in the Chemical Industry, Fort Lauderdale, FA, (1990).

47. R. L. CLARKE, 2nd European Conference on Electrochemical Processing, Innovation and progress, Moat House International, Glasgow, U. K. (1993).

48. X. G. ZHANG, *in* Corrosion and Electrochemistry of Zinc, Plenum Press New York,

NY, USA, (1996). p. 250.

49. D.L. PIRON, *in* The Electrochemistry of Corrosion, Nace Houston, (1994), p. 169.

50. D.W. SHOESMITH, Kinetics of Aqueous Corrosion, ASM Handbook, 9th Edition, Vol 13, p. 35, (1986).

51. R.W. SCHUTZ, Corrosion of Titanium and Titanium Alloys, ASM Handbook, 9th Edition, Vol 13, pp. 669-696, (1986).

52. J. P. HIRTH,. *in* Hydrogen embrittlement and Stress Corrosion Cracking, *Edited by* R. GIBALA and R.F. HEHEMANN, American Society for Metals, Ohio, USA, 1984, pp.30-38.

53. Encyclopedia of Electrochemistry of elements, *Edited by* A.J. BARD, Marcel Dekker Inc., New York, NY, USA,1976, Vol V, p.365.

54. Corrosion and Corrosion Protection Handbook, Seconf Edition, *Edited by* P. A. SCHWEITZER, Marcel Dekker Inc., New York, NY, 1988, pp.3187-212.

55. W.D. CALLISTER, Materials Science and Engeneering, John Willey and Sons, New York, NY, 1990, p. 587.

56. D. SCHLAIN, Corrosion Properties of Titanium, Bureau of Mines Bulletin, 1964. p. 619.

57. K. O. GRAY, Mater. Prot., **3**, 46 (1964).

58. M.E. STRAUMANIS and P.C. CHEN, J. Electrochem. Soc., **98**, 234, (1951).

59. T. FUKUZUKA, K. SHIMOGORI, H. SATOH and F. KAMIKUBO, in Titanium'8O Science and Technology, The Metallurgical Society, pp. 2631-2638, 1980.

60. S. HRAPOVIC, G. VATANKHAH, B. LUAN, and G. JERKIEWICZ, *in* Environmental Degradation of materials and Corrosion Control in Metals, *Edited by* M. Elboujdaini, E. Ghali, METSOC, CIM, Montréal, Canada, (1999).

61. L.D. BURKE, Chapter 4 *in* R.E. WHITE, J.O'M. BOCKRIS and B.E. CONWAY, Modern Aspects of Electrochemistry, **18**, New York, NY, 1986.

62. N.V. PARTHASARADHY, Practical Electroplating Handbook, Prentice Hall,

Englewood Cliffs, (1989).

63. H. ANGERSTEIN-KOZLOWSKA, *in* Comprehensive Treatise of Electrochemistry, Vol. 9, Ch. 1, *Edited by* E. YEAGER, J.O'M. BOCKRIS, B.E. CONWAY, S. SARANGAPANI, Plenum Press, New York, NY, USA, (1984).

64. A. ZOLFAGHARI, Ph. D. Thesis, Université de Sherbrooke, Canada, (1998).

65. EBONEX® Electrodes for Electrometallurgy, ICI Ebonex Technologies Inc. (Product Description), (1996).

66. G.J. LEFFETT *in* Surface Analysis-The Principal Techniques, *Edited by* J.C. VICKERMAN, John Wiley & Sons, England, p. 406, (1997).

67. N. WINOGRAD and S.W. GAARENSTROOM *in* Physical Methods in Modern Chemical Analysis, *Edited by* T. KUWANA, Academic Press, New york, NY, USA, Vol. 2, p. 126-161, (1980).

68. M. RUBEL, R. HAASH, P. MROZEK, A. WIECKOWSKI, C.DE PAULLI, S. TRASATTI, Vacuum, **45**, 423, (1994).

69. G. ERTL, J. KŰPPERS, Low Energy Electrons and Surface Chemistry, VCH, New York, NY, USA, (1985).

70. J.F. WATTS, An Introduction to Surface Analysis by Electron Spectroscopy, Oxford University Press, New York, NY, USA, (1990).

71. Hanboook of X-Ray Photoelectron Spectroscopy, *Edited by* J.F. MOULDER, Perkin Elmer, Eden Prairie, MN, USA, (1992).

72. P. PEDEFERRI, Drawings on Titanium, Cooperativa Libraria Universitaria del Politecnico, Milano, Italia, (1981).

73. C. MADORE, O. PIOTROWSKI, D. LANDOLT, J. Electrochem. Soc., **146**, 2526, (1999).

74. M. STERN, H. WISSENBRG, J. Electrochem. Soc., **106**, 755 (1959).

75. J. TAFEL, Z. Phys. Chem., **50**, 641, (1905).

76. B.E. CONWAY, Theory and Principles of Electrode Processes, Ronald Press,

New York, NY, (1965).

77. B.E. CONWAY, B.V. TILAK, Advances in Catalysis, Vol 38, Ch. 1, Academic Press, New York, NY, USA, (1992).

78. Electrodes of Conductive Metallic oxides, *Edited by* S. TRASATTI, Elsevier Scientific Publishing Company, Part 1, **6**, p. 324, New York, NY, USA, (1980).

79. S. TRASATTI and P. KURTZWEIL, Platinum Met. Rev., **38**, 46, (1994).

80. B.E. CONWAY, Electrochemical Supercapacitors, Kluwer Academic Plenum Publishers, New York, NY, USA, (1999).

81. J. O'M. BOCKRIS and T. OTAGAWA, J. Electrochem. Soc., **131**, 290, (1984).

82. R. BOGGIO, A. CARUGATI, and S. TRASATTI, J. Appl. Electrochem., **17**, 828, (1987).

83. S. TRASATTI and D. A. PETRII, Pure Appl. Chem. **63**, 711, (1991).

84. P. SIVIGLIA, A. DAGHETTI, and S. TRASATTI, Colloids Surf., **7**, 15 (1983).

85. ANDERSSON, S.; COLLEN, B. KUYLENSTIERNA, U. MAGNELI, Acta Chem. Scand.,**11**, 1641, (1957).

86. R.R. MILLER-FOLK, R.E. NOFTLE, D. PLETCHER, J. Electroanal. Chem., **274**, 257, (1989).

87. R.E. GRAVES, D. PLETCHER, R.L. CLARKE, F.C.J. WALSH, J. Appl. Electrochem., **21**, 848, (1991).